Université de Montréal

Quantifying diffusion in biofilms: from model hydrogels to living biofilms

par
Mahmood Golmohamadi

Département de chimie
Faculté des Arts et des Sciences

Thèse présentée à la Faculté des études supérieures et postdoctorales
en vue de l'obtention du grade de Ph.D.
en Chimie

Juillet 2012

Université de Montréal
Faculté des études supérieures et postdoctorales

Cette thèse intitulée:

Quantifying diffusion in biofilms: from model hydrogels to living biofilms

Présentée par:
Mahmood Golmohamadi

a été évaluée par un jury composé des personnes suivantes:

Michel Lafleur, président-rapporteur
Kevin J. Wilkinson, directeur de recherche
Suzanne Giasson, membre du jury
Reghan Hill, examinateur externe
Alain Vincent, représentant du doyen de la FAS

Résumé

Les biofilms sont des communautés de microorganismes incorporés dans une matrice exo-polymérique complexe. Ils sont reconnus pour jouer un rôle important comme barrière de diffusion dans les systèmes environnementaux et la santé humaine, donnant lieu à une résistance accrue aux antibiotiques et aux désinfectants. Comme le transfert de masse dans un biofilm est principalement dû à la diffusion moléculaire, il est primordial de comprendre les principaux paramètres influençant les flux de diffusion. Dans ce travail, nous avons étudié un biofilm de *Pseudomonas fluorescens* et deux hydrogels modèles (agarose et alginate) pour lesquels l'autodiffusion (mouvement Brownien) et les coefficients de diffusion mutuels ont été quantifiés. La spectroscopie par corrélation de fluorescence a été utilisée pour mesurer les coefficients d'autodiffusion dans une volume confocal de ca. 1 μm^3 dans les gels ou les biofilms, tandis que les mesures de diffusion mutuelle ont été faites par cellule de diffusion. En outre, la voltamétrie sur microélectrode a été utilisée pour évaluer le potentiel de Donnan des gels afin de déterminer son impact sur la diffusion.

Pour l'hydrogel d'agarose, les observations combinées d'une diminution du coefficient d'autodiffusion et de l'augmentation de la diffusion mutuelle pour une force ionique décroissante ont été attribuées au potentiel de Donnan du gel. Des mesures de l'effet Donnan (différence de -30 mV entre des forces ioniques de 10^{-4} et 10^{-1} M) et l'accumulation correspondante d'ions dans l'hydrogel (augmentation d'un facteur de 13 par rapport à la solution) ont indiqué que les interactions électrostatiques peuvent fortement influencer le flux de diffusion de cations, même dans un hydrogel faiblement chargé tel que l'agarose. Curieusement, pour un gel plus chargé comme l'alginate de calcium, la variation de la force ionique et du pH n'a donné lieu qu'à de légères variations de la diffusion de sondes chargées dans l'hydrogel. Ces résultats suggèrent qu'en influençant la diffusion du soluté, l'effet direct des cations sur la structure du gel (compression et/ou gonflement induits) était beaucoup plus efficace que l'effet Donnan. De même, pour un biofilm bactérien, les coefficients d'autodiffusion étaient pratiquement constants sur toute une gamme de force ionique (10^{-4}-10^{-1} M), aussi bien pour des petits solutés chargés négativement ou positivement (le rapport du coefficient d'autodiffusion dans biofilm sur

celui dans la solution, $D_b/D_w \approx 85$ %) que pour des nanoparticules ($D_b/D_w \approx 50$ %), suggérant que l'effet d'obstruction des biofilms l'emporte sur l'effet de charge.

Les résultats de cette étude ont montré que parmi les divers facteurs majeurs qui affectent la diffusion dans un biofilm environnemental oligotrophe (exclusion stérique, interactions électrostatiques et hydrophobes), les effets d'obstruction semblent être les plus importants lorsque l'on tente de comprendre la diffusion du soluté. Alors que les effets de charge ne semblaient pas être importants pour l'autodiffusion de substrats chargés dans l'hydrogel d'alginate ou dans le biofilm bactérien, ils ont joué un rôle clé dans la compréhension de la diffusion à travers l'agarose. L'ensemble de ces résultats devraient être très utiles pour l'évaluation de la biodisponibilité des contaminants traces et des nanoparticules dans l'environnement.

Mots-clés : agarose, alginate de calcium, autodiffusion, biofilm, cellule de diffusion, diffusion mutuelle, potentiel de Donnan, spectroscopie de corrélation de fluorescence, voltamétrie sur microélectrode.

Abstract

Biofilms are primarily communities of microorganisms embedded in a complex exopolymer matrix. They are thought to play an important role as diffusive barriers in environmental systems and human health, resulting in increased resistance to disinfectants and antibiotics. Since mass transport in a biofilm is primarily due to molecular diffusion, it is critical to understand the main parameters influencing diffusive fluxes in a biofilm. In this thesis, a *Pseudomonas fluorescens* biofilm and two model hydrogels, (agarose and calcium alginate), were investigated. Both self-diffusion (Brownian motion) and mutual diffusion coefficients were quantified. Fluorescence correlation spectroscopy was used to measure the self-diffusion coefficients in a ca. 1 μm^3 confocal volume in the gels or biofilms, whereas a diffusion cell setup was employed for mutual diffusion measurements. In addition, microelectrode voltammetry was used to evaluate Donnan potential of the gels in order to determine its impact on diffusion.

For the agarose hydrogel, the combined observations of a decreasing self-diffusion coefficient coupled with increasing mutual diffusion as a function of a decreasing ionic strength have been attributed to the gel's Donnan potential. Measurements of the Donnan effect (difference of -30 mV between ionic strengths of 10^{-4} and 10^{-1} M) and the corresponding accumulation of ions in the hydrogel (13x enhancement with respect to the bulk solution) indicated that electrostatic interactions can strongly influence the diffusive flux of cations, even in a weakly charged hydrogel, such as agarose. Somewhat surprisingly, for a more highly charged gel such as calcium alginate, varying ionic strength and pH resulted in only small changes to the diffusion of charged probes in the hydrogel. These results suggested that the direct effect of the cations on gel structure (due to an induced swelling or compression) was much more effective than the Donnan effect when influencing solute diffusion. Similarly, for a bacterial biofilm, self-diffusion coefficients were virtually constant across a range of examined ionic strengths (10^{-4}-10^{-1} M) for both negatively and positively charged small solutes ($D_b/D_w \approx 85\%$) and nanoparticles ($D_b/D_w \approx 50\%$), suggesting that the obstruction effect of the biofilms again overwhelmed the charge effect.

The results of this work indicated that among the various major factors affecting diffusion in an oligotrophic environmental biofilm (steric exclusion, hydrophobic and electrostatic interactions), obstruction effects appeared to be the most important when attempting to understand the solute diffusion. While charge effects did not appear to be important to the self-diffusion of charged substrates in the alginate hydrogel or bacterial biofilm, they were key to understanding diffusion through another gel, with numerous biomedical and environmental applications, i.e. agarose. These results should be extremely useful when evaluating the bioavailability of the trace contaminants and nanoparticles in the environment.

Keywords: agarose, biofilm, calcium alginate, Donnan Potential, diffusion cell, fluorescence correlation spectroscopy, microelectrode voltammetry, mutual diffusion, nanoparticles, self-diffusion.

Table of contents

List of tables

List of figures

List of abbreviations

A	Surface area
a	Activity
b	Background factor
CPS	Counts per second
c	Concentration
c_w	Concentration in bulk solution
c_g	Concentration in hydrogel
C	Coulomb
d_H	Hydrodynamic diameter
D	Dalton
D	Diffusion coefficient
D^s	Self-diffusion coefficient
D^m	Mutual diffusion coefficient
D_w	Diffusion coefficient in water
D_g	Diffusion coefficient in hydrogel
D_g^s	Self diffusion coefficient in hydrogel
D_g^m	Mutual diffusion coefficient in hydrogel
DET	Diffusion equilibrium technique
DPSS	Diode-pumped solid-state laser
F	Faraday constant
F	Opposing force
FCS	Fluorescence Correlation Spectroscopy
GF-AAS	Graphite furnace atomic absorption spectrometry
GDL	D-glucono-δ-lactone
$G(\tau)$	Autocorrelation function
h	Hour
Hz	Hertz
I	Ionic strength
$I_\circ$	The peak maximum excitation intensity of laser beam
I^L	Limiting current
J	Flux

K	Boltzman constant
kD	Kilodalton
L	Liter
m	Meter
m	Mass
mV	Milivolt
mL	Mililiter
M	Molarity
n	Number of electrons transferred
n	Number of particles in the confocal volume
nM	Nanomolar
$nTiO_2$	Titanium oxide nanoparicle
nAu	Gold nanoparticle
nSi	Silicon nanoparticle
nm	Manometer
N	Average number of particles in the confocal volume
NA	Numeric aperture of objective
NP	Nanoparticle
Oregon 1C/Org 1C	Oregon green 488 carboxylic acid, succinimidyl ester
Oregon 2C/Org 2C	Oregon green 488 carboxylic acid
P	Pressure
p	The confocal volume shape factor
PAA	Polyacrylic acid
PDDA	Poly diallyl dimethyl ammonium chloride
q	Fluorescence quantum efficiency
R	The universal gas constant
R6G	Rhodamine 6G
R123	Rhodamine 123
RB	Rhodamine B
R110	Rhodamine 110
s	Second
S	Swelling factor

TMRM	Tetramethylrhodamine, methyl ester
t	Time
T	Temperature
V_{eff}	The effective confocal volume
V	Volume
x	Distance
z	Charge number of the electrolytes
z_{g}	Charge number of the functional groups in the gel
α	Degree of anomalous diffusion
η	Viscosity of solution
ε	Absorptivity coefficient
ℓ	Gel thickness
μ	Micron
μW	Microwatt
Π	The electrostatic (Donnan) partition coefficient
$\Pi D_{\text{g}}^{\text{m}}$	Apparent mutual diffusion coefficient
ρ	Volume charge density of the gel
ς	Retardation factor
τ	Delay lag time
τ_{T}	Triplet time
ω_{xy}	Transversal radii of the confocal volume
ω_{z}	Longitudinal radii of the confocal volume
ψ_{D}	Donnan potential
ζ	Zeta potential
Γ	Triplet fraction

To my lovely parents,

Acknowledgements

Special thanks goes to my supervisor, Professor Kevin Wilkinson, for his knowledge and sustainable efforts in creating the opportunity of this Ph.D. for me. I would like to thank him for his prompt feedback, constant guidance, incredible patience and full support in editing my manuscripts.

I would like to take the opportunity to express my sincere gratitude to all the people whose support contributed to the success of this project. I would like to thank my parents, my family, my friends, and also my primary, secondary, high school and university teachers, professors as well as colleagues in Iran and Canada. Also, I would like to think Lana for her lovely support in Canada.

In addition, I extend my appreciation to my fellow colleagues in the research laboratory, all the post-docs and graduate students, who helped me and shared their experiences and knowledge during my Ph.D. project.

I would like to thank the department of chemistry of University de Montreal for their generous support and for providing all the materials needed to accomplish my Ph.D. project. Also thanks to the professors who evaluated my Ph.D. exam, Dr. Robert Prud'homme, Dr. André Beauchamp, Dr. Sébastien Sauvé, Dr Jean-Francois Masson, Dr. Radu Iftimie, and Dr. Karen Waldron.

I would like to thank Jean-François, Martin, Yves, Louis, Cédric, and also Amira and Sylvie for their generous technical support and for providing the necessary materials during my Ph.D. project.

Finally, I would also like to thank the members of the doctoral committee who examined my Ph.D. thesis, Dr. Michel Lafleur, Dr. Suzanne Giasson and Dr. Reghan Hill.

Chapter 1

Introduction

1.1. Overview

Biofilms are important in the fields of human health[1], industrial production[2] and the natural environment, among others[3]. In industrial environments, biofilms are often problematic, resulting in the contamination of food industry products or the biocorrosion of equipment. In the public health field, they can be associated with infectious diseases[4-6] or infect the surfaces of medical implants[7-10]. Furthermore, many household surfaces are the target of biofilms, leading to higher incidences of illnesses associated with pathogenic organisms. In natural environments, biofilms are involved with numerous biogeochemical activities, including the immobilisation of toxic metals[11] or the creation of oxygen depletion zones[12] in lakes and rivers, potentially leading to toxic algal blooms[13].

A biofilm is a collection of microorganisms, embedded within a three dimensional matrix of extracellular polymers (EPS)[14, 15]. The inhomogeneous distribution of cell clusters encapsulated in EPS and the presence of void volumes (water channels) inside the biofilms, have been well documented by confocal laser scanning microscopy (CLSM)[16, 17]. Indeed, EPS form the backbone of the clusters, water channels and intercluster voids[18, 19], all of which contribute to the overall heterogeneous structure of the biofilm. The EPS matrix is often in contact with a surface, where it remains even when cells are removed due to death or shear forces[20]. Biofilm formation, in general, is a complex biological phenomenon, consisting of a succession of several different steps: reversible then irreversible attachment of biological cells to a surface, formation of microcolonies, coalescence of growing microcolonies to form a macrocolony and cell dispersal. This model[21], however, still needs more validation by different experimental techniques. Nonetheless, these observations led to the development of the ‘mushroom-like’ model, which describes the biofilms as a series of mushroom-shaped columns attached to a surface (c.f. Fig. 1.1)[22].

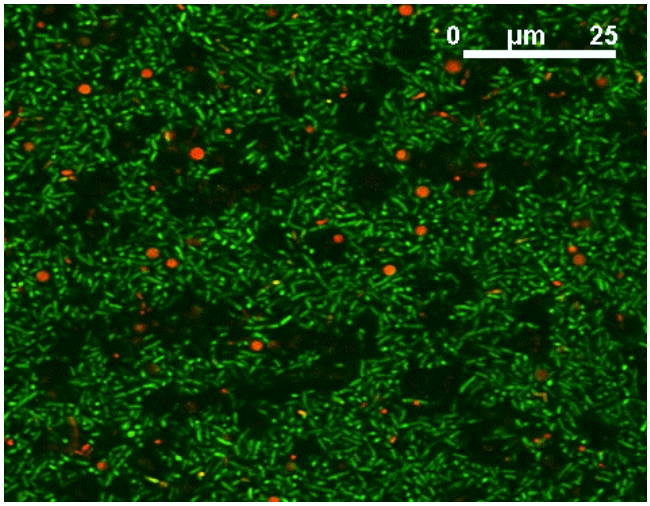

Figure 1.1. Confocal laser scanning microscopy (CLSM) image of a *P. fluorescens* biofilm grown in the presence of 10^{-5} M Fe(III). Bacterial cells have been stained with the Live/Dead *Bac*Lightkit (green-fluorescent SYTO 9 stain / red-fluorescent propidium iodide stain) in order to show viable cells in green and dead cells in red. The sample was excited with the 488 nm line of an Ar ion laser.

Biofilm EPS consists mainly of diverse biomacromolecules including: polysaccharides, peptidoglycans, lipids, polyphenols, proteins, nucleic acids and humic materials. The EPS render the biofilm morphologically diverse, chemically heterogeneous and dynamic. EPS may vary in chemical and physical properties but they mainly consist of polysaccharides. Some of these polysaccharides are neutral and some are polyanionic. Also, uronic acid compounds (D-glucuronic, D-galactouronic and mannuronic) as well as ketal linked pyruvate enhance the anionic properties of EPS. These compounds become important in the presence of ions which can increase the crosslinking between the ionisable functional groups on the polymer backbone. For example, for alginate (and some biofilms), the presence of calcium may serve to strengthen the hydrogel. The hexose residues constitute the backbone of the EPS. Moreover, as the EPS in some biofilms are negatively charged, they can strongly bind water and act as a cation exchanger. The presence of hydrophobic carbon chains can also lead to enhanced local concentrations of organic molecules in the biofilm. Based on the microorganisms and the age of biofilm, the amount of EPS may vary. Furthermore, inside the biofilm, compounds including ions and

macromolecules such as proteins, DNA, lipids and humic substances may also be found. EPS production is, mainly, affected by nutrient status of the growth medium. For example, nitrogen and phosphate limitation can promote the EPS production[23].

Mass transport in biofilms has been primarily attributed to molecular diffusion, particularly in the inner part of the biofilm, i.e., in the local zones of EPS far from the surface of the cluster[24]. The presence of the EPS matrix is thought to increase the resistance of organisms in the biofilm to both environmental stress and antimicrobial agents[25-28] when compared to the planktonic forms of the same organisms[29]. It has been postulated that the increased resistance results from reduced diffusion within the biofilm.[30] Indeed, the increased resistance to disinfection[31] as well as the increased residence time of a tracer in a bioreactor[32] have been attributed to a diffusion limitation. The density, thickness and stickiness of the EPS depend largely on the strain of bacteria and the conditions under which they are grown.

In this thesis, we are interested in quantifying diffusion in a biofilm with respect to both its characteristics and to the nature of the diffusing solutes. Our investigation is designed to help us better understand the diffusion phenomena which are key to understanding biofilm function (both cells and the matrix) with respect to numerous applications. For example, information on diffusion is needed to predict the mobility of the nutrient and metabolic end-products, to determine the activity of biofilms, to characterize antibiotic penetration in biofilms and to better control remediation processes. Nonetheless, given that the biofilm is both chemically and physically heterogeneous, two model polysaccharide hydrogels, prepared from agarose and alginate, were first studied. Although diffusion in biofilms has been investigated by other authors, much of their research has focused on obstruction effects. Little work has been performed on quantifying the role of charge when variably charged solutes interact with the charged EPS in a biofilm. Therefore, in addition to quantifying of the effects due to the sizes of the diffusing solutes, the role of electrostatic interactions between the (mainly) negatively charged EPS and variably charged solutes were examined in more detail. To attain these objectives, a number of modern analytical techniques including the diffusion equilibration cell technique (DET),

microelectrode-based voltammetry and fluorescence correlation spectroscopy have been employed.

1.2. Diffusion

The transport of solutes in the pores of hydrogels and biofilms can be characterized either in terms of Brownian motion (reflected by a *self*-diffusion coefficient) or by a concentration gradient driven diffusive flux (reflected by a *mutual*-diffusion coefficient).

1.2.1 Self-diffusion

Self-diffusion (also called *intra*diffusion[33]) refers to the diffusion of: (i) a one component system, for example, the diffusion of water in water; (ii) a binary or multicomponent system, such as Na^+ in aqueous KCl[34]. In the latter case, the term *tracer* diffusion is often used in literature. Indeed, the thermodynamic factor, $d\ln a_i/d\ln X_i$, which appears in equations describing mutual diffusion (where a is the activity and X is the mole fraction of component i, see below), becomes unity for the diffusing species. Brownian forces cause the molecules to undergo some average mean-squared displacement ($< r^2 >$) in dimension (d) over time, t[35]:

$$\left\langle r^2 \right\rangle = 2d\, D^s\, t \tag{1-1}$$

where D^s is the self-diffusion coefficient. The Stokes-Einstein Equation has been derived from Equation 1-1 with d=2 and Stokes' law, under the assumption of a solid spherical particle:

$$D^s = \frac{k\,T}{3\,\pi\,\eta\,d_H} \tag{1-2}$$

where k is Boltzmann constant, T is the temperature, η is the viscosity of solution and d_H is the hydrodynamic diameter of the solute. This equation is often used to estimate the radii of

particles when the self-diffusion coefficient of the particles and the viscosity of the solution are known.

1.2.2 Mutual diffusion

In contrast, *mutual* diffusion refers to the relaxation of fluctuations or gradients. The movement of particles between two points in the system occurs in order to attain the equilibrium of chemical potential between two points[36]. Accordingly, when a substance moves at constant temperature and pressure, the work that is performed can be described with respect to the opposing force, which is considered a thermodynamic force:

$$F = -\left(\frac{\partial \mu_{\mathrm{i}}}{\partial x}\right)_{\mathrm{T,P}} \tag{1-3}$$

where μ_{i} is the chemical potential change in the x direction. The flux of material, J, is proportional to this force and can be described by:

$$J = -D^{\mathrm{m}} \frac{c}{RT}\left(\frac{\partial \mu_{\mathrm{i}}}{\partial x}\right) \tag{1-4}$$

where D^{m} is the mutual diffusion coefficient, R is the universal gas constant and c is the concentration. Flux is a time independent parameter in this equation. The chemical potential of compound i, μ_{i}, is dependent upon the temperature, T, pressure, P, compound activity, a_{i}, and long range electrostatic interactions[37]:

$$\mu_{\mathrm{i}} = \mu_{\mathrm{i}}^{0} + V_{\mathrm{i}}(\mathrm{p} - \mathrm{p}^{0}) + RT \ln a_{\mathrm{i}} - S_{\mathrm{i}}(T - T^{0}) + \mu_{\mathrm{i,el}} \tag{1-5}$$

where $\mu_{\mathrm{i,el}}$ accounts for the electrostatic interactions and S_{i} for entropy of component i. When changes in pressure and temperature are negligible, Equation 1-5 becomes:

$$\mu_{\mathrm{i}} = \mu_{\mathrm{i}}^{0} + RT \ln a_{\mathrm{i}} + \mu_{\mathrm{i,el}} \tag{1-6}$$

In dilute solutions, the activity can be replaced by the concentration. Combination of equations 1-4 and 1-6 gives:

$$J = -D^{\mathrm{m}} \frac{c}{RT}\left(\frac{RT}{c} \frac{\partial c}{\partial x} + \frac{\partial \mu_{\mathrm{el}}}{\partial x} \right) \tag{1-7}$$

which is Fick's first law. In Equation 1-7, there are contributions from a concentration gradient and electrostatic charges. If no charges are present, then $\partial \mu_{el} / \partial x$ approaches zero and the equation can be simplified to:

$$J = -D^{\mathrm{m}} \frac{\partial c}{\partial x} \tag{1-8}$$

In a binary system composed of one type of gel in bulk solution such as the gel-water systems that are studied later in this thesis, the concentration of solute in the gel (c_{i}) can be related to that in water (c_{aq}) by an overall partition coefficient, Φ_{i} [38]:

$$c_{\mathrm{i}} = c_{\mathrm{aq}} \Phi_{\mathrm{i}} \tag{1-9}$$

where i indicates the gel phase (i=1 for one gel in water). Equation 1-9 can be applied to multi-phase systems. For example, for a multi-phase system, consisting of many pieces of different types of gels (each gel considered as a single phase) in one bulk solution, the total concentration of solute in the bulk water will be distributed among the different gel components. Equation 1-9 can be extended to the multi-phase system using Equation 1-10:

$$c_{\mathrm{i,total}} = c_{\mathrm{aq}} \sum_{i=1}^{N} \Phi_{\mathrm{i}} \tag{1-10}$$

where $c_{\mathrm{i,\ total}}$ represents the total concentration of the solute which can only be found in gel phases. As mentioned above, for a binary system (one hydrogel in water), $\sum_{i=1}^{N} \Phi_i$ is equal to the overall partition coefficient of the solute in the hydrogel, i.e., Φ, and it is equal to 1 in the case of no interaction of the solute with the gel. The partition coefficient results from steric (θ), electrostatic (Π) and chemical (α) interactions such that[39]:

$$\Phi = \theta \, \Pi \, \alpha \tag{1-11}$$

where θ, α, and Π are the partition coefficients for purely steric, chemical, and electrostatic interactions, respectively.

A lowering of the ionic strength in the bulk solution can lead to an electrostatic effect (Donnan effect) and deviations from the expected response based upon Equation 1-11. The Donnan effect is due to an electric potential difference of hydrogel with respect to the bulk medium. When the Donnan potential of the gel is significant, especially at lower ionic strengths, the effective diffusion coefficient, D_e, for a one gel component in water should be used by taking into account partitioning [39]:

$$D^m = \frac{D_e}{\Phi_:} \tag{1-12}$$

1.3. Diffusion in hydrogels

Hydrogels are used in a large number of pharmaceutical, biological and environmental applications[40-42]. The diffusion of solutes into, through and out of gels is often a key to understanding their function. Among key points, it is important to understand how the hindered diffusion of solutes inside the gels is governed by specific and nonspecific interactions.

The rate of steady-state diffusion of solute through a hydrogel depends upon physical (e.g. obstruction[43]) and chemical (e.g. hydrogen bonding, electrostatic effects[39]) interactions between the diffusing solutes and the (primarily) carbohydrate matrix of the hydrogel. It will depend upon the physicochemical properties of both the hydrogel and the diffusing molecules, including solute size[44] and charge[45]. Among the additional ***solute*** parameters affecting diffusion, it is also necessary to take into account the shape of the solute, its hydrophilic and hydrophobic character, and the hydration of the solute molecules. Moreover, since the charge of the solute is important, the ionic strength and the pH of the bulk solution can also have an important impact on diffusion. With respect to the ***hydrogel***, its water content (so called volume fraction) and the extent of gel crosslinking[46] are the primary factors which control the diffusion and partitioning of solutes. The pore size and the pore size distribution determine the 'tortuosity' of the solute displacement in the gel. In addition, hydrodynamic drag –the proximity of solute to the polymer-solvent interface– has an impact on the mobility of the solutes[47]. Note that for a charged gel, the

"effective proximity" can be modified by the ionic strength of the bulk solution, which affects the thickness of the Debye layer. The latter effect may result in a Donnan exclusion effect, which is especially important at lower ionic strengths. As above, the pH may additionally affect the diffusion by modulating interactions between the solutes and the hydrogel[40, 41].

Based upon the above discussion, it is not surprising that mass transport in the hydrogels is influenced by both the pH and ionic strength. For example, it was previously reported that the diffusion of small ions, proteins, and surfactants[48, 49] was affected by the ionic strength and pH of the bulk solution[50]. Furthermore, for highly charged gels such as alginate and polyacrylamide, the Donnan potential difference has been shown to result in a significant partitioning of charged solutes. Nonetheless, the role of the Donnan effect on the diffusion of charged solutes still requires further investigation.

1.4. Donnan potential of a charged hydrogel

A hydrogel such as agarose or alginate can be considered as a membrane with a porous *homogeneous* matrix. Assuming a uniform distribution of the fixed charges throughout the polymer structure, an electrical potential difference[51] is established when the membrane is in equilibrium with a bulk solution. In general, there are two different approaches to model the Donnan effect. The first approach[52] considers the electrical difference as a surface potential (Fig. 1.2a). In this model, all the charges are considered to be located at the membrane surface and unable to penetrate into the membrane. This model can be expressed as:

$$\psi_{\mathrm{S}} = \frac{RT}{z\mathrm{F}} \arcsin\left[\frac{\sigma}{\left(8c\varepsilon_{\mathrm{r}}\varepsilon_0 RT\right)^{1/2}}\right] \tag{1-13}$$

where ψ_s is the surface potential, σ is the surface charge density of the hydrogel, ε_r the relative permittivity of the solution, ε_0 the permittivity of a vacuum, z represents the charge valence of the electrolytes, F is the Faraday constant and c is the concentration of bulk electrolyte.

In the second approach[53], the electrical difference is modeled as the Donnan equilibrium potential. This model is mostly used to study mass transport through hydrogels (Fig. 1.2b) and can be expressed as:

$$\psi_{\mathrm{D}} = \frac{RT}{z\mathrm{F}} \arcsin\left(\frac{z_{\mathrm{g}}\rho}{2zc}\right) \tag{1-14}$$

where z represents the charge valence of the electrolytes, z_{g} is the charge valence of the functional groups in the gel, ρ is the charge density of the gel and c is the bulk electrolyte concentration in the medium. The Donnan potential of the hydrogel can be predicted according to Equation 1-14[54]. The concentration of the charged functional groups of a hydrogel can be measured using an acid-base titration of a piece of hydrogel. The charge density (ρ ; C/kg) of the hydrogel can be obtained according to Equation 1-15:

$$\frac{|\rho|}{\mathrm{F}} = Q \tag{1-15}$$

where Q is the concentration of the charged functional groups in the hydrogel[54].

Equation 1-14 was later modified based on the assumption of Mauro[55], in which a Poisson-Boltzmann distribution was applied, leading to a continuous Donnan potential extending over a distance on the order of $1/\kappa$ (κ is the Debye-Hückel parameter) on both sides of the sharp interface (Fig. 1.2c). In fact, at the interface between the gel and bulk solution, both the gel segment density and the fixed charge density drop sharply to zero.[56]

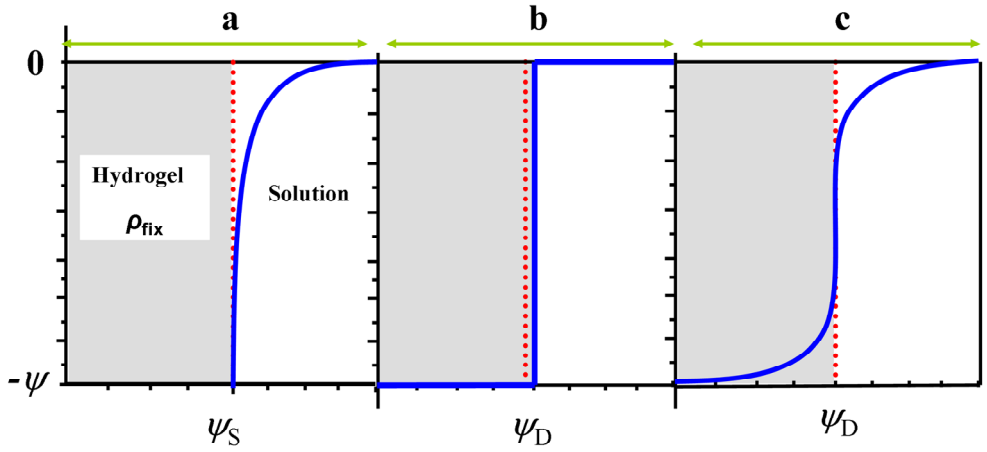

Figure 1.2. Schematic representation of the potential distribution (blue solid line) near the membrane surface (red dotted line) using (a) a surface potential (ψ_S), (b) a discontinuous Donnan potential (ψ_D), (c) a continuous Donnan potential (ψ_D).

The Donnan partition coefficient can be estimated according to Equation 1-16 as follows[57,58]:

$$\Pi = e^{\frac{-2F\psi_D}{RT}} \tag{1-16}$$

where the Donnan partition coefficient, Π, represents the enhancement of metal ions in the gel that are due to electrostatic effects. The Donnan partition coefficient can be compared to the overall partition coefficient that is obtained by dividing the measured metal concentration that is extracted from an equilibrated hydrogel using nitric acid, $[M^{2+}]_g$, with that measured in the bulk solution, $[M^{2+}]_w$. Extracted concentrations can be measured by atomic absorption spectroscopy or inductively coupled plasma mass spectrometry.

1.5. Diffusion models in hydrogels

Mass transport retardation in a gel, due to the blocking of the diffusion path by the gel polymer chains, can be evaluated by a retardation factor:

$$\varsigma = \frac{D_g}{D_w} \tag{1-17}$$

A number of models have been developed in order to predict the retardation factor. These models are based upon the solute properties (e.g. hydrodynamic radius), the gel network structure (gel concentration and mesh size[59, 60]) and solvent properties (e.g. free volume[61]). The hindered diffusion of solutes has been well documented for agarose[59, 62] and alginate[43] gels.

Obstruction models consider the gel chains as rigid obstacles that allow the passage of the diffusing solutes through the openings among the chains. In fact, when the solutes pass through a matrix, they are forced to move around these chains. As a result, the diffusion path tends to be longer than that in free solution, leading to the hindered mobility of solutes. Some models based on the obstruction theory are Maxwell–Fricke's[63], Mackie and Meares's[64], Ogston's[65] and the Hard Sphere Theory[66] model. It has been shown that the deviation of theoretical diffusion values from the experimental ones increases as the concentration of the polymer increases[43] or when as the solute size[67] becomes larger (in which case, hydrodynamic effects are non-negligible).

Hydrodynamic models are based on the Stokes-Einstein relation (Eq. 1-2). In this case, solutes are considered as spheres that diffuse at a constant velocity in the bulk solution. These models consider a frictional drag close to the polymer chains, which slows down the diffusion of the solutes. Hence, the expression of the magnitude of this effect is the core of the hydrodynamic models. Different models have been developed including Cukier's[68], Altenberger's[69] and Phillies's[70] models in addition to the reptation scaling[71] model. Although most of these models can fit experimental data for small size solutes or in dilute solutions, fits often deviated from the theoretical predictions for larger solutes in more concentrated polymer solutions. In addition, the different assumptions used in the models appeared to affect the model fits.

Free volume theory models are based on the random movements of solvent molecules through void volumes or 'free volumes'. Solutes are modeled as jumping from void to void. The polymer chains of the hydrogel contribute to the availability of these voids. Accordingly, as the polymer concentration is increased, the concentration of these

voids decreases, leading to more diffusion retardation as compared with that seen in weakly concentrated gel-solvent systems. Also, the mesh size of the polymer network can be determinant in relation to the size of the solutes as solutes can diffuse when their sizes are smaller than the sieves of the polymer network. Fujita's[72], and Peppas and Reinhart's [73] models have been developed, based on the free volume theory.

1.6. Diffusion in biofilms

In planktonic cultures, the bulk flow of a fluid (convection) rather than the random molecular motion (diffusion) is responsible for the transport of the solutes (except in the immediate vicinity of the cells). In microbial biofilms, diffusion becomes the main mechanism for transport of solutes because biofilms and the substratum to which it is anchored, reduce the fluid flow. This reduction in fluid flow occurs through the locally high cell densities and the presence of EPS in the biofilm. Diffusion is also the predominant transport process within cell aggregates[74, 75] and biofilm clusters[30], at least for small solutes[76]. Nonetheless, convection can also be involved in the diffusion process in the voids and water channels of the biofilm[77, 78]. Solutes in a biofilm are involved in two main events: (i) diffusion into the biofilm; (ii) interaction with the organisms in the biofilm. Generally, nutrient or pollutant species must diffuse through the gel matrix in order to reach the biofilm embedded bacteria, which are often found deep inside the biofilm. Solute transport is hindered[79,80] by the presence of bacterial cells, EPS and inorganic materials, which act as obstacles to diffusion (i.e. greater tortuosity), generally leading to the observation of a smaller diffusion coefficient in the biofilm with respect to that in water[38]. For example, as compared to planktonic cells, the higher resistance of biofilms to heavy metals has been thought to be due to the presence of EPS[81]. The reduction of the diffusive flux in the biofilm has, in general, been attributed to an exclusion effect due to steric interactions with the EPS[82] or to the interaction of solutes with the EPS (binding[83] or electrostatic effect[84]).

A concentration gradient of metabolic substrates and microbial species have been shown to occur during the biofilm formation process[85, 86]. For example, gradients have been observed for oxygen, nitrite and pH[87] using microelectrodes[88]. Furthermore, the mobility of

solutes (nutrients, oxygen and biocides) have been shown to be significantly hindered by the bacterial clusters, even though these elements diffuse easily in the voids of the biofilms[75]. Heterogeneous nutrient gradients can lead to the heterogeneous growth of microorganisms into biofilms[89] resulting in local microniches[90]. These local microniches render the biofilm even more complex with diverse coexisting environments. Indeed, the changing microbial community is an adaptive response resulting in a continual reorganization of the EPS matrix[91, 92].

In general, the value of the diffusion coefficient in the biofilm will be reduced compared to that in water, due to the presence of microbial cells, extracellular polymers and other materials including the abiotic particles or gas bubbles that are trapped in the biofilm. Generally speaking, diffusion coefficients in the biofilm voids are close to those in the water. Nonetheless, given the presence of soluble EPS in the biofilm voids, increased viscosity may be responsible for a slightly decreased solute mobility[93]. It would appear that the determining factor for both microbial behaviour (cell-matrix ratio, biofilm thickness) and solute diffusion is more due to the architecture of the biofilm than to its physiological properties. Indeed, it has been shown that the limitations to diffusion in biofilms are primarily caused by the EPS of the biofilm matrix[18]. Limitations in mass transport are mainly dependent on the biofilm structure (density and porosity of the EPS) rather than, for example, biofilm thickness [94].

Moreover, the compositions of EPS vary in different biofilms, and the free diffusion of solutes is highly dependent upon the biofilm composition. For example, it has been shown that the diffusion of anionic beads larger than 55 nm was hindered in the EPS of *S. maltophilia*, however in the biofilm of *L. lactis*, 14 nm anionic beads were slowed[18]. In addition, different shapes of the fluorescence correlation spectroscopy (FCS) correlation curves in various zones of EPS confirmed the impact of EPS heterogeneity on diffusion[84]. The compactness of the EPS also increased the diffusion time of the particles, indicating an EPS density effect on the mobility of particles[18]. Furthermore, the difference in the diffusion of several FITC-dextrans in two different biofilms of *S. maltophilia* and *L. lactis* was consistent with the dissimilarity in the spatial architecture of these biofilms. Indeed, the *S. maltophilia* biofilm had a mushroom-like structure while *L. lactis* biofilm appeared to be

composed of an assembly of cells embedded in a highly hydrated uniform matrix[95]. Finally, it recently has been shown that the cell wall properties of genetically engineered hydrophilic and hydrophobic cells of *L. lactis* had an impact on the diffusion of nanoparticles in biofilms[96].

The first mechanism by which the EPS have an impact on the mobility of solutes is via the obstruction effect. Obstruction occurs either by blocking the diffusion path, rendering a longer diffusion path or by the exclusion of solute by the biomass of the biofilm, resulting in a slower diffusion. When using more compact biofilms (larger volume fraction of the biofilm) smaller values were determined for the diffusion coefficients, indicating the role of EPS in hindering the movement of probes in the biofilm[38]. The impact of the biofilm density on diffusion has been shown for glucose, acetate, phenol, sucrose and lactate. In these cases, the value of D_g/D_w was reduced as a function of the volume fraction of biofilm[38]. For fluorescence probes, both the absence of signal and/or quenching of the signal have been observed in biofilm, indicating the impact of EPS on diffusion, due either to exclusion effects or specific interactions[97] with the diffusing solutes[18]. Also, for anionic and cationic beads of various sizes, distortions of FCS correlations in local zones of the EPS indicated the significant impact of particle size on diffusion in the EPS[18]. A similar effect has been shown for dextrans. In most cases, diffusion values in EPS were smaller than those in water[80, 98]. Also, when the diffusion of dextrans with a vast range of molar masses were measured by CLSM in the same biofilm, D_g/D_w decreased systematically as a function of the increasing sizes of the dextrans[99]. Nonetheless, the difference in diffusion coefficients that were observed for dextran probes with similar sizes strongly suggested that other factors, such as solute charge, were involved in transport of solutes.

Diffusive transport can be hindered by both steric effects and electrostatic interactions with the charged components of the biofilm. As is the case for hydrogels, the polymer matrix of the biofilm consists of variably charged local zones that depend upon the local pH and ionic strength. These local zones can have significant impact on the incoming solutes. For example, a substantial reduction in the relative diffusion coefficients (D_g/D_w) of the charged ions: NH_4^{+}[1100], Li^{+}[1101], HCO_3^{-} and NO_3^{-}[1102] with respect to non-charged solutes in a biofilm was attributed to the electrostatic effect. In addition, a reduction in the

diffusion of cationic antibiotics[103-108], quaternary ammonium compounds[82, 83], cationic amine-modified latex beads[18], Zn^{2+} [81] and silver nanoparticles[109] has been attributed to electrostatic interactions within (negatively charged) biofilms. In addition, the slow diffusion of ceylpyridinium chloride (CPC) into the *Streptococcus mutans* biofilm appears to be due to charge interactions between ammonium groups of CPC and EPS of the biofilm[82]. Furthermore, the reduced value of D_g/D_w (0.4) for fluorescein as compared to that of larger molecules (0.56-0.90) was thought to be due to the electrostatic sorption of the probes to the EPS [98]. Large negative Donnan potentials may lead to increased electrostatic interactions of the biofilm with charged solutes[110], resulting in higher concentrations of cations in the biofilm as compared to the bulk medium. Numerous functional groups in the biofilm will show a pH dependency over environmentally relevant pH. Conversely, no impact of charge on the diffusion of small charged ions was reported by Siegrist et al.[111]. In that case, convective mass transport, i.e., the turbulent fluid motions in the upper layers of a flow cell, were thought to predominate.

The diffusion coefficient also depends on the temperature (T) and viscosity (η)[112]. Indeed, local variations in the temperature and viscosity can lead to large variations in the diffusion coefficients in various zones of the EPS. These factors and their impact on diffusion have been poorly investigated for biofilms.

Due to the above competing physical, chemical and electrostatic effects in a biofilm, it is no wonder that there are numerous contradictory reports of increased or decreased diffusive fluxes for ions of different charges and biofilms of different natures. Clearly, there is little consensus on the values of diffusion coefficients in biofilms[38].

1.7. Techniques for measuring biofilm structure

In order to relate biofilm structure to function, it is necessary to characterize the biofilms. Biofilm development and structure have been analysed using fluorescence microscopy, differential interference contrast (DIC), transmission electron microscopy (TEM), scanning electron microscopy (SEM), atomic force microscopy (AFM) and

confocal laser scanning microscopy (CLSM). Useful information about the surfaces, morphology and arrangement of biofilms have been obtained by transmission electron microscopy (TEM) and scanning electron microscopy (SEM)[22]. However, the samples need to be dehydrated in order to use these techniques; the risk of the structural misconception arises for the biofilms. In contrast, CLSM can provide researchers with *in situ* analysis. CLSM gives insights into the structure of biofilm, including cell clusters separated by channels[75]. Confocal microscopy has also been used in order to measure the diffusion in biofilm based on the imaging of fluorescence markers[99]. On the other hand, the disadvantage of CLSM is that it requires fluorescence markers in order to stain and visualize the biofilm. In addition, techniques such as particle image velocimetry coupled with CSLM have been used to characterize the biofilm structure, however this technique is only applicable for large size particles (~100 nm)[75]. The use of specific microelectrodes or *ex situ* analysis following extraction of polymers has also been reported[92, 113]. These approaches are invasive and have poor resolution, which renders difficult dynamic observations of biofilms over time.

1.8. Techniques for diffusion measurements

1.8.1 Measuring self-diffusion coefficients

Various techniques such as pulsed-field gradient spin-echo nuclear magnetic resonance (PFG-SE-NMR), fluorescence recovery after photobleaching (FRAP) and fluorescence correlation spectroscopy (FCS), have been used to measure self-diffusion coefficients.

NMR– The technique of PFG-SE-NMR[114, 115] has been used as an effective technique to measure diffusion in gels and biofilms. The basic principle of the PFG-SE-NMR technique is the fact that the Larmor frequency of a nucleus is proportional to the local magnetic field[116]. Two magnetically equivalent nuclei resonate at a different Larmor frequency if the nuclei are located at different positions along the magnetic field gradient. This technique can measure self-diffusion coefficients for all NMR-detectable solutes[116].

For biological systems such as biofilms, proton NMR[114] is very applicable. However, the water which dominates most biofilms (~ 98%) is mainly measured in the diffusion measurements. The technique is fast, non-destructive, and capable of multicomponent measurements using very small volumes. Furthermore, information about the structure of matrix can be obtained[115, 117].

FRAP- An intense but brief laser light is pointed at a spot inside the sample containing the fluorescent probe[118]. The recovery of fluorescence in the bleached zone is monitored as a function of time. Diffusion coefficients can be obtained from a two dimensional model describing the recovery profile. FRAP has widely been used in biological systems such as biofilms[95, 119] as it is considered a high resolution technique which can provide information about the local structure as well. FRAP is not practical in applications in which very low concentrations (nM) of probe is used. Information about molecules in the diffusion spot is limited given that FRAP measures the Brownian motions of molecules that diffuse from outside the diffusion region[29, 95, 120-123].

FCS- This technique has been used in this thesis and its theory is explained in detail in Chapter 2 (section 2.2).

1.8.2 Measuring mutual diffusion coefficients

Uptake and release from gel beads or slices- In this technique, solutes are first entrapped in small gel pieces that are placed in a solution that initially contains no solute. Small aliquots of solution are periodically sampled in order to monitor solute concentrations and concentration data, are interpreted with appropriate models in order to obtain the diffusion coefficients[124].

Concentration gradient profile techniques- In this technique, concentration gradients in the matrix are monitored. This monitoring is obtained with (1) destructive methods in which the gel is sliced and the concentration of solute is determined or (2) non-destructive methods in which the concentration profile is scanned over as a function of distance using NMR imaging[125], fluorescence[126], UV-VIS[127], Raman[128] or IR techniques.

Concentrations in the matrix are measured and plotted versus time or distance and the appropriate model is used to determine the diffusion coefficients[124].

Microelectrode Voltammetry- This technique has been explained in detail in Chapter 2 (section 2.3). It can be used to measure diffusion in hydrogels and biofilms. It only determines diffusion of the electrosensitive molecules indirectly. It has mainly been used for measuring diffusion in gels.

Diaphragm cell- This technique has been used in this thesis and is explained in Chapter 2 (section 2.4).

Fluorescence correlation spectroscopy[129] (FCS) constitutes a powerful tool for the study of molecular dynamics. In this technique, a small number of molecules in a micro-volume (confocal volume) are excited and the emitted signal is analyzed. FCS is a non-invasive technique which is appropriate to study the biological media[130-132]. The small concentration of probes and the vast range of probes are the other advantages of this technique. The important events that should be considered in FCS measurements are the photodamage and photobleaching phenomena. These factors can be minimised by modifying the laser intensity and by using a two photon excitation system instead of classical confocal detection[133].

In recent years, optical microscopy allowed for the *in situ* observation of EPS. For example, one can track the mobility of the free molecules over time with time lapse imaging. However, this technique measures the average diffusion coefficients over the macrostructure distance and thus molecular diffusion is hard to evaluate[134]. Furthermore, fluorescence recovery after photobleaching (FRAP) has been developed in order to study mass transport phenomenon in biofilm matrix[29, 95, 98, 99]. This technique is limited to very low concentrations of fluorescence probe.

1.8.3 Mutual versus self diffusion coefficients

A major difference between mutual and self-diffusion measurements is related to the different time and length scales for each technique. The time and length scales are generally shorter for self-diffusion than mutual diffusion coefficient measurements. For example, for FRAP and FCS, the diffusion spot volume is on the order of femtoliters and the diffusion time occurs on the scale of ms-s. For NMR, this time is even shorter. In contrast, for mutual diffusion techniques, the times and distances are longer, e.g., hours and millimetres (uptake and release technique) or days and centimetres (concentration gradient technique, Raman spectroscopy[135]).

1.9. Objectives

The overall objective of this dissertation was to better understand the effects of both particle and matrix charge on the diffusion of solutes and nanoparticles in a biofilm. Given the complexity of biofilms, two polysaccharide hydrogels, agarose and alginate, were first used as the simple models of the biofilm matrix in order to better relate structure to function (i.e. diffusion) in a biofilm. Both the self and mutual diffusion were examined in the hydrogels in order to better understand the contributions of electrostatic, obstruction, hydrodynamic or specific (binding) effects on the diffusion mechanism. Results observed for model gels were used to explain some of the behaviour observed for solute diffusion in the more complex biofilms.

In Chapter 3, the weakly charged agarose hydrogel was studied. Both self and mutual diffusion were characterized (using diffusion cells and fluorescence correlation spectroscopy). Microelectrode voltammetry was used to quantify the Donnan effect. In Chapter 4, self-diffusion coefficients were measured in a highly charged, calcium alginate hydrogel, which was very representative of biofilm EPS. Self-diffusion was measured under several conditions of ionic strength, pH and medium composition using FCS. In addition, the roles of cations on the structure of the hydrogel were carefully quantified. Finally, in Chapter 5, a *P. fluorescens* biofilm was produced and self-diffusion coefficients

were measured for a number of physicochemical conditions including solute charges and sizes.

1.10. References

1.Beikler, T.; Flemmig, T. F. Oral biofilm-associated diseases: trends and implications for quality of life, systemic health and expenditures. *Periodontology 2000* **2011,** 55, 87-103.

2.Li, X. Z.; Hauer, B.; Rosche, B. Single-species microbial biofilm screening for industrial applications. *Applied microbiology and biotechnology* **2007,** 76, 1255-1262.

3.Lebert, I.; Leroy, S.; Talon, R. Effect of industrial and natural biocides on spoilage, pathogenic and technological strains grown in biofilm. *Food microbiology* **2007,** 24, 281-287.

4.Suzuki, T.; Yamazaki, Y. The biofilm formation in infectious diseases. *Rinsho Biseibutshu Jinsoku Shindan Kenkyukai Shi* **2005,** 16, 165-167.

5.Hamal, P.; Ostransky, J.; Dendis, M.; Horvath, R.; Ruzicka, F.; Buchta, V.; Vejsova, M.; Sauer, P.; Hejnar, P.; Raclavsky, V. A case of endocarditis caused by the yeast *Pichia fabianii* with biofilm production and developed in vitro resistance to azoles in the course of antifungal treatment. *Medical mycology* **2008,** 46, 601-605.

6.Costerton, J. W. Anaerobic biofilm infections in *cystic fibrosis*. *Molecular cell* **2002,** 10, 699-700.

7.Steinberg, D.; Blank, O.; Rotstein, I. Influence of dental biofilm on release of mercury from amalgam exposed to carbamide peroxide. *Journal of biomedical materials research. Part B, Applied biomaterials* **2003,** 67, 627-631.

8.Seneviratne, C. J.; Zhang, C. F.; Samaranayake, L. P. Dental plaque biofilm in oral health and disease. *Chinese Journal of Dental Research* **2011,** 14, 87-94.

9.Latorre, A. A.; Van Kessel, J. S.; Karns, J. S.; Zurakowski, M. J.; Pradhan, A. K.; Boor, K. J.; Jayarao, B. M.; Houser, B. A.; Daugherty, C. S.; Schukken, Y. H. Biofilm in milking equipment on a dairy farm as a potential source of bulk tank milk contamination with *Listeria monocytogenes*. *Journal of dairy science* **2010,** 93, 2792-2802.

10.Juhler, S.; Revsbech, N. P.; Schramm, A.; Herrmann, M.; Ottosen, L. D.; Nielsen, L. P. Distribution and rate of microbial processes in an ammonia-loaded air filter biofilm. *Applied and environmental microbiology* **2009,** 75, 3705-3713.

11.Canstein, H. F.; Li, Y.; Felske, A.; Wagner-Dobler, I. Long-term stability of mercury-reducing microbial biofilm communities analyzed by 16S-23S rDNA interspacer region polymorphism. *Microbial ecology* **2001,** 42, 624-634.

12.Stoodley, P.; Debeer, D.; Longwell, M.; Nistico, L.; Hall-Stoodley, L.; Wenig, B.; Krespi, Y. P. Tonsillolith: not just a stone but a living biofilm. *Otolaryngology--head and neck surgery* **2009,** 141, 316-321.

13.Patil, J. S.; Anil, A. C. Biofilm diatom community structure: influence of temporal and substratum variability. *Biofouling* **2005,** 21, 189-206.

14.Flemming, H. C.; Wingender, J. Relevance of microbial extracellular polymeric substances (EPSs) - Part I: Structural and ecological aspects. *Water Science and Technology* **2001,** 43, 1-8.

15.Flemming, H. C.; Neu, T. R.; Wozniak, D. J. The EPS matrix: the "house of biofilm cells". *Journal of Bacteriology* **2007,** 189, 7945-7947.

16.Caldwell, D. E.; Korber, D. R.; Lawrence, J. R. Imaging of bacterial-cells by fluorescence exclusion using scanning confocal laser microscopy *Journal of Microbiological Methods* **1992,** 15, 249-261.

17.Wagner, M.; Ivleva, N. P.; Haisch, C.; Niessner, R.; Horn, H. Combined use of confocal laser scanning microscopy (CLSM) and Raman microscopy (RM): investigations on EPS-matrix. *Water Research* **2009,** 43, 63-76.

18.Guiot, E.; Georges, P.; Brun, A.; Fontaine-Aupart, M. P.; Bellon-Fontaine, M. N.; Briandet, R. Heterogeneity of diffusion inside microbial biofilms determined by fluorescence correlation spectroscopy under two-photon excitation. *Photochemistry and Photobiology* **2002,** 75, 570-578.

19.Stewart, P. S.; Franklin, M. J. Physiological heterogeneity in biofilms. *Nature Reviews Microbiology* **2008,** 6, 199-210.

20.O'Toole, G. A. To build a biofilm. *Journal of Bacteriology* **2003,** 185, 2687-2689.

21.Monds, R. D.; O'Toole, G. A. The developmental model of microbial biofilms: ten years of a paradigm up for review. *Trends in Microbiology* **2009,** 17, 73-87.

22.Wimpenny, J.; Manz, W.; Szewzyk, U. Heterogeneity in biofilms. *Fems Microbiology Reviews* **2000,** 24, 661-671.

23.Donlan, R. M.; Costerton, J. W. Biofilms: Survival mechanisms of clinically relevant microorganisms. *Clinical Microbiology Reviews* **2002,** 15, 167.

24.Golmohamadi, M.; Davis, T. A.; Wilkinson, K. J. Diffusion and partitioning of cations in an agarose hydrogel. *The Journal of Physical Chemistry A* **2012,** 116, 6505-6510.

25.Mah, T.-F. C.; O'Toole, G. A. Mechanisms of biofilm resistance to antimicrobial agents. *Trends in Microbiology* **2001,** 9, 34-39.

26.Gilbert, P.; Allison, D. G.; McBain, A. J. Biofilms in vitro and in vivo: do singular mechanisms imply cross-resistance? *Journal of Applied Microbiology* **2002,** 92, 98s-110s.

27.Stewart, P. S.; Costerton, J. W. Antibiotic resistance of bacteria in biofilms. *Lancet* **2001,** 358, 135-138.

28.Stewart, P. S. Mechanisms of antibiotic resistance in bacterial biofilms. *International Journal of Medical Microbiology* **2002,** 292, 107-113.

29.Bryers, J. D.; Drummond, F. Local macromolecule diffusion coefficients in structurally non-uniform bacterial biofilms using fluorescence recovery after photobleaching (FRAP). *Biotechnology and Bioengineering* **1998,** 60, 462-473.

30.deBeer, D.; Stoodley, P. Relation between the structure of an aerobic biofilm and transport phenomena. *Water Science and Technology* **1995,** 32, 11-18.

31.Chen, X.; Stewart, P. S. Chlorine penetration into artificial biofilm is limited by a reaction-diffusion interaction. *Environmental Science & Technology* **1996,** 30, 2078-2083.

32.Sangi, M. R.; Halstead, M. J.; Hunter, K. A. Use of the diffusion gradient thin film method to measure trace metals in fresh waters at low ionic strength. *Analytica Chimica Acta* **2002,** 456, 241-251.

33.Albright, J. G.; Mills, R. A study of diffusion in the ternary system, labeled urea-urea-water, at 25° by measurements of the Intradiffusion coefficients of urea. *The Journal of Physical Chemistry* **1965,** 69, 3120-3126.

34.Holte, O.; Tonnesen, H. H.; Karlsen, J. Effect of charge and size of diffusing probe on the diffusion through calcium alginate gel matrices. *Pharmazie* **2007,** 62, 914-918.

35.Einstein, A. On the motion of small particles suspended in liquids at rest required by the molecular-kinetic theory of heat. *Annalen der Physik (Leipzig)* **1905,** 17, 549-560.

36.Lobo, V. M. M. *Mutual and self-diffusion coefficients: a common confusion*, Department of Chemistry – University of Coimbra, 3049 Coimbra – Portugal (Personal Communication). **2012**.

37.Wesselingh, J. A., *Mass transfer in multicomponent mixtures*. Delf University Press: Delf, 2000.

38.Stewart, P. S. A review of experimental measurements of effective diffusive permeabilities and effective diffusion coefficients in biofilms. *Biotechnology and Bioengineering* **1998,** 59, 261-272.

39.Fatin-Rouge, N.; Milon, A.; Buffle, J.; Goulet, R. R.; Tessier, A. Diffusion and partitioning of solutes in agarose hydrogels: the relative influence of electrostatic and specific interactions. *Journal of Physical Chemistry B* **2003,** 107, 12126-12137.

40.Hamidi, M.; Azadi, A.; Rafiei, P. Hydrogel nanoparticles in drug delivery. *Advanced Drug Delivery Reviews* **2008,** 60, 1638-1649.

41.Degryse, F.; Smolders, E.; Zhang, H.; Davison, W. Predicting availability of mineral elements to plants with the DGT technique: a review of experimental data and interpretation by modelling. *Environmental Chemistry* **2009,** 6, 198-218.

42.Town, R. M.; Yezek, L. P.; van Leeuwen, H. P. Stripping chronopotentiometry at scanned deposition potential (SSCP). Part 8. Metal speciation analysis in gels. *Journal of Electroanalytical Chemistry* **2006,** 589, 203-211.

43.Amsden, B. Solute diffusion in hydrogels. An examination of the retardation effect. *Polymer Gels and Networks* **1998,** 6, 13-43.

44.Petit, J. M.; Zhu, X. X.; Macdonald, P. M. Solute probe diffusion in aqueous solutions of poly(vinyl alcohol) as studied by pulsed-gradient spin-echo NMR spectroscopy. *Macromolecules* **1996,** 29, 70-76.

45.Johansson, L.; Skantze, U.; Lofroth, J. E. Diffusion and interaction in gels and solutions .6. Charged systems. *Journal of Physical Chemistry* **1993,** 97, 9817-9824.

46.Amsden, B. Solute diffusion within hydrogels. Mechanisms and models. *Macromolecules* **1998,** 31, 8382-8395.

47.Cukier, R. I. Diffusion of Brownian spheres in semidiluted polymer-solutions *Macromolecules* **1984,** 17, 252-255.

48.Narita, T.; Gong, J. P.; Osada, Y. Kinetic study of surfactant binding into polymer gel. Experimental and theoretical analyses. *Journal of Physical Chemistry B* **1998,** 102, 4566-4572.

49.Narita, T.; Gong, J.; Osada, Y. Enhanced velocity of surfactant binding after the volume collapse of an oppositely charged gel. *Macromolecular Rapid Communications* **1997,** 18, 853-857.

50.Kalis, E. J. J.; Davis T. A.; Town, R. M.; van Leeuwen, H. P. Impact of pH on Cd(II) partitioning between alginate gel and aqueous media. *Environmental Chemistry* **2009,** 6, 305–310.

51.Ohshima, H.; Ohki, S. Donnan potential and surface-potential of a charged membrane. *Biophysical Journal* **1985,** 47, 673-678.

52.Verwey, E. J. W. Theory of the stability of lyophobic colloids. *Journal of Physical and Colloid Chemistry* **1947,** 51, 631-636.

53.Teorell, T. Transport processes and electrical phenomena in ionic membranes. *Progress in Biophysics and Biophysical Chemistry* **1953,** 3, 305-369.

54.Ohshima, H.; Kondo, T. Relationship among the surface potential, Donnan potential and charge density of ionpenetrable membranes. *Biophysical Chemistry* **1990,** 38, 117–122.

55.Mauro, A. Space charge regions in fixed charge membranes and associated property of capacitance. *Biophysical Journal* **1962,** 2, 179-&.

56.Ohshima, H.; Kondo, T. Membrane-potential and Donnan potential. *Biophysical Chemistry* **1988,** 29, 277-281.

57.Van Leeuwen, H. P.; Davis, T. A.; Yezek, L. P.; Pinheiro, J. P. Measurement of Donnan potentials in gels by in situ microelectrode voltammetry. *Journal of Electroanalytical Chemistry* **2005,** 584, 100-109.

58.Davis, T. A.; Kalis, E. J.; Pinheiro, J. P.; Town, R. M.; van Leeuwen, H. P. Cd(II) Speciation in Alginate Gels. *Environmental Science & Technology* **2008,** 42, 7242-7247.

59.Johnson, E. M.; Berk, D. A.; Jain, R. K.; Deen, W. M. Hindered diffusion in agarose gels: test of effective medium model. *Biophysical Journal* **1996,** 70, 1017-1023.

60.Clague, D. S.; Phillips, R. J. Hindered diffusion of spherical macromolecules through dilute fibrous media. *Physics of Fluids* **1996,** 8, 1720-1731.

61.Lustig, S. R.; Peppas, N. A. Solute diffusion in swollen membranes. IX. Scaling laws for solute diffusion in gels. *Journal of Applied Polymer Science* **1988,** 36, 735-747.

62.Pluen, A.; Netti, P. A.; Jain, R. K.; Berk, D. A. Diffusion of macromolecules in agarose gels: comparison of linear and globular configurations. *Biophysical Journal* **1999,** 77, 542-552.

63.Waggoner, R. A.; Blum, F. D.; Macelroy, J. M. D. Dependence of the solvent diffusion-coefficient on concentration in polymer-solutions. *Macromolecules* **1993,** 26, 6841-6848.

64.Mackie, J. S.; Meares, P. The Diffusion of electrolytes in a cation-exchange resin membrane .1. Theoretical. *Proceedings of the Royal Society of London Series a-Mathematical and Physical Sciences* **1955,** 232, 498-509.

65.Ogston, A. G.; Preston, B. N.; Wells, J. D. On the transport of compact particles through solutions of chain-polymers. *Proceedings of the Royal Society of London. A. Mathematical and Physical Sciences* **1973,** 333, 297-316.

66.Johansson, L.; Elvingson, C.; Loefroth, J. E. Diffusion and interaction in gels and solutions. 3. Theoretical results on the obstruction effect. *Macromolecules* **1991,** 24, 6024-6029.

67.Mackie, J. S.; Meares, P. The Diffusion of electrolytes in a cation-exchange resin membrane. I. Theoretical. *Proceedings of the Royal Society of London. Series A. Mathematical and Physical Sciences* **1955,** 232, 498-509.

68.Cukier, R. I. Diffusion of Brownian spheres in semidilute polymer solutions. *Macromolecules* **1984,** 17, 252-255.

69.Altenberger, A. R.; Tirrell, M.; Dahler, J. S. Hydrodynamic screening and particle dynamics in porous-media, semidilute polymer-solutions and polymer gels. *Journal of Chemical Physics* **1986,** 84, 5122-5130.

70.Phillies, G. D. J. Universal scaling equation for self-diffusion by macromolecules in solution. *Macromolecules* **1986,** 19, 2367-2376.

71.de Gennes, P. G. Reptation of a polymer chain in the presence of fixed obstacles. *The Journal of Chemical Physics* **1971,** 55, 572-579.

72.Fujita, H., Diffusion in polymer-diluent systems
Fortschritte Der Hochpolymeren-Forschung. In Springer Berlin / Heidelberg: 1961; Vol. 3, pp 1-47.

73.Peppas, N. A.; Reinhart, C. T. Solute diffusion in swollen membranes. Part I. A new theory. *Journal of Membrane Science* **1983,** 15, 275-287.

74.de Beer, D.; Stoodley, P.; Lewandowski, Z. Measurement of local diffusion coefficients in biofilms by microinjection and confocal microscopy. *Biotechnology and Bioengineering* **1997,** 53, 151-158.

75.Stoodley, P.; Debeer, D.; Lewandowski, Z. Liquid flow in biofilm systems. *Applied and Environmental Microbiology* **1994,** 60, 2711-2716.

76.Libicki, S. B.; Salmon, P. M.; Robertson, C. R. The effective diffusive permeability of a nonreacting solute in microbial cell aggregates. *Biotechnology and Bioengineering* **1988,** 32, 68-85.

77.de Beer, D.; Stoodley, P.; Roe, F.; Lewandowski, Z. Effects of biofilm structures on oxygen distribution and mass transport. *Biotechnology and Bioengineering* **1994,** 43, 1131-1138.

78.Lewandowski, Z.; Stoodley, P.; Altobelli, S. Experimental and conceptual studies on mass transport in biofilms. *Water Science and Technology* **1995,** 31, 153-162.

79.Peulen, T. O.; Wilkinson, K. J. Diffusion of nanoparticles in a biofilm. *Environmental Science & Technology* **2011,** 45, 3367-3373.

80.Thurnheer, T.; Gmur, R.; Shapiro, S.; Guggenheim, B. Mass transport of macromolecules within an in vitro model of supragingival plaque. *Applied and Environmental Microbiology* **2003,** 69, 1702-1709.

81.Teitzel, G. M.; Parsek, M. R. Heavy metal resistance of biofilm and planktonic Pseudomonas aeruginosa. *Applied and Environmental Microbiology* **2003,** 69, 2313-2320.

82.Marcotte, L.; Therien-Aubin, H.; Sandt, C.; Barbeau, J.; Lafleur, M. Solute size effects on the diffusion in biofilms of Streptococcus mutans. *Biofouling* **2004,** 20, 189-201.

83.Sandt, C.; Barbeau, J.; Gagnon, M.-A.; Lafleur, M. Role of the ammonium group in the diffusion of quaternary ammonium compounds in *Streptococcus mutans* biofilms. *Journal of Antimicrobial Chemotherapy* **2007,** 60, 1281-1287.

84.Zhang, Z.; Nadezhina, E.; Wilkinson, K. J. Quantifying diffusion in a biofilm of *Streptococcus mutans*. *Antimicrobial Agents and Chemotherapy* **2011,** 55, 1075-1081.

85.Sternberg, C.; Christensen, B. B.; Johansen, T.; Nielsen, A. T.; Andersen, J. B.; Givskov, M.; Molin, S. Distribution of bacterial growth activity in flow-chamber biofilms. *Applied and Environmental Microbiology* **1999,** 65, 4108-4117.

86.Wentland, E. J.; Stewart, P. S.; Huang, C. T.; McFeters, G. A. Spatial variations in growth rate within Klebsiella pneumoniae colonies and biofilm. *Biotechnology Progress* **1996,** 12, 316-321.

87.Xu, K. D.; Stewart, P. S.; Xia, F.; Huang, C. T.; McFeters, G. A. Spatial physiological heterogeneity in Pseudomonas aeruginosa biofilm is determined by oxygen availability. *Applied and Environmental Microbiology* **1998,** 64, 4035-4039.

88.Ramsing, N. B.; Kuhl, M.; Jorgensen, B. B. Distribution of sulfate-reducing bacteria, O_2, and H_2S in photosynthetic biofilms determined by oligonucleotide probes and microelectrodes. *Applied and Environmental Microbiology* **1993,** 59, 3840-3849.

89.Schramm, A.; Larsen, L. H.; Revsbech, N. P.; Ramsing, N. B.; Amann, R.; Schleifer, K. H. Structure and function of a nitrifying biofilm as determined by in situ hybridization and the use of microelectrodes. *Applied and Environmental Microbiology* **1996,** 62, 4641-4647.

90.Santegoeds, C. M.; Ferdelman, T. G.; Muyzer, G.; de Beer, D. Structural and functional dynamics of sulfate-reducing populations in bacterial biofilms. *Applied and Environmental Microbiology* **1998,** 64, 3731-3739.

91.Barken, K. B.; Pamp, S. J.; Yang, L.; Gjermansen, M.; Bertrand, J. J.; Klausen, M.; Givskov, M.; Whitchurch, C. B.; Engel, J. N.; Tolker-Nielsen, T. Roles of type IV pili, flagellum-mediated motility and extracellular DNA in the formation of mature multicellular structures in Pseudomonas aeruginosa biofilms. *Environmental Microbiology* **2008,** 10, 2331-2343.

92.Lawrence, J. R.; Swerhone, G. D. W.; Kuhlicke, U.; Neu, T. R. In situ evidence for microdomains in the polymer matrix of bacterial microcolonies. *Canadian Journal of Microbiology* **2007,** 53, 450-458.

93.Stewart, P. S. Diffusion in biofilms. *Journal of Bacteriology* **2003,** 185, 1485-1491.

94.Debeer, D.; Stoodley, P.; Roe, F.; Lewandowski, Z. Effects of biofilm structures on oxygen distribution and mass-transport. *Biotechnology and Bioengineering* **1994,** 43, 1131-1138.

95.Waharte, F.; Steenkeste, K.; Briandet, R.; Fontaine-Aupart, M. P. Diffusion measurements inside biofilms by image-based fluorescence recovery after photobleaching (FRAP) analysis with a commercial confocal laser scanning microscope. *Applied and Environmental Microbiology* **2010,** 76, 5860-5869.

96.Habimana, O.; Steenkeste, K.; Fontaine-Aupart, M. P.; Bellon-Fontaine, M. N.; Kulakauskas, S.; Briandet, R. Diffusion of Nanoparticles in Biofilms Is Altered by Bacterial Cell Wall Hydrophobicity. *Applied and Environmental Microbiology* **2011,** 77, 367-368.

97.Govan, J. R. W.; Fyfe, J. A. M.; McMillan, C. Instability of Mucoid *Pseudomonas-Aeruginosa*-fluctuation and improved stability of the mucoid form in shaken culture. *Journal of General Microbiology* **1979,** 110, 229-232.

98.Takenaka, S.; Pitts, B.; Trivedi, H. M.; Stewart, P. S. Diffusion of macromolecules in model oral biofilms. *Applied and Environmental Microbiology* **2009,** 75, 1750-1753.

99.Lawrence, J. R.; Wolfaardt, G. M.; Korber, D. R. Determination of diffusion coefficients in biofilms by confocal laser microscopy. *Applied and Environmental Microbiology* **1994,** 60, 1166-1173.

100.Williamson, K.; McCarty, P. L. Verification studies of bioflm model for baterial substrate utilization. *Journal Water Pollution Control Federation* **1976,** 48, 281-296.

101.Nilsson, B. K.; Karlsson, H. T. Diffusion rates in a dense matrix of methane-producing microorganisms. *Journal of Chemical Technology and Biotechnology* **1989,** 44, 255-260.

102.Arvin, E.; Kristensen, G. H. Effect of denitrification on the pH in biofilms. *Water Science and Technology* **1982,** 14, 833-848.

103.Kim, H.-J.; Michael Gias, E. L.; Jones, M. N. The adsorption of cationic liposomes to Staphylococcus aureus biofilms. *Colloids and Surfaces A: Physicochemical and Engineering Aspects* **1999,** 149, 561-570.

104.Ahmed, K.; Gribbon, P.; Jones, M. N. The application of confocal microscopy to the study of liposome adsorption onto bacterial biofilms. *Journal of Liposome Research* **2002,** 12, 285-300.

105.Suci, P. A.; Geesey, G. G.; Tyler, B. J. Integration of Raman microscopy, differential interference contrast microscopy, and attenuated total reflection Fourier transform infrared spectroscopy to investigate chlorhexidine spatial and temporal distribution in *Candida albicans* biofilms. *Journal of Microbiological Methods* **2001,** 46, 193-208.

106.Gordon, C. A.; Hodges, N. A.; Marriott, C. Antibiotic interaction and diffusion through alginate and exopolysaccharide of cystic fibrosis-derived *Pseudomonas-Aeruginosa*. *Journal of Antimicrobial Chemotherapy* **1988,** 22, 667-674.

107.Nichols, W. W.; Dorrington, S. M.; Slack, M. P. E.; Walmsley, H. L. Inhibition of tobramycin diffusion by binding to alginate. *Antimicrobial Agents and Chemotherapy* **1988,** 32, 518-523.

108.Campanac, C.; Pineau, L.; Payard, A.; Baziard-Mouysset, G.; Roques, C. Interactions between biocide cationic agents and bacterial biofilms. *Antimicrobial Agents and Chemotherapy* **2002,** 46, 1469-1474.

109.Lin, C. A.; Sperling, R. A.; Li, J. K.; Yang, T. Y.; Li, P. Y.; Zanella, M.; Chang, W. H.; Parak, W. J. Design of an amphiphilic polymer for nanoparticle coating and functionalization. *Small* **2008,** 4, 334-341.

110.Lee, S. P.; Nicholls, J. F. Diffusion of charged ions in mucus gel-effect of net charge. *Biorheology* **1987,** 24, 565-569.

111.Siegrist, H.; Gujer, W. Mass-transfer mechanisms in a heterotrophic biofilm. *Water Research* **1985,** 19, 1369-1378.

112.Converti, A.; Zilli, M.; Arni, S.; Di Felice, R.; Del Borghi, M. The effects of temperature and viscosity on glucose diffusivity through *Saccharomyces cerevisiae* biofilms. *Canadian Journal of Chemical Engineering* **1999,** 77, 618-626.

113.Zhou, X. H.; Qiu, Y. Q.; Shi, H. C.; Yu, T.; He, M.; Cai, Q. A New approach to quantify spatial distribution of biofilm kinetic parameters by In situ determination of oxygen uptake rate (OUR). *Environmental Science & Technology* **2009,** 43, 757-763.

114.Vogt, M.; Flemming, H. C.; Veeman, W. S. Diffusion in Pseudomonas aeruginosa biofilms: a pulsed field gradient NMR study. *Journal of Biotechnology* **2000,** 77, 137-146.

115.Renslow, R. S.; Majors, P. D.; McLean, J. S.; Fredrickson, J. K.; Ahmed, B.; Beyenal, H. *In situ* effective diffusion coefficient profiles in live biofilms using pulsed-field gradient nuclear magnetic resonance. *Biotechnology and Bioengineering* **2010,** 106, 928-937.

116.Stilbs, P. Fourier transform pulsed-gradient spin-echo studies of molecular diffusion. *Progress in Nuclear Magnetic Resonance Spectroscopy* **1987,** 19, 1-45.

117.Gagnon, M. A.; Lafleur, M. Self-diffusion and mutual diffusion of small molecules in high-set curdlan hydrogels studied by P-31 NMR. *Journal of Physical Chemistry B* **2009,** 113, 9084-9091.

118.Moussaoui, M.; Benlyas, M.; Wahl, P. Diffusion of proteins in Sepharose Cl-B gels. *Journal of Chromatography* **1992,** 591, 115-120.

119.Orgad, O.; Oren, Y.; Walker, S. L.; Herzberg, M. The role of alginate in Pseudomonas aeruginosa EPS adherence, viscoelastic properties and cell attachment. *Biofouling* **2011,** 27, 787-798.

120.Wahl, P. Fluorescence recovery after photobleaching of suspensions of vacuoles. *Biophysical Chemistry* **1996,** 57, 225-237.

121.Wahl, P.; Azizi, F. Fluorescent recovery after photobleaching (FRAP) of a fluorescent transferrin internalized in the late transferrin endocytic compartment of living A431 cells: Theory. *Biochimica Et Biophysica Acta-Biomembranes* **1997,** 1327, 69-74.

122.Oubekka, S. D.; Briandet, R.; Waharte, F.; Fontaine-Aupart, M. P.; Steenkeste, K. Image-based fluorescence recovery after photobleaching (FRAP) to dissect vancomycin diffusion-reaction processes in Staphylococcus aureus biofilms. *Clinical and Biomedical Spectroscopy and Imaging Ii* **2011,** 8087.

123.Birmingham, J. J.; Hughes, N. P.; Treloar, R. Diffusion and binding measurements within oral biofilms using fluorescence photobleaching recovery methods. *Philosophical Transactions of the Royal Society of London Series B-Biological Sciences* **1995,** 350, 325-343.

124.Gagnon, M. A.; Lafleur, M. Comparison between nuclear magnetic resonance profiling and the source/sink approach for characterizing drug diffusion in hydrogel matrices. *Pharmaceutical Development and Technology* **2011,** 16, 651-656.

125.Kwak, S.; Viet, M. T.; Lafleur, M. Self- and mutual-diffusion coefficients measurements by 31P NMR 1D profiling and PFG-SE in dextran gels. *J Magn Reson* **2003,** 162, 198-205.

126.Labille, J.; Fatin-Rouge, N.; Buffle, J. Local and average diffusion of nanosolutes in agarose gel: The effect of the gel/solution interface structure. *Langmuir* **2007,** 23, 2083-2090.

127.Dunmire, E. N.; Plenys, A. M.; Katz, D. F. Spectrophotometric analysis of molecular transport in gels. *J Control Release* **1999,** 57, 127-140.

128.Kwak, S.; Lafleur, M. Raman spectroscopy as a tool for measuring mutual-diffusion coefficients in hydrogels. *Applied Spectroscopy* **2003,** 57, 768-773.

129.Elson, E. L.; Magde, D. Fluorescence correlation spectroscopy .1. Conceptual basis and theory. *Biopolymers* **1974,** 13, 1-27.

130.Weiss, S. Fluorescence spectroscopy of single biomolecules. *Science* **1999,** 283, 1676-1683.

131.Brock, R.; Hink, M. A.; Jovin, T. M. Fluorescence correlation microscopy of cells in the presence of autofluorescence. *Biophys J* **1998,** 75, 2547-2557.

132.Widengren, J.; Rigler, R. Review -Fluorescence correlation spectroscopy as a tool to investigate chemical reactions in solutions and on cell surfaces. *Cellular and Molecular Biology* **1998,** 44, 857-879.

133.Mertz, J.; Xu, C.; Webb, W. W. Single molecule detection by two-photon excited fluorescence. *Optics Letters* **1995**, 20, 2532-2534.

134.Rani, S. A.; Pitts, B.; Stewart, P. S. Rapid diffusion of fluorescent tracers into Staphylococcus epidermidis biofilms visualized by time lapse microscopy. *Antimicrobial Agents and Chemotherapy* **2005,** 49, 728-732.

135.Martinez, A. R.; Granon, F. S.; Perez, F. R.; Colorado, A. C. P.; Edwards, H. G. M. Mass diffusion transport Studies of lithium sulfate in aqueous solutions using Raman spectroscopy. *Applied Spectroscopy* **1995,** 49, 1131-1136.

Chapter 2

Optimization of the experimental methods used to quantify diffusion

2.1. Overview

In this thesis, self-diffusion coefficients were measured in equilibrated systems of water, hydrogels and biofilms using ***fluorescence correlation spectroscopy***. Mutual diffusion coefficients in the agarose hydrogel were determined from the diffusive flux generated from a concentration gradient between two halves of a ***custom-built diffusion cell***. ***Microelectrode voltammetry*** was employed to evaluate the Donnan potential of the gels, which was then used to interpret the observed mutual diffusion fluxes. In this chapter, the theory and optimization of each of these three key analytical techniques is discussed. Parts of sections 2.3 and 2.4 were previously published as the supporting information in M. Golmohamadi, T.A. Davis and K.J. Wilkinson, *J. Phys. Chem*. A.[1] (chapter 3). Those sections have been slightly edited here and have not been reproduced in chapter 3.

2.2. Fluorescence correlation spectroscopy (FCS)

2.2.1 FCS theory

Fluorescence correlation spectroscopy (FCS) was first developed by D. Magde *et al.*[2] in the early 1970's to study chemical reaction rates and translational diffusion coefficients. FCS is based on the temporal analysis of fluorescence intensity fluctuations. In fact, the kinetics of any phenomenon which arises from fluorescence fluctuations can be observed by FCS and thus FCS has been used to characterize translational diffusion[3-9] but also rotational diffusion[10], active transport[11], rates of conformational changes[12], concentrations,[13] and various kinetic phenomena such as intersystem crossing between

singlet and triplet states[14] and photobleaching[15]. In a typical FCS experiment, time-lag correlations are obtained from either the correlation of the fluorescence intensity signal with itself (autocorrelation) or the correlation with a second signal (cross-correlation). Data are fitted to a theoretical model (Fig. 2.1) in order to separate various photochemical phenomena from diffusion.

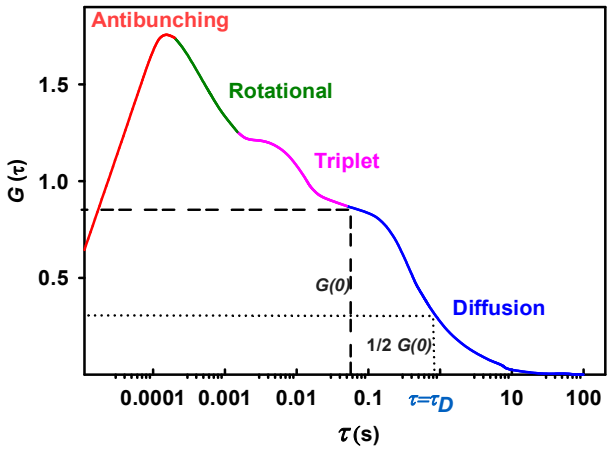

Figure 2.1. Typical autocorrelation function of the fluorescence intensity fluctuations. In FCS, generally only the times longer than 0.01 ms (blue line) are used to derive solute diffusion times (τ_D).

Briefly, in order to perform an FCS experiment, a laser is used as light source. The incident beam passes through a dichroic beam splitter and is focused into the sample using a high numerical aperture (NA) microscope objective. Fluorescence emission is collected by the same objective, passed through the dichroic filter and focussed onto the confocal pinhole. Because of the pinhole, only a fraction of the emission reaches the detector and light from out-of-focus regions is thus greatly attenuated. Photons are detected by either a photomultiplier tube (PMT) or an avalanche photo diode (APD), equipped with a suitable band pass filter, which rejects ambient and elastically scattered light.

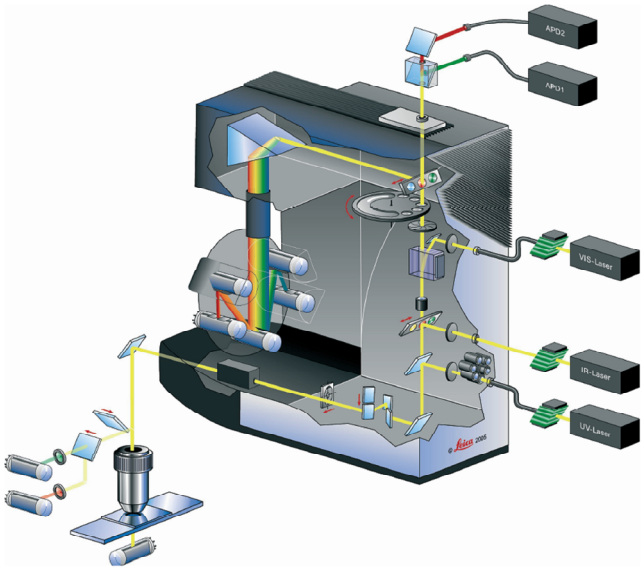

Figure 2.2. The principles of confocal microscopy. The excitation laser is focused into the confocal volume via a microscope objective. Fluorescence emission is collected by the same objective, passes through a dichroic mirror and is focused towards the pinhole. Photons passing through the pinhole are collected by an APD or PMT detector. Image taken from the Leica user manual.

The autocorrelation function, $G(\tau)$, is defined in terms of the fluorescence fluctuations:

$$G(\tau) = \frac{< \delta F(t)\, \delta F(t+\tau) >}{< F(t) >^2} \qquad (2\text{-}1)$$

where $F(t)$ is the fluorescence signal at time t, $<F(t)>$ is the average fluorescence intensity $< F(t) >= 1/\mathrm{T} \int_0^{\mathrm{T}} F(t)\, dt$ where T is the measurement time, $\delta F(t)$ is the fluctuation of fluorescence at time t and $\delta F(t)=F(t)-<F(t)>$. The autocorrelation function does not depend on the time at which the measurement is recorded. For FCS, $F(t)$ is determined by:

$$F(t) = H\, \Omega \sum_{i=1}^{n} \int_v W_i(r).c_i(r,t)\, d_v \qquad (2\text{-}2)$$

where n is the number of fluorescent species, H is a constant, $\Omega=\varepsilon\, q\, I_\circ$ in which ε is the absorptivity coefficient, q is the fluorescence quantum efficiency, $I_\circ$ is the maximum

amplitude of special intensity distribution of the excitation laser beam, c_i *(r,t)* is the number density for the i[th] species and the function *W(r)* is defined as:

$$W(r) = I(r)\,\beta(r)/I_{\circ} \tag{2-3}$$

in which *I*(r) is the excitation distribution, β(r) is the optical transfer function of the objective-pinhole combination and $I_{\circ}$ is constant during FCS. The fluctuation function of the fluorescence signal, $\delta F(t)$ in Equation 2-1 corresponds to:[16]

$$\delta F(t) = H\,\Omega \sum_{i=1}^{n} \int_{v} W_i(r).\delta\left(c_i(r,t)\right) d_v \tag{2-4}$$

Substitution of $\delta F(t)$ from Equation 2-4 with that in Equation 2-1 assuming one single particle with constant brightness and small fluctuations gives[17]:

$$G(\tau) = \frac{\int_{v}\int_{v'} W(r')W(r) < \delta c_i(r,t)\,\delta c_i(r',t+\tau) > dv\,dv'}{< c >^2 \left(\int_{v} W(r).dv\right)^2} \tag{2-5}$$

Equation 2-5 is the autocorrelation function typically used in FCS to measure diffusion coefficients based upon fluctuations of the fluorescence intensity. In order to derive the correlation function for normal diffusion in a confocal volume, the simplest case is to consider one particle which has the constant brightness (Equation 2-2). By applying diffusion theory (Fick's Law), we can obtain the following Equation[18]

$$G(\tau) = \frac{1}{< N >} \cdot \left(1 + \frac{\tau}{\tau_D}\right)^{-1} \left(1 + \frac{1}{p^2} \cdot \frac{\tau}{\tau_D}\right)^{-1/2} \tag{2-6}$$

where the factor *p* is related to the confocal shape and is defined as $p=\omega_z/\omega_{xy}$ in which ω_{xy} and ω_z are the transversal and longitudinal radii of the confocal volume, respectively, and $< N > = < c > \omega_{xy}^2\,\pi^{3/2}\,\omega_z$ where *c* is the concentration of diffusing solute in confocal volume. The diffusion coefficient of a molecule or particle passing through the confocal volume can be obtained from the diffusion times (τ_D) determined from Equation 2-6[19]

$$\tau_D = \frac{\omega_{xy}^2}{4D^s} \tag{2-7}$$

When the molecules are found in the triplet state, the triplet state signals can be correlated using[20]:

$$G(\tau) = \frac{1}{N}\frac{\Gamma}{(1-\Gamma)}e^{-\tau/\tau_T} \tag{2-8}$$

where Γ is the triplet fraction and τ_Γ is the triplet time. Generally, the autocorrelation function for the normal diffusion of a molecule with a triplet state can be obtained by combining the Equations 2-6 and 2-8 to give[21]

$$G(\tau) = \frac{1}{<N>}\left(1+\frac{\Gamma}{(1-\Gamma)}e^{-\tau/\tau_T}\right)\left(1+\frac{\tau}{\tau_D}\right)^{-1}\left(1+\frac{1}{p^2}\cdot\frac{\tau}{\tau_D}\right)^{-1/2} \tag{2-9}$$

where $< N >$ is the total number of fluorescence molecules in either state. In this case, the amplitude *G(0)* is no longer equal to the inverse of the average number of particles in the confocal volume, *N*, rather[22]

$$G(0) = \frac{1}{<N>(1-\Gamma)} \tag{2-10}$$

For most FCS experiments that were performed in this thesis, $\tau_D >> \tau_\Gamma$ and the correlation resulted simply from a sum of the diffusion and the triplet contributions. Nonetheless, the triplet contributions can also be accounted for in the data analysis by lowering the data acquisition frequency or by selecting the type of fluorescence probes whose triplet states are negligible and can only fitted with Equation 2-6.

In the case where *n* non-interacting species with constant brightness diffuse through the confocal volume, e.g. in the case of a nanoparticle that has been labelled with a small fluorescence probe, Equation 2-10 assumes no cross-correlation between the two components i and j and gives[23]

$$G(\tau)=\frac{1}{<N>}\left(\begin{array}{l} f\left(1+\frac{\tau}{\tau_{\mathrm{D,i}}}\right)^{-1}\left(1+\frac{1}{p^2}\frac{\tau}{\tau_{\mathrm{D,i}}}\right)^{-1/2}+ \\ (1-f)\left(1+\frac{\tau}{\tau_{\mathrm{D,i}}}\right)^{-1}\left(1+\frac{1}{p^2}\frac{\tau}{\tau_{\mathrm{D,i}}}\right)^{-1/2} \end{array}\right) \tag{2-11}$$

where f is the fraction of particles with diffusion times of τ_D and N is the total number of particles in the confocal volume. If the triplet state is included, Equation 2-11 becomes:

$$G(\tau)=\frac{1}{<N>}\left(\begin{array}{l} f\left(1+\frac{\Gamma}{(1-\Gamma)}e^{-\tau/\tau_T}\right)\left(1+\frac{\tau}{\tau_{\mathrm{D,i}}}\right)^{-1}\left(1+\frac{1}{p^2}\frac{\tau}{\tau_{\mathrm{D,i}}}\right)^{-1/2}+ \\ (1-f)\left(1+\frac{\Gamma}{(1-\Gamma)}e^{-\tau/\tau_T}\right)\left(1+\frac{\tau}{\tau_{\mathrm{D,i}}}\right)^{-1}\left(1+\frac{1}{p^2}\frac{\tau}{\tau_{\mathrm{D,i}}}\right)^{-1/2} \end{array}\right) \tag{2-12}$$

For the non-Brownian diffusion of solutes when Fick's law is not applicable, the diffusion time can be described by a modified version of Equation 2-7

$$\tau_D{}^{\alpha} = \frac{\omega_{xy}^{2}}{4D^{s}} \tag{2-13}$$

where α indicates the degree of anomalous diffusion. For values $\alpha<1$, diffusion is considered as sub-diffusion, which is often the case for macromolecules entrapped in the pores of gel of a similar size. When $\alpha>1$, the diffusion is called super-diffusion, for which diffusion appears to be faster than Brownian motion. By substituting Equation 2-13 in Equation 2-6, the anomalous diffusion model gives[24, 25]:

$$G(\tau)=\frac{1}{<N>}\left(1+\left(\frac{\tau}{\tau_{\mathrm{D,i}}}\right)^{\alpha}\right)^{-1}\left(1+\frac{1}{p^2}\left(\frac{\tau}{\tau_{\mathrm{D,i}}}\right)^{\alpha}\right)^{-1/2} \tag{2-14}$$

and finally, the model can be expanded to a two component model:

$$G(\tau)=\frac{1}{<N>}\left(\begin{array}{l} f\left(1+\left(\frac{\tau}{\tau_{D,i}}\right)^{\alpha}\right)^{-1}\left(1+\frac{1}{p^2}\left(\frac{\tau}{\tau_{D,i}}\right)^{\alpha}\right)^{-1/2}+ \\ (1-f)\left(1+\left(\frac{\tau}{\tau_{D,i}}\right)^{\alpha}\right)^{-1}\left(1+\frac{1}{p^2}\left(\frac{\tau}{\tau_{D,i}}\right)^{\alpha}\right)^{-1/2} \end{array}\right) \quad (2\text{-}15)$$

The correct form of the model to be employed depends on the geometry of the confocal volume and the kinetics of the fluorescence dye. The model should, in general, be selected on the basis of (i) whether diffusion process are involved with multiple interacting or non-interacting components; (ii) whether the components seem to indicate that anomalous diffusion is involved; and (iii) whether a cross-correlation occurs among the different fluorescence signals.

The effective FCS confocal volume, V_{eff}, can be obtained from equation 2-5 at τ=0:

$$G(0)=\frac{1}{<c>}\frac{\int W^2(r)dr}{\left(\int W(r)dr\right)^2} \quad (2\text{-}16)$$

Since the τ_D value can also be obtained from Equation 2-1 at τ=0:

$$G(0)=\frac{<\delta F(t)^2>}{<F>^2}=\frac{<F^2>-<F>^2}{<F>^2}=\frac{<N^2>-<N>^2}{<N>^2}=\frac{1}{<N>} \quad (2\text{-}17)$$

By combining Equations 2-16 and 2-17, one arrives at[26]

$$V_{eff}=\frac{\left(\int W(r)dr\right)^2}{\int W^2(r)dr} \quad (2\text{-}18)$$

Under the assumption of a three-dimensional Gaussian distribution for the confocal volume (Fig. 2.3.), one obtains[26]

$$W(r) = \exp\left(-\frac{2\left(x^2 + y^2\right)}{\omega_{xy}^2}\right)\exp\left(-\frac{2z^2}{\omega_z^2}\right) \quad (2\text{-}19)$$

where ω_{xy} and ω_z define $1/e_2$ values of $W(r)$ in the lateral and axial axis, respectively. This assumption implies that the highest probability of fluorescence detection is for the particles at the center of the confocal volume and that fluorescence decay is greater in the radial direction than the axial direction, i.e. $\omega_{xy} < \omega_z$. The effective confocal volume can be obtained from substituting Equation 2-19 into Equation 2-18 to give:

$$V_{\text{eff}} = \omega_{xy}^2 \pi^{3/2} \omega_z \quad (2\text{-}20)$$

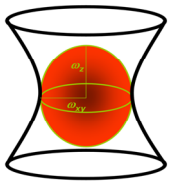

Figure 2.3. The three dimensional Gaussian distribution assumed to derive the confocal volume function

Finally, the role of removing data points from the autocorrelation function can be seen in Fig. 2.4 in which fluorescence intensity fluctuations at time t are delayed by the lag time of τ. In general, increased lag time leads to reduced correlation value, $G(\tau)$.[27]

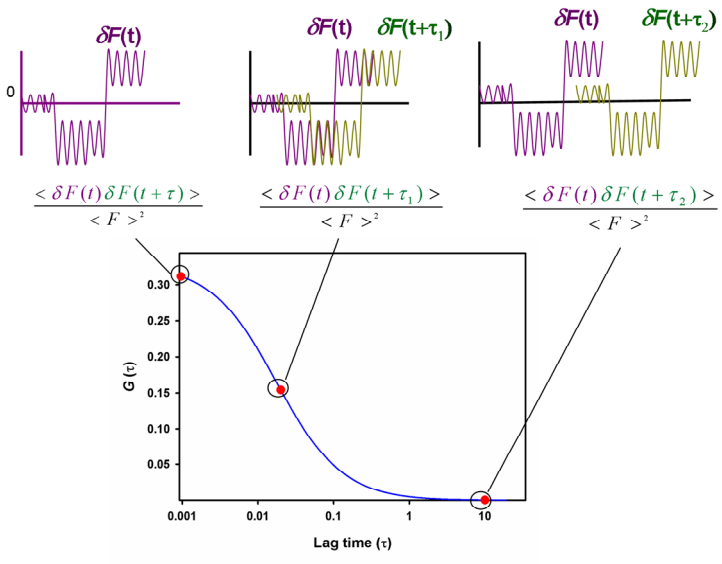

Figure 2.4. The typical correlation curve of FCS from autocorrelation of fluorescence fluctuations.

2.2.2 FCS materials and methods

FCS measurements in this thesis were performed on a Leica TCS SP5 laser scanning microscope using an Ar (argon) 488 nm/20 mW, DPSS (Diode-pumped solid-state laser) 561 nm/10 mW or a HeNe 633 nm/10 mW laser source for the fluorescence excitation, with a confocal microscope stand equipped with a water immersion objective (NA 1.2). Fluorescence emission was followed at 500-530 nm and/or 607-683 nm. The confocal volume was calibrated by fitting autocorrelation decays for rhodamine 110 (R110) at concentrations of 2.5, 5, 10 and 20 nM using an excitation wavelength of 488 nm. R110 has a diffusion coefficient of 4.40 x10^{-10} m^2 s^{-1} [3]. Calibration of the confocal volume was used to obtain absolute values for the diffusion coefficients. Dimensions of the confocal volume are obtained by fitting with following model:

$$G(\tau) = \frac{1}{N}\left(1+\left(\frac{4D^s\tau}{\omega_{xy}^2}\right)\right)^{-1}\left(1+\frac{1}{p^2}\left(\frac{4D^s\tau}{\omega_{xy}^2}\right)\right)^{-1/2} \quad (2\text{-}21)$$

Given that the laser power will affect the size of confocal volume, it was initially optimized in order to determine the optical saturation limit of the fluorophore. Furthermore,

in the case of increased background of fluorescence signal (Fig. 2.1) in more complex system as biofilms, the factor *b* can be added to the Equation 2-21 to gives

$$G(\tau) = \frac{1}{N}\left(1+\left(\frac{4D^s\tau}{\omega_{xy}^2}\right)\right)^{-1}\left(1+\frac{1}{p^2}\left(\frac{4D^s\tau}{\omega_{xy}^2}\right)\right)^{-1/2} + b \qquad (2\text{-}22)$$

to avoid overestimation in measurement of diffusion coefficient (more information for the issue of background can be seen in Fig. S5.2 of supporting information of chapter 5).

2.2.3 FCS results and discussion

As the excitation intensity is increased, the molecule/particle spends more and more time in a non-excitable state. This phenomenon is called the optical saturation. Optical saturation can arise from: (i) *Excited state saturation* (the fluorophore is still in the excited state when the next photons arrive); (ii) *Triplet state saturation* (the fluorophore has a long-lived triplet state and can no longer be excited until it returns to the ground state; (iii) *Non-fluorescing states* (intersystem conversion of fluorescence signal); and (iv) *Photobleaching* (due to laser beam)[28]. In order to investigate the influence of optical saturation on the correlation function, a series of FCS measurements with different laser intensities were performed for 5 nM of R110. The fluorescence emission is presented as a function of laser power in Fig. 2.5.

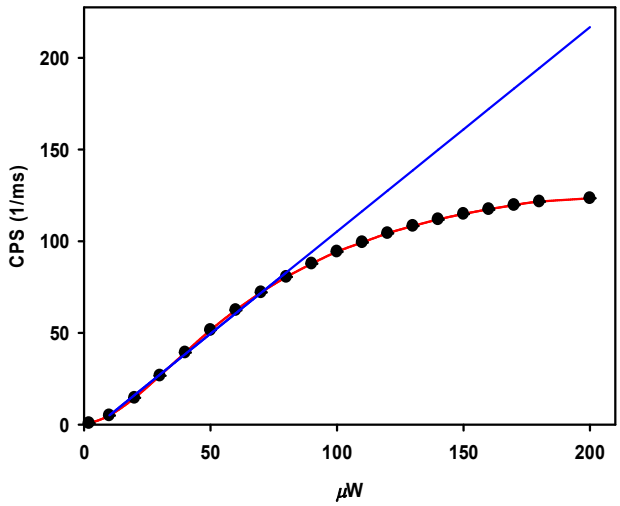

Figure 2.5. Emission intensity (counts per second: CPS) as a function of laser intensity for rhodamine 110 (R110); c=5 nM in water (I=10^{-2} M, pH=6); laser: Ar at 488 nm; acquisition frequency 10^5 Hz; acquisition time =60 sec; blue line: fitted curve of the linear section of curve.

For laser powers higher than 90 μW, a deviation from the linear range of fluorescent emissions, resulting from optical saturation, was visible. The corresponding dimensions of confocal volume and number of molecules in the confocal volume are shown in Fig. 2.6.

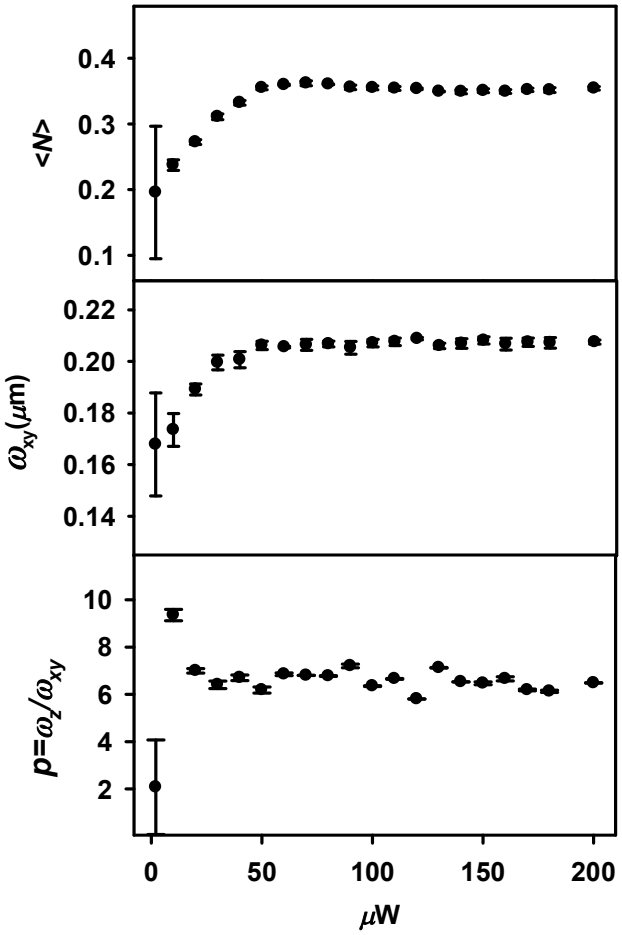

Figure 2.6. The number of fluorescence molecules in the confocal volume, <N>, lateral (ω_{xy}) dimension of the confocal volume and the ratio, $p=\omega_z/\omega_{xy}$, as a function of laser power intensity for R110. Values were obtained from ISS software; c=5 nM in water (I=10^{-2} M; pH=6); laser: Ar at 488 nm; acquisition frequency 10^5 Hz; acquisition time =60 s.

It can be seen in Fig. 2.6 that the correlation amplitude, $G(0)=1/<N>$, deceasing, meaning an increase of the number of particles (N) in $V_{eff.}$ Hence, a laser power as 60 μW was chosen for subsequent FCS calibrations. The autocorrelation curve for 5 nM of R110 is given in Fig. 2.7.

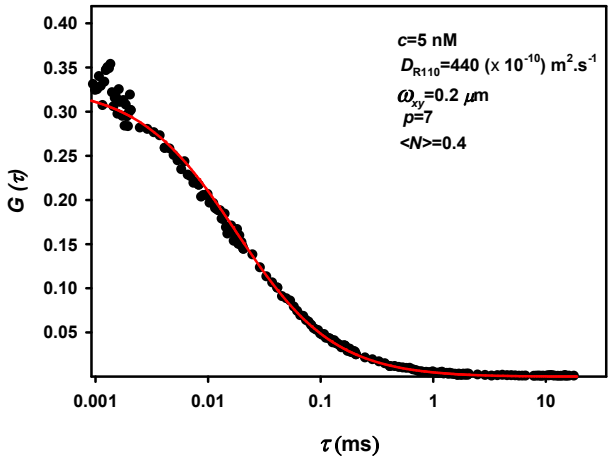

Figure 2.7. Autocorrelation function of 5 nM of R110 for a laser power of 60 μW; acquisition time=60 s; acquisition frequency=10^6 Hz (resolution time =1 μs); D_{R110}=4.40 $\times 10^{-10}$ $m^2.s^{-1}$; ω_{xy}=0.2, p=7, N=0.4; red lines are fitted curves provided by the ISS software under the assumption of 3D Gaussian model.

The second determinant factor in the FCS calibration is the concentration of the fluorescence dye in the confocal volume. In order to evaluate the role of fluorophore concentration on the calibration, a series of R110 concentrations were evaluated. Correlation curves with their respective fits are shown for a low and high extreme concentration (Fig. 2.8). The raw data can be correlated well for two of example concentrations. The resulting parameters for concentration from 1-10 nM for R110 are plotted in Fig.2.9.

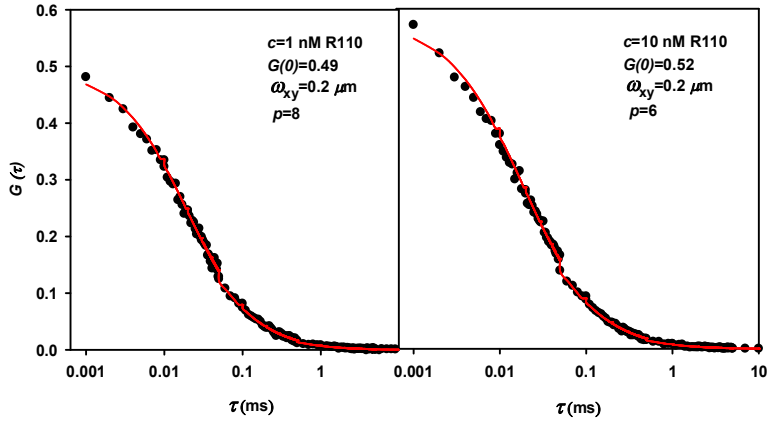

Figure 2.8. Correlation curves for two concentrations of R110; D_{R110}=4.4 x10^{-10} $m^2.s^{-1}$; acquisition time=60 s; acquisition frequency=10^6 Hz (resolution time =1 μs); red lines are fitted curves provided by the ISS software under the assumption of 3D Gaussian model.

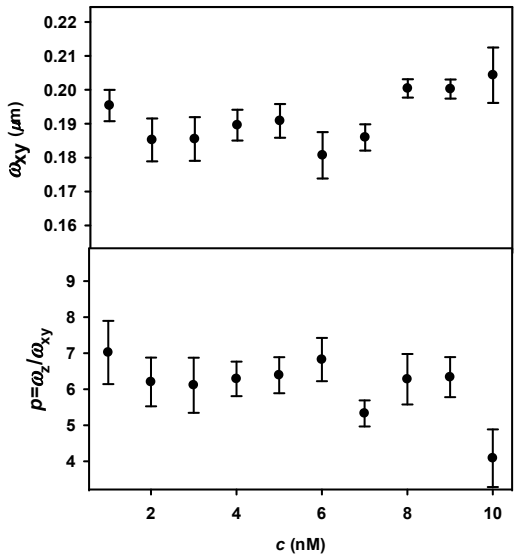

Figure 2.9. The dimensions of confocal volume (ω_{xy} and $p=\omega_z/\omega_{xy}$) for the concentrations of R110 in water from 1-10 nM (I=10^{-2} M; pH=6). The autocorrelation data was fitted with the 3D Gaussian model; laser: Ar at 488 nm; laser intensity=60 μW; acquisition time =60 s; acquisition frequency=10^5 Hz (resolution time=10 μs); D_{R110} =4.40 ×10^{-10} $m^2.s^{-1}$.

As it can be seen from Fig. 2.9, R110 concentrations between 1 and 10 nM could be used to calibrate the FCS technique. Indeed, fluorophore concentration had minimal effect on the calculated confocal volume dimensions.

2.3. Determination of the Donnan potentials by microelectrode voltammetry

2.3.1 Voltammetric theory

Fast transport rates, low capacitive currents and a low iR drop (i as current and R as resistance) are the characteristics of a microelectrode voltammetry, which make it applicable in low ionic strength. The flux of the solute determines the steady-state current of a microelectrode. Hence, accurate measurements of the concentrations of electroactive metal ions in the solutions are possible.[29] Diffusion coefficients of a metal ion in solution can be obtained by an inlaid gold (Au) microelectrode[30] through the use of Equation 2-23[31]:

$$I^{\mathrm{L}} = 4n\mathrm{F}D^{\mathrm{m}}c\,r_0 \tag{2-23}$$

where c is the bulk concentration of the electroactive ion, r_0 is the radius of the microelectrode, n is the number of electrons transferred, and F is the Faraday constant, I^{L} is the steady-state current, and D^{m} is mutual diffusion coefficient. Typically, microelectrodes with radii smaller than 25 μm produce steady-state voltammograms on the time scale of a few tenths of a second[32] (Fig. 2.10).

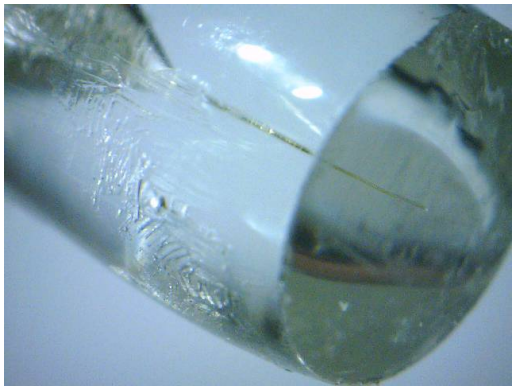

Figure 2.10. The Gold microelectrode in a glass support (r_0=25 μm).

Uncompensated immobile charges in the hydrogels will lead to the development of a Donnan potential[33]. In this case, the negative potential of the gel will result in an increased concentration of cations in the gel with respect to the bulk medium.[34] The Donnan potential for a symmetrical *z*-*z* electrolyte is given by[35]

$$\psi_{\mathrm{D}} = \frac{RT}{z\mathrm{F}} \operatorname{arcsin\,h}\left(\frac{z_{\mathrm{g}}\rho}{2\mathrm{F}zc}\right) \tag{2-24}$$

where z represents the valence of the electrolytes, z_{g} is the valence of the functional groups in the gel, ρ (C/m^3) the volume charge density of the gel and c is the bulk electrolyte concentration in the medium. Other expressions have been derived for more complex electrolyte mixtures[36].

For a more complex mixture of 2-1 and 1-1 (e.g., $Cd(NO_3)_2$ + $NaNO_3$), Ohshima and Kondo derived the following set of expressions[33]:

$$-\frac{1-\eta}{2}e^{-y} - \frac{\eta}{3}e^{-2y} + \frac{3-\eta}{6}e^{y} - \frac{\rho}{2c_1 + 3c_2} = 0 \tag{2-25}$$

$$y = \frac{\mathrm{F}\psi_{\mathrm{D}}}{RT} \tag{2-26}$$

$$\eta = \frac{3c_2}{c_1 + 3c_2} \tag{2-27}$$

where c_1 and c_2 are the concentrations of 1:1 and 2:1 electrolytes, respectively. The functional groups in the agarose hydrogel are normally carboxylate groups and other functional groups such as sulfonate, which have a negative value for z_g. The protonation of the functional group sites needs to be considered for pH values in the range of the relevant pK_a of the gel.

2.3.2 Voltammetric materials and methods

The gold microelectrodes (diameter of gold wire: r_0= 25 μm) were purchased from CH Instruments, Inc. The microelectrodes were processed in the lab, based on the approach of Brendel and Luther.[30] The gold electrode was extensively polished (1000 and 2400 grit silica carbide polishing paper; polishing cloth (DP-NAP, Struers) and successively finer diamond pastes (9, 6, 3, 1, 0.25 μm, Struers) with DP-Lubricant (Red, HG, Struers)) using a custom-made polisher built by the chemistry workshop. The microelectrode tip was sonicated between each polishing step.

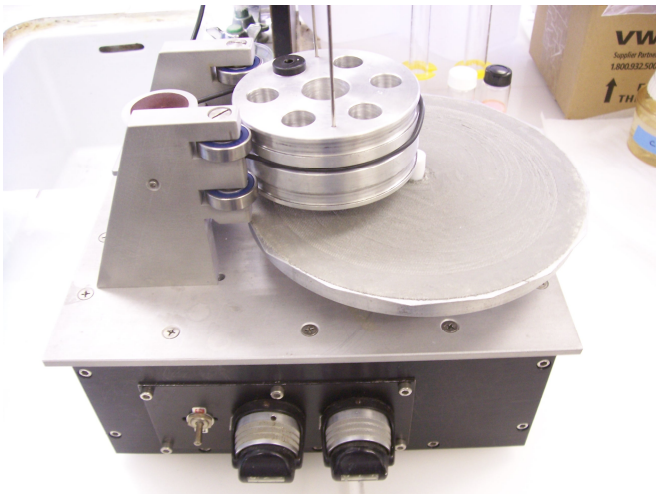

Figure 2.11. The instrument used to polish the gold microelectrode

Voltammetric measurements were made using an Ecochemie μAutolab III potentiostat combined with a Metrohm 663 VA stand. Mercury was plated onto the gold electrode at -0.4 V (vs. Ag-AgCl-3M KCl/ 0.25M KNO_3) in deoxygenated 5x10^{-3} M Hg

$(CH_3COO)_2$ and 0.1 M $HClO_4$ (until 65-70 μC of charge had accumulated). Amalgam formation between Hg and Au was controlled according to the procedure of Brendel, P. J. and Luther, G. W.[30] A custom-made Faraday cage was used to protect the microelectrode from excessive background found in the environment which microelectrode used. DC voltammetry was performed using the following conditions: initial potential -0.4 V; step potential 0.15 mV; scan rate 1.5 mV/s. A transient chronoamperometric Cd^{2+} (cadmium cation) reduction was performed using a deposition potential, E_d, of -0.8 V. Reductions were performed in solution and then in the gel. For the measurements in the gel, the microelectrode tip was placed in direct contact with the gel surface while the reference electrode remained in solution. For voltammetry experiments, an amalgamated gold electrode was used as the working electrode; a glassy carbon electrode was employed as the counter electrode and an Ag-AgCl electrode was employed as the reference electrode. The schematic of the microelectrode voltammetry cell is depicted in Fig.2.12.

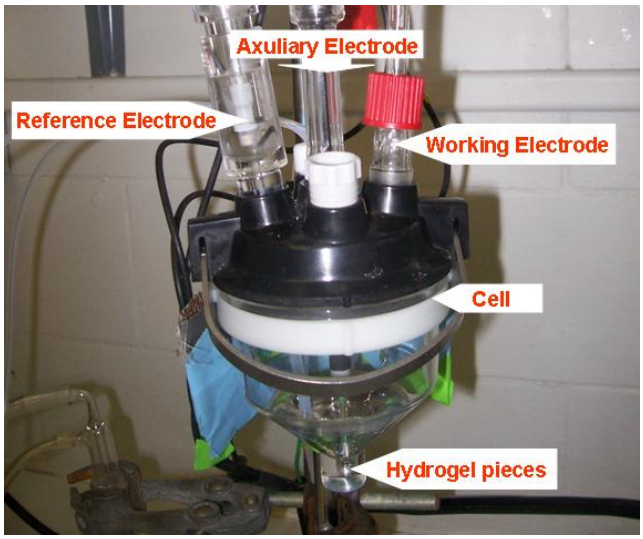

Figure 2.12. Photo of the electrochemical cell for microelectrode voltammetry

When measurements are made in the bulk solution and after the slow insertion of a microelectrode into the hydrogel, Donnan potentials can be determined in two ways: first, directly from the shift in the voltammetric Cd half-wave potential, which is equivalent to the Donnan potential:

$$\Delta E_{1/2} = E_{1/2_g} - E_{1/2_w} \tag{2-28}$$

where $E_{1/2}$ is the half-wave potential and ΔE is the difference in half-wave potentials (Fig. 2.13), and secondly, from the ratio of limiting currents:

$$\Pi = \frac{\left[Cd^{2+}\right]_g}{\left[Cd^{2+}\right]_w} = e^{\frac{-2F\psi_D}{RT}} = \frac{I_g^L}{I_w^L} \times \frac{D_w^m}{D_g^m} \qquad (2\text{-}29)$$

where the (Donnan) partition coefficient, Π, represents the enhancement of metal in the gel due to electrostatic effects[37,38], R is the gas constant, and I_g^L / I_w^L is the ratio of limiting currents measured in gel and water, respectively.

2.3.3 Voltammetric results and discussion

The characteristic diffusion-limited, steady-state voltammetric wave is shown in Fig. 2.13 for a gel in Donnan equilibrium with a solution containing the electroactive metal ion.

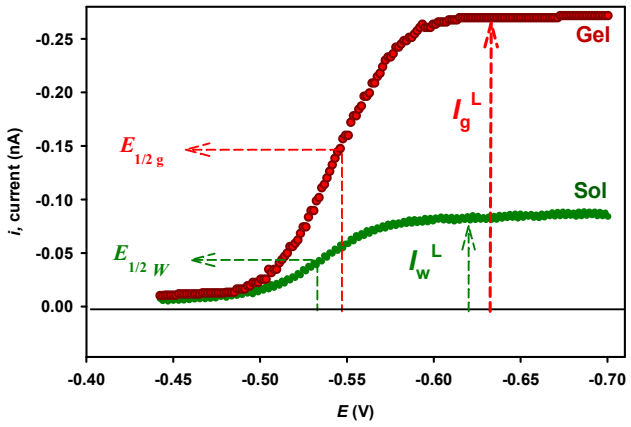

Figure 2.13. Metal ion voltammogram obtained from a gel-sol system in Donnan equilibrium. The important features are the limiting current (I^L) and half-potential, $E_{1/2}$ in gel (g) and water solution (w).

The voltammogram is first obtained in solution (subscript "W" in Fig. 2.13) and subsequently, the microelectrode is placed into contact with the surface of the gel (subscript

"g" in Fig. 2.13). The concentration of the metal ion was much smaller than the electrolyte concentration so that the migration effect for diffusion in the gel should be negligible.

Transient voltammetry was performed to reveal whether Cd bound to the gel phase could contribute to the Cd flux at the electrode surface. When the reduction current, *I*, is plotted as a function of time, the area under the curve corresponds to the amount of Cd that is reduced at the electrode surface. The hatched areas in Figure 2.14 represent the transient responses for the gel and for water prior to the attainment of the steady-state current (symbolized by the horizontal line). As shown in Fig. 2.14, an upward shift in the (negative) steady-state current was observed for measurements performed in the gel. Nonetheless, the nature of the transient response was similar in solution and in the gel with the apparent attainment of steady-state conditions after a few seconds. The combination of an increased steady-state current and a similar transient response strongly suggests that the voltammetric technique was only measuring diffusion limited Cd within the pores of hydrogel and not Cd bound to the hydrogel [39]. These curves are consistent with results from the paper (chapter 3;Fig. 3.3b) showing that the electrostatic partition coefficient was nearly identical to the overall partition coefficient.

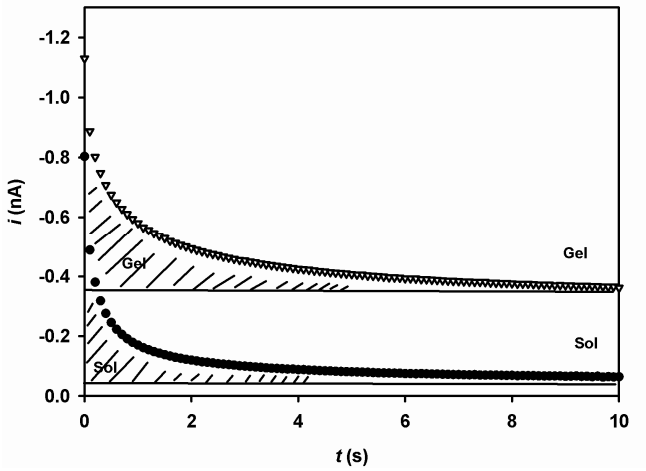

Figure 2.14. Current transient for Cd ion reduction at E_d = -0.8 V in the gel and in solution, c_{Cd}=10^{-5} M, *I*= 5 x10^{-4} M, r_0 (diameter of microelectrode)= 25 μm.

2.4. Diffusion equilibration technique (DET)

2.4.1 DET theory

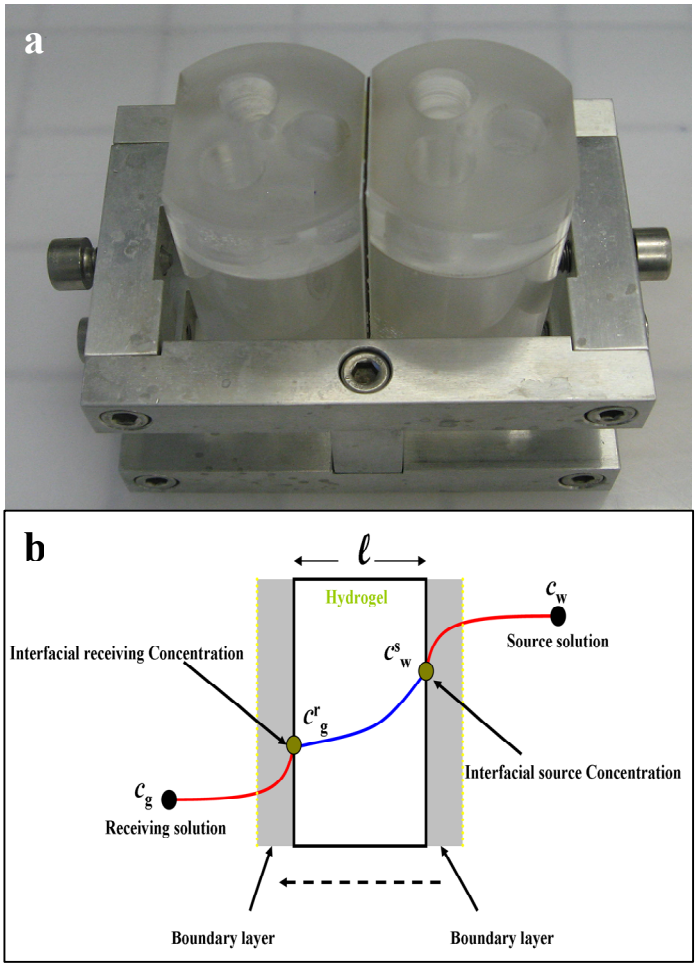

Figure 2.15. (a) The diaphragm diffusion cell used to measure mutual diffusion coefficients; (b) schematic of the concentration profile in the diffusion cell. Symbols employed correspond to: ℓ, the gel thickness; c_w, the concentration of solute (metal) in the source solutions; c_g, the concentration of solute (metal) in the receiving solution.

A photo and a schematic of the diffusion cell are given in Fig. 2.15. In the diffusion cell, the steady-state flux of a solute passing through a hydrogel can be given by[40]

$$J = D_g^m \frac{dc_g}{dx} \quad (2\text{-}30)$$

where D_g^m (cm^2 s^{-1}) is the mutual diffusion coefficient of the solute and c_g is its concentration in the hydrogel, and x is the thickness of hydrogel. Equation 2-1 can be rewritten as[41]:

$$J = D_g^m \frac{(c_g^s - c_g^r)}{\ell} \tag{2-31}$$

where ℓ is the gel thickness and c_g^s and c_g^r are the concentrations of the solute at the gel/source and gel/receiving solution interfaces, respectively. For an ionic solute, the electrostatic partition coefficient at both interfaces of the hydrogel, i.e. the total concentration of the ion in the gel with respect to that in the solution is given by:

$$\Pi = \frac{c_g^s}{c_w^s} = \frac{c_g^r}{c_w^r} \tag{2-32}$$

where c_w^s and c_w^r are the total concentrations of the ions in the source and receiving solutions, respectively. Note that in Equation 2-32, the chemically bound Cd concentration was neglected as it does not diffuse. Hence, total partition coefficient (Equation 1-12) was simplified to the electrostatic partition or (Donnan) partition coefficient Π (Equation 2-32) as steric (θ) and chemical (α) partitions can be considered 1 for small cations in weakly charged agarose.

If the diffusion boundary layer thicknesses at both interfaces are negligible then the flux can be obtained by combining Equations 2-31 and 2-32:

$$J = \frac{\Pi D_g^m (c_w^s - c_w^r)}{\ell} \tag{2-33}$$

Since the flux (mol cm^{-2} min^{-1}) is simply the change in the number of moles of solute over time (dN/dt) for a given surface of hydrogel, A, it is possible to determine the mutual diffusion coefficient of the ion in the gel from the measured change in concentration (N/V) of a given volume, V, of receptor solution:

$$\frac{dc}{dt} = \frac{A\Pi D_g^m (c_w^s - c_w^r)}{V\ell} \tag{2-34}$$

Typically, ΠD_g^m can be obtained from the slope of the steady-state (linear) increase of concentration in a receiving solution (initial concentration=0, Fig. 2.16). The electrostatic partition factor Π can be obtained from the electrochemical measurements (above).

2.4.2 DET materials and methods

The diffusion cell (also referred to as a *diaphragm cell*) is made up of two plastic compartments (containing the source and receiving solutions, separated by a small piece of hydrogel). The assembly is held together by a metal frame (Fig. 2.15). The solutions are stirred with a magnetic stirrer attached to a glass rod at rates determined by a digital stirrer. Identical volumes (100 mL) of an electrolyte solution are introduced into both compartments. A small volume (0.2-0.3 mL) of concentrated sample solution is added to the source compartment at the same time as an identical volume of the carrier solution (electrolyte without sample ions) is added to the receiving compartment. During the diffusion experiment, 1 mL samples are simultaneously removed from both compartments at appropriate time intervals (5 to 10 min) for further analysis of Cd ions with GF-AAS spectroscopy. Cd concentrations were determined using graphite furnace atomic absorption spectrometry (GF-AAS, Varian AA240Z) while $R6G^+$ concentrations were quantified used fluorescence measurements (Tecan spectrophotometer, Infinite200).

2.4.3 DET results and discussion

Typically, ΠD_g^m is obtained from the slope of the steady-state (linear) increase of concentration in a receiving solution (initial concentration=0, Figure 2.16).

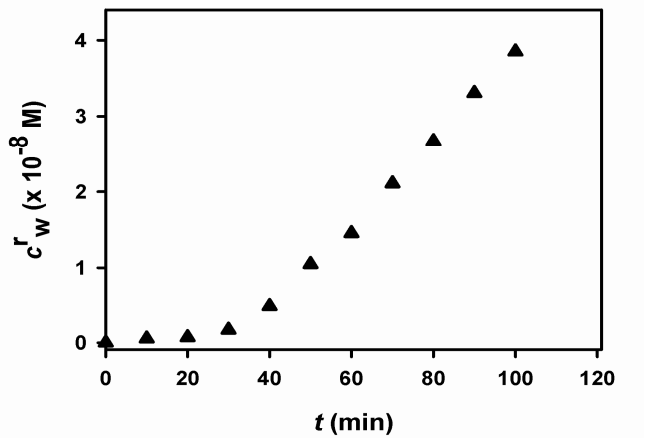

Figure 2.16. Cd concentration in the receiving compartment of a diffusion cell as a function of time; c= 10^{-5} M (I=10^{-4} M; pH=6), Cd measured by GF-AAS. The slope calculated here was 6x10^{-10} M min^{-1} (A=6.84 cm^2, ℓ =0.095 cm, V=100 cm^3).

2.5. References

1.Golmohamadi, M.; Davis, T. A.; Wilkinson, K. J. Diffusion and partitioning of cations in an agarose hydrogel. *The Journal of Physical Chemistry A* **2012,** 116, 6505-6510.

2.Magde, D.; Elson, E.; Webb, W. W. Thermodynamic fluctuations in a reacting system—measurement by fluorescence correlation spectroscopy. *Physical Review Letters* **1972,** 29, 705-708.

3.Gendron, P. O.; Avaltroni, F.; Wilkinson, K. J. Diffusion coefficients of several rhodamine derivatives as determined by pulsed field gradient-nuclear magnetic resonance and fluorescence correlation spectroscopy. *Journal of Fluorescence* **2008,** 18, 1093-1101.

4.Lead, J.; Wilkinson, K. J.; Starchev, K.; Canonica, S.; Buffle, J. Determination of diffusion coefficients of humic substances by fluorescence correlation spectroscopy: role of solution conditions. *Environmental Science & Technology* **2000,** 34, 1365-1369.

5.Lee, J.; Lee, Y.; Kim, S. W. Measurement of the diffusion coefficients of single molecules by using fluorescence correlation spectroscopy with a software correlator. *Journal of the Korean Physical Society* **2011,** 59, 3171-3176.

6.Han, Y.; Lee, J.; Lee, Y.; Kim, S. W. Measurement of the diffusion coefficients of fluorescence beads and quantum dots by using fluorescence correlation spectroscopy. *Journal of the Korean Physical Society* **2011,** 59, 3177-3181.

7.Weiss, M.; Hashimoto, H.; Nilsson, T. Anomalous protein diffusion in living cells as seen by fluorescence correlation spectroscopy. *Biophysical Journal* **2003,** 84, 4043-4052.

8.Gennerich, A.; Schild, D. Anisotropic diffusion in mitral cell dendrites revealed by fluorescence correlation spectroscopy. *Biophysical Journal* **2002,** 83, 510-522.

9.Rigler, R.; Mets, U.; Widengren, J.; Kask, P. Fluorescence correlation spectroscopy with high count rate and low-background-analysis of translational diffusion. *European Biophysics Journal with Biophysics Letters* **1993,** 22, 169-175.

10.Pieper, C. M.; Enderlein, J. Fluorescence correlation spectroscopy as a tool for measuring the rotational diffusion of macromolecules. *Chemical Physics Letters* **2011,** 516, 1-11.

11.Kohler, R. H.; Schwille, P.; Webb, W. W.; Hanson, M. R. Active protein transport through plastid tubules: velocity quantified by fluorescence correlation spectroscopy. *Journal of Cell Science* **2000,** 113, 3921-3930.

12.Schuttpelz, M.; Schoning, J. C.; Doose, S.; Neuweiler, H.; Peters, E.; Staiger, D.; Sauer, M. Changes in conformational dynamics of mRNA upon AtGRP7 binding studied by fluorescence correlation spectroscopy. *Journal of the American Chemical Society* **2008,** 130, 9507-9513.

13.Enderlein, J.; Gregor, I.; Patra, D.; Dertinger, T.; Kaupp, U. B. Performance of fluorescence correlation spectroscopy for measuring diffusion and concentration. *Chemphyschem* **2005,** 6, 2324-2336.

14.Stromqvist, J.; Nardo, L.; Broekmans, O.; Kohn, J.; Lamperti, M.; Santamato, A.; Shalaby, M.; Sharma, G.; Di Trapani, P.; Bondani, M.; Rigler, R. Binding of Biotin to Streptavidin: A combined fluorescence correlation spectroscopy and time-resolved fluorescence study. *European Physical Journal-Special Topics* **2011,** 199, 181-194.

15.Widengren, J.; Rigler, R. Mechanisms of photobleaching investigated by fluorescence correlation spectroscopy. *Bioimaging* **1996,** 4, 149-157.

16.Jameson, D.; Ross, J.; Albanesi, J. Fluorescence fluctuation spectroscopy: ushering in a new age of enlightenment for cellular dynamics. *Biophysical Reviews* **2009,** 1, 105-118.

17.Krichevsky, O.; Bonnet, G. Fluorescence correlation spectroscopy: the technique and its applications. *Reports on Progress in Physics* **2002,** 65, 251-297.

18.Ries, J.; Schwille, P. Fluorescence correlation spectroscopy. *Bioessays* **2012,** 34, 361-368.

19.Cabalero-George, C.; Sorkalla, T.; Bermingham, E.; Haberlein, H. Fluorescence correlation spectroscopy (FCS) a powerful biophysic method for drug discovery: study of Alexa532-endothelia 1 binding on the endothelia ETA receptor on living cells. *Planta Medica* **2008,** 74, 1156-1157.

20.Gosch, M.; Rigler, R. Fluorescence correlation spectroscopy of molecular motions and kinetics. *Advanced Drug Delivery Reviews* **2005,** 57, 169-190.

21.Beranova, L.; Humpolickova, J.; Hof, M. Principles and applications of fluorescence lifetime correlation spectroscopy. *Optical Sensors 2009* **2009,** 7356.

22.Widengren, J.; Mets, U.; Rigler, R. Fluorescence correlation spectroscopy of triplet-states in solution - a theoretical and experimental-study. *Journal of Physical Chemistry* **1995,** 99, 13368-13379.

23.Leng, X. J.; Starchev, K.; Buffle, J. Adsorption of fluorescent dyes on oxide nanoparticles studied by fluorescence correlation spectroscopy. *Langmuir* **2002,** 18, 7602-7608.

24.Malchus, N.; Weiss, M. Elucidating anomalous protein diffusion in living cells with fluorescence correlation spectroscopy-facts and pitfalls. *Journal of fluorescence* **2010,** 20, 19-26.

25.Weiss, M.; Hashimoto, H.; Nilsson, T. Anomalous protein diffusion in living cells as seen by fluorescence correlation spectroscopy. *Biophys J* **2003,** 84, 4043-4052.

26.Hess, S. T.; Webb, W. W. Focal volume optics and experimental artifacts in confocal fluorescence correlation spectroscopy. *Biophysical Journal* **2002,** 83, 2300-2317.

27.Schwille, P.; Ries, J. Principles and applications of fluorescence correlation spectroscopy (FCS). *Biophotonics: Spectroscopy, Imaging, Sensing, and Manipulation* **2011**, 63-85.

28.Gregor, I.; Patra, D.; Enderlein, J. Optical saturation in fluorescence correlation spectroscopy under continuous-wave and pulsed excitation. *Chemphyschem* **2005,** 6, 164-170.

29.Luther, G. W.; Reimers, C. E.; Nuzzio, D. B.; Lovalvo, D. In situ deployment of voltammetric, potentiometric. and amperometric microelectrodes from a ROV to determine dissolved O_2, Mn, Fe, S(-2), and pH in porewaters. *Environmental Science & Technology* **1999,** 33, 4352-4356.

30.Brendel, P. J.; Luther, G. W. Development of a gold amalgam voltammetric microelectrode for the determination of dissolved Fe, Mn, O_2, and S(-II) in porewaters of marine and fresh-Water sediments. *Environmental Science & Technology* **1995,** 29, 751-761.

31.A.J. Bard, L. R. F., *Electrochemical Methods: Fundamentals and Applications*. second ed.; Wiley, New York: 2001.

32.Luther, G. W.; Brendel, P. J.; Lewis, B. L.; Sundby, B.; Lefrancois, L.; Silverberg, N.; Nuzzio, D. B. Simultaneous measurement of O_2, Mn, Fe, I^-, and S(-II) in marine pore waters with a solid-state voltammetric microelectrode. *Limnology and Oceanography* **1998,** 43, 325-333.

33.Ohshima, H.; Kondo, T. Relationship among the surface-potential, Donnan potential and charge-density of ion-penetrable membranes. *Biophysical Chemistry* **1990,** 38, 117-122.

34.Davis, T. A.; Kalis, E. J. J.; Pinheiro, J. P.; Town, R. M.; Van Leeuwen, H. P. Cd(II) speciation in alginate gels. *Environmental Science & Technology* **2008,** 42, 7242-7247.

35.Ohshima, H.; Ohki, S. Donnan potential and surface-potential of a charged membrane. *Biophysical Journal* **1985,** 47, 673-678.

36.Ohshima, H.; Kondo, T. Relationship among the surface potential, Donnan potential and charge density of ionpenetrable membranes. *Biophysical Chemistry* **1990,** 38, 117–122.

37.Van Leeuwen, H. P.; Davis, T. A.; Yezek, L. P.; Pinheiro, J. P. Measurement of Donnan potentials in gels by in situ microelectrode voltammetry. *Journal of Electroanalytical Chemistry* **2005,** 584, 100-109.

38.Davis, T. A.; Kalis, E. J.; Pinheiro, J. P.; Town, R. M.; Van Leeuwen, H. P. Cd(II) speciation in alginate gels. *Environmental Science & Technology* **2008,** 42, 7242-7247.

39.Kalis, E. J. J.; Davis, T. A.; Town, R. M.; Van Leeuwen, H. P. Impact of ionic strength on Cd(II) partitioning between alginate gel and aqueous media. *Environmental Science & Technology* **2009,** 43, 1091-1096.

40.Fatin-Rouge, N.; Milon, A.; Buffle, J.; Goulet, R. R.; Tessier, A. Diffusion and partitioning of solutes in agarose hydrogels: the relative influence of electrostatic and specific interactions. *Journal of Physical Chemistry B* **2003,** 107, 12126-12137.

41.Stewart, P. S. A review of experimental measurements of effective diffusive permeabilities and effective diffusion coefficients in biofilms. *Biotechnology and Bioengineering* **1998,** 59, 261-272.

42.Takenaka, S.; Pitts, B.; Trivedi, H. M.; Stewart, P. S. Diffusion of macromolecules in model oral biofilms. *Applied and Environmental Microbiology* **2009,** 75, 1750-1753.

43.Marcotte, L.; Therien-Aubin, H.; Sandt, C.; Barbeau, J.; Lafleur, M. Solute size effects on the diffusion in biofilms of Streptococcus mutans. *Biofouling* **2004,** 20, 189-201.

44.Thurnheer, T.; Gmur, R.; Shapiro, S.; Guggenheim, B. Mass transport of macromolecules within an in vitro model of supragingival plaque. *Applied and Environmental Microbiology* **2003,** 69, 1702-1709.

45.Bryers, J. D.; Drummond, F. Local macromolecule diffusion coefficients in structurally non-uniform bacterial biofilms using fluorescence recovery after photobleaching (FRAP). *Biotechnol Bioeng* **1998,** 60, 462-473.

Chapter 3

Diffusion and partitioning of cations in an agarose hydrogel

Mahmood Golmohamadi, Thomas A. Davis and Kevin J. Wilkinson, Journal of Physical Chemistry A, 116, 2012, p 6505.

3.1. Abstract

In the majority of applications using hydrogels, it is necessary to understand how solutes diffuse and interact with the solid phase. In this paper, a low melt 1.5% agarose hydrogel was characterized by measuring diffusion coefficients and the gel's Donnan potential as a function of ionic strength (10^{-4}-10^{-1} M) and pH (3-7). Self and mutual diffusion coefficients were determined in the hydrogel for Cd^{2+} and a charged rhodamine derivative. Self-diffusion was measured by fluorescence correlation spectroscopy whereas mutual diffusion was evaluated using a diffusion cell. In contrast to the results observed for the diffusion cell, self-diffusion of rhodamine 6G increased from 50% to 90% of that found in water as the ionic strength increased from 10^{-4} to 10^{-1} M (pH=6). The combined observations of a decreasing diffusive flux in parallel with an increasing diffusion coefficient were attributed to the gel's Donnan potential. Gel Donnan potentials were evaluated from voltammetrically determined Cd(II) concentrations, obtained using an Au amalgam microelectrode. Donnan potentials varied from -30 mV to 0 mV as the ionic strength increased from 10^{-4} to 10^{-1} M (pH=6). At the low ionic strengths, Donnan potentials of this magnitude accounted for a 13x enhancement of Cd^{2+} concentrations in the hydrogel, which was consistent with measurements obtained by a nitric acid extraction of the gel (15x) and able to explain the apparent discrepancy between mutual and self-diffusion measurements. Finally, the overall diffusion of the positively charged substrates decreased as the pH was decreased from 12 to 3.

3.2. Introduction

Hydrogels, including agarose, are used in a large number of pharmaceutical, biological and environmental applications[1-3]. Agarose consists of a 3D polymer network of linear agarobiose units that are associated through hydrogen bonds and hydrophobic interactions[4, 5]. The structure of the gel will vary, depending upon chemical factors such as purity and concentration and physical factors including the cooling rate during gel formation. Pore size distributions ranging from 1 to 900 nm have been determined by neutron scattering[6], transmission electron microscopy (TEM)[7], and atomic force microscopy (AFM)[8].

The diffusion of solutes into, through and out of gels is often a key to understanding their function. The rate of steady-state diffusion of a solute through a hydrogel will depend upon physical (e.g. obstruction[9-11]) and chemical (e.g. hydrogen bonding, electrostatic effects[12, 13]) interactions between the two phases, which are dependent upon the physicochemical properties of both the solute and the gel. For example, solute size[14] and charge[15] and the extent of gel crosslinking[16] have been well documented to affect diffusion in hydrogels. For highly charged gels such as alginate and polyacrylamide, the Donnan potential difference, ψ_D, at the gel-water interface, can result in a significant partitioning of charged solutes[17-19] due to ionic interactions and hydrogen bonding. For agarose, the negative charge resulting from sulfonate, ester sulfate, ketal pyruvate, and carboxylic functional groups can also lead to significant Donnan potentials[12] resulting in both an accumulation of cations in the gel[12] and a modification of its effective pore size due to Debye layer effects. The diffusive properties of agarose result from a complex interplay among chemical and electrostatic partitioning and obstruction effects that have only rarely been systematically studied or have given contradictory results[20, 21].

In this paper, several techniques were coupled in order to better understand the important factors controlling diffusion in a low melt agarose hydrogel under conditions of variable pH and ionic strength. Measurements of Donnan potential were determined by *in situ* voltammetry while self and mutual diffusion coefficients were determined by fluorescence correlation spectroscopy (FCS) and diffusion equilibration, respectively. The results demonstrate that the charge of the hydrogel had a strong influence on its diffusive

properties and that it was critical to distinguish between measurements of self and mutual diffusion when quantifying solute mobility.

3.3. Theory

3.3.1 Measurements of mutual diffusion

In diffusion cell experiments, the presence of a chemical gradient from a source to a receiving compartment drives the diffusive flux, J_{diff}, of solute across a thin layer of hydrogel. Steady-state measurements of chemical fluxes can be employed to determine mutual diffusion coefficients (chapter 2) [22]:

$$\frac{dc}{dt} = \frac{A\Pi D_g^m (c_w^s - c_w^r)}{V\ell} \qquad (3\text{-}1)$$

where D_g^m ($cm^2\ s^{-1}$) is the average mutual diffusion coefficient of a given compound across a slice of gel of thickness, ℓ, A is the exposed surface area of the gel, Π is the electrostatic partition coefficient, V is the volume of the source cell, dc/dt is the measured initial rate of increase of the compound in the receiving solution and c_w^s and c_w^r are the initial concentrations in the source and receiving compartments, respectively. For a given thickness of a slice of gel (ℓ=0.95 mm) and volume of source compartment (V=100 mL), ΠD_g^m can be determined from the observed increase in concentration in the receiving compartment with time.

3.3.2 Measurements of self-diffusion

In fluorescence correlation spectroscopy (FCS), the delay lag time, τ, of a fluorescent probe is measured in a small volume that is defined by the optics of a confocal microscope. Variations of the fluorescence intensity are attributed to the translational

diffusion of fluorophores into and out of the confocal volume. Diffusion times are determined from an autocorrelation function, *G(t)*:

$$G(\tau) = b + \left(\frac{1}{N}\right)\left(1+\frac{\tau}{\tau_{\mathrm{D}}}\right)^{-1}\left(1+\frac{\tau}{p^2\tau_{\mathrm{D}}}\right)^{-\frac{1}{2}} \qquad (3\text{-}2)$$

where b is the limiting value of $G(\tau)$ for $\tau \to \infty$; N is the average number of fluorescent particles diffusing through the confocal volume, τ is the measurement time and p is the structure parameter (ratio of the transversal, ω_{xy}, to the longitudinal, ω_{z}, dimension of the confocal volume: $p = \omega_{\mathrm{z}}/\omega_{\mathrm{xy}}$). Self-diffusion coefficients, D^{s}, were determined from the characteristic diffusion time, τ_D, that a fluorescent probe pass through in the confocal volume:

$$D^{\mathrm{s}} = \frac{\omega_{xy}^2}{4\tau_D} \qquad (3\text{-}3)$$

Prior to measurements, ω_{xy} was obtained from a calibration of the dimensions of the confocal volume, using rhodamine 110 (R110), which has a known diffusion coefficient of 4.42×10^{-10} $\mathrm{m^2\,s^{-1}}$ [23].

3.3.3 Measurement of Donnan potential (ψ_{D}) and the Donnan partition coefficient (Π).

For an inlaid-disk microelectrode, the experimentally acquired, diffusion-limited, steady state current, I^{L}, can be used to determine the electroactive concentration of an element[22]:

$$I^{\mathrm{L}} = 4n\mathrm{F}D^{\mathrm{m}}c\,r_0 \qquad (3\text{-}4)$$

where c and D^{m} refer to the concentration and (mutual) diffusion coefficient of the electroactive species in the bulk solution, w, or in the gel, g; r_0 is the radius of the microelectrode, n is the number of electrons transferred and F is the Faraday constant. When measurements are made in the bulk solution and after the slow insertion of a

microelectrode into the hydrogel, Donnan potentials can be determined in two ways: first, directly from the shift in the voltammetric Cd half-wave potential (Eq. 2-28, chapter 2), which is equal to Donnan potential, and second, from the ratio of limiting currents with Equation 3-5 as follows:

$$\Pi = \frac{\left[Cd^{2+}\right]_g}{\left[Cd^{2+}\right]_w} = e^{\frac{-2F\psi_D}{RT}} = \frac{I_g^L}{I_w^L} \times \frac{D_w^m}{D_g^m} \qquad (3\text{-}5)$$

where the Donnan partition coefficient represents the enhancement of metal in the gel due to electrostatic effects[18,19], R is the gas constant (8.314 J.mol^{-1}.K^{-1}), T is the temperature (295 K) and I_g^L / I_w^L is the ratio of limiting currents measured in gel and water, respectively.

3.4. Materials and methods

3.4.1 Chemicals

A standard, low melt agarose (Bio-Rad, 162-0100) was used without further purification. A 1.5% gel was prepared by first dissolving the solid in ultrapure water (R>18 MΩ cm, total organic carbon <2 μg C L^{-1}). The mixture was then covered, heated (90 ^{o}C) and stirred for 40-60 minutes. The warm, clear solution was transferred into preheated (70 ^{o}C) gel-casting assemblies and left to slowly cool to its gelling temperature (< 37 ^{o}C). Where required, ionic strength was adjusted using $NaNO_3$ (Sigma, suprapur). Rhodamine 6G (R6G) was purchased from Sigma-Aldrich. Cd(II) solutions were prepared from $Cd(NO_3)_2$ (Sigma).

3.4.2 Diffusion equilibration (mutual diffusion coefficients)

In the diffusion cell measurements, the agarose hydrogel was placed between two compartments (the source and the receiving solutions) that contained identical volumes

(100 mL) of mechanically stirred solutions. Gels were first left to equilibrate overnight in an electrolyte solution containing no Cd^{2+}/$R6G^{+}$. On the day of the experiment, solutions with identical ionic strengths were prepared in the presence (source compartment) or absence (receiving compartment) of 10^{-5} M Cd^{2+}/$R6G^{+}$. Small volumes (0.3 mL) of solution were sampled from both compartments at 5-10 min. intervals to a maximum of 2 hours. Cd concentrations were determined using graphite furnace atomic absorption spectrometry (GF-AAS, Varian AA240Z) while $R6G^{+}$ concentrations were quantified used fluorescence measurements (Tecan spectrophotometer, Infinite200). Following measurements with Cd^{2+} or $R6G^{+}$, the gel and diffusion cell were tested for micro tears in the gel by repeating the experiment with Dextran blue (Molar mass= 2,000,000 D; Sigma) and monitoring absorbance (620 nm, Tecan spectrophotometer) in the receiving solution.

3.4.3 Fluorescence correlation spectroscopy (self-diffusion coefficients)

Diffusion coefficients of fluorescent probes were measured by FCS using a Leica TCS SP5 laser scanning microscope equipped with an argon ion laser functioning at 488 nm. An avalanche photodiode detector was used to quantify fluorescence intensity fluctuations. A small quantity (0.25 mL) of liquid agarose (60 ^{o}C) was introduced into each of the 8 wells of an FCS optical cell and cooled to room temperature. Electrolyte solutions containing $R6G^{+}$ (typically 2×10^{-8} M) were added to the top of the gel and left to equilibrate overnight. At least 1 hour before FCS measurements, the solutions were renewed. Diffusion coefficients were measured in both the hydrogel and in water (identical pH and ionic strength). Results are presented as the mean and standard deviation of triplicate measurements, with each measurement being the average obtained from 8 different locations within the same gel. At each location, an acquisition time of 100 s was used in order to attain a good signal-to-noise ratio.

3.4.4 Voltammetry (Donnan potential and Donnan partition coefficients)

Conventional steady-state voltammetry was used to determine free Cd^{2+} in solution and in the gel according to the method previously outlined by Davis et al[18,24]. In brief, small pieces of the gels were equilibrated for 2 weeks in solutions at defined pH and ionic strength. Over 2 weeks, solutions were renewed 6 times in order to ensure that they had a constant Cd concentration (10^{-5} M; verified by GF-AAS) and pH (pH electrode, pH adjusted if necessary). For experiments examining the effect of pH, pH adjustments were performed with either HNO_3 (Fluka) or NaOH (Sigma-Aldrich) and ionic strengths were adjusted to 5×10^{-4} M with $NaNO_3$ (Sigma). For experiments evaluating the role of ionic strength, $NaNO_3$ was used as the electrolyte and pH was held constant at pH 6.0. Gel/solution samples were purged overnight with nitrogen in order to remove all traces of oxygen prior to their transfer to the electrochemical cell. Voltammetric measurements were made on an Ecochemie μAutolab III potentiostat combined with a Metrohm 663 VA stand. An amalgamated gold electrode (diameter of gold wire: r_0= 25 μm, CH instruments) was used as the working electrode; a glassy carbon electrode was employed as the counter electrode and an Ag-AgCl electrode was employed as the reference electrode. The gold electrode was extensively polished (1000 and 2400 grit silica carbide polishing paper; polishing cloth and successively finer diamond pastes (9, 6, 3, 1, 0.25 μm, Struers)). The electrode tip was sonicated between each polishing step. Mercury was plated onto the gold electrode at -0.4 V (vs. Ag-AgCl-3M KCl/ 0.25M KNO_3) in deoxygenated $5x10^{-3}$ M $Hg(CH_3COO)_2$ and 0.1 M $HClO_4$ (until 65-70 μC of charge had accumulated). Amalgam formation between Hg and Au was controlled according to the procedure of Brendel *et al*.[24] A custom-made Faraday cage was used to protect the microelectrode from excessive background. DC voltammetry was performed using the following conditions: initial potential -0.4 V; step potential 0.15 mV; scan rate 1.5 mV/s. A transient chronoamperometric Cd^{2+} reduction was performed using a deposition potential, E_d, of -0.8 V. Reductions were performed in solution and then in the gel. For the measurements in the gel, the microelectrode tip was placed in direct contact with the gel surface while the reference electrode remained in solution. For each data point, 8-10 measurements were performed in order to ensure a reproducible signal.

3.4.5 Chemical extraction (partition coefficients)

Cd associated with gel pieces that had been equilibrated with Cd was determined after by placing the pieces into a 0.1 M HNO_3 acid solution over 3-4 days. The volumes of circular gel pieces were determined by precisely measuring their thickness with callipers before and after equilibration. Cd determinations were performed by GF-AAS.

3.5. Results and discussion

3.5.1 Role of ionic strength on mutual diffusion

For the diffusion cell experiments, Cd^{2+} or $R6G^{+}$ concentrations were followed in the source and receiving compartments. In the receiving compartment, a short lag period (ca. 20 min., supporting information) was observed, which was attributed to equilibration of the $Cd^{2+}/R6G^{+}$ with the binding sites in the hydrogel. Subsequently, a constant solute flux (linear increase of the solute in the receiving compartment with time) was measured. Concentration-time slopes (dc/dt) obtained from this steady-state regime were used to determine the *apparent* mutual diffusion coefficient in the gel (ΠD_g^m) for different ionic strengths (Eq. 3-1, Fig. 3.1). For both Cd and R6G, the diffusive flux through the gel *decreased* substantially as ionic strength increased over the range of 10^{-4} to 10^{-1} M. Values obtained at high ionic strengths were very similar to literature values for the diffusion coefficients in water [12], however, values obtained at low ionic strength, greatly exceeded those found in water. Such an observation strongly suggested that the cations were being concentrated in the gel (i.e. $\Pi > 1$), thereby increasing the chemical gradient driving the diffusion.

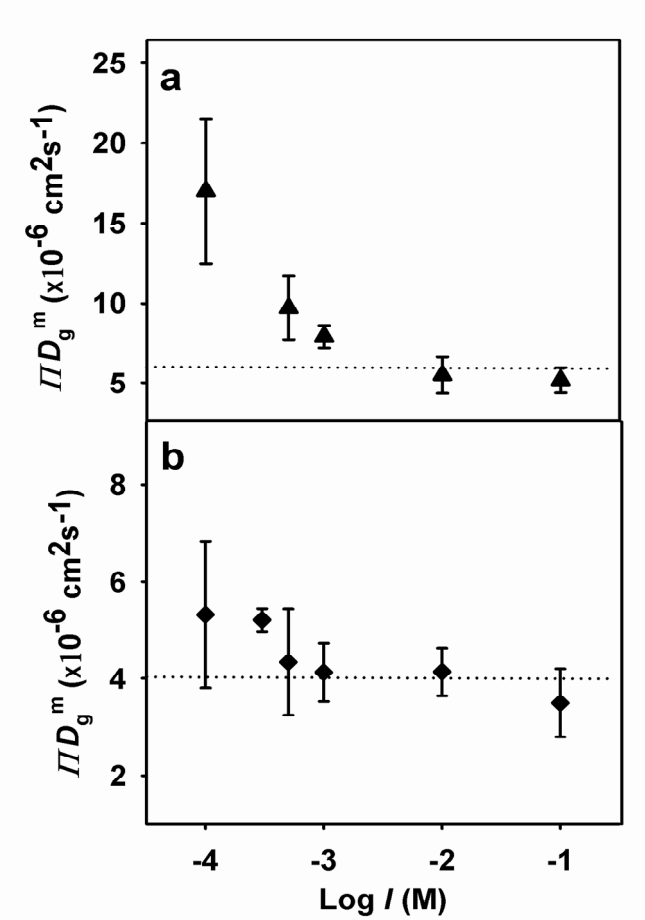

Figure 3.1. Apparent mutual diffusion coefficients (ΠD_g^m) as a function of ionic strength in a low melt (1.5%) agarose for: (a) Cd^{2+} (▲), $c_{Cd}=10^{-5}$ M, pH=6.0; (b) $R6G^+$ (♦), $c_{R6G}=10^{-5}$ M, pH=6.0. Error bars indicate standard deviations obtained on 3-6 replicate measurements. Literature values of the diffusion coefficients in water are indicated by the two dashed lines: $D_w = 6.2\times10^{-6}$ cm^2s^{-1} for Cd^{2+} and $D_w = 4.1\times10^{-6}$ cm^2s^{-1} for $R6G^+$ [12]

3.5.2 Role of ionic strength on self-diffusion

FCS can be used to obtain self-diffusion coefficients of the fluorescent R6G. At pH 6, R6G has a net charge of +1 and a similar size as the hydrated Cd^{2+}. In the aqueous phase, there may have been a small (4%) decrease in D_g^s from 10^{-4} to 10^{-1} M (Figure 3-2a, open points), which has previously been attributed to a partial dimerization of the probe[23, 25] at

the high ionic strengths. In this study, the magnitude of the decrease, if present, was small and not statistically significant.

Measurements in the gel are performed in a small volume defined by the confocal optics (ca. 1 μm^3) of the microscope. Effects due to gel inhomogeneities can be averaged out by performing measurements at several different locations. In this study, 8 measurements were performed over a total xy displacement of ca. 0.5 mm. For $R6G^+$ in the gel, self-diffusion coefficients (Fig. 3.2a, solid points) clearly increased as a function of increasing I (ca. 30%) with a resulting increase in the D^s_g/D^s_w values. An increase in D^s_g could be attributed to a weakened Coulombic attraction of the cationic R6G for the negatively charged gel or to an increase in the effective pore size of the gel due to a decreasing Debye layer (with increasing ionic strength).

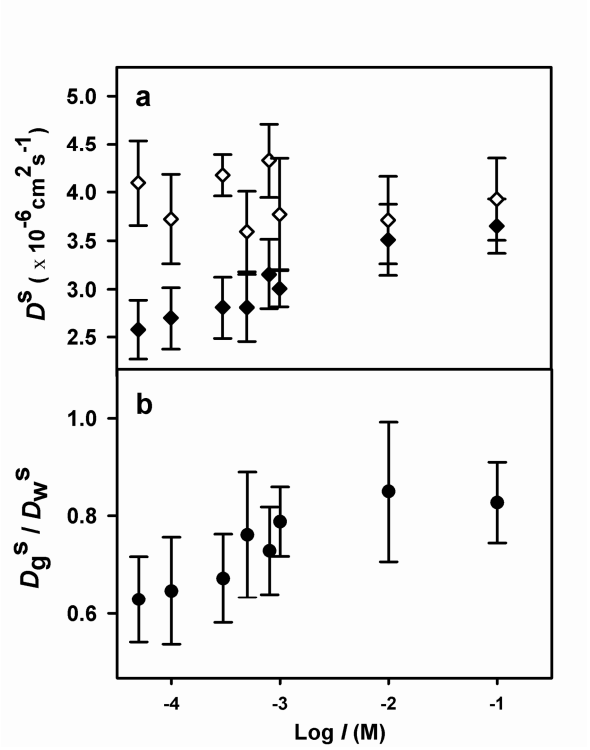

Figure 3.2**.** Self-diffusion coefficients for (a) $R6G^+$ in water, D^s_w (◊), and in the low melt (1.5%) agarose hydrogel, D^s_g (♦), as a function of ionic strength, $c_{R6G}=2\times10^{-8}$ M, pH=6.0; (b) D^s_g / D^s_w values obtained from diffusion experiments examining R6G at various ionic strengths (pH=6). Error bars indicate standard deviations obtained on triplicate measurements.

The observation of a *decreasing* mutual diffusion (Fig. 3.1) concurrent with *increasing* self-diffusion coefficients (Fig. 3.2a) was initially counter-intuitive. Our hypothesis to explain the apparent contradiction was that mutual diffusion was increasing due to an increased chemical partitioning at low ionic strength whereas, self-diffusion would decrease due to the aforementioned increase in the effective pore size or partial binding of the probe. Indeed, larger concentrations of the cations in the gel (bound and free) should have relatively little impact on the FCS measurements of the self-diffusion coefficient–a constant background fluorescence due to probe binding is ignored in the analysis of the autocorrelation function (only fluctuations on the order of $\leq$ *ca.* 500 ms are taken into account in the analysis). The potential role of chemical partitioning on the diffusive flux is examined in the following sections.

3.5.3 Role of ionic strength on Donnan potentials

Donnan potentials were obtained from the shifts in half-potential, $\psi_D(E)$, observed for the same range of I values as above. As expected, Donnan potentials were largest for the lowest ionic strengths, especially $I \leq 10^{-3}$ M (e.g. -32 mV at $I=10^{-4}$ M, Fig. 3.3a). Large Donnan potentials will increase the concentration of cations in the gel, leading to an increased flux of cations and a larger diffusive flux. [26] Indeed, calculations of the Donnan partition coefficient (Eq. 3-5) showed that at an ionic strength of 10^{-4} M, free Cd^{2+} was about 12x higher within the gel as compared to the bulk solution (Fig. 3.3b, c). Total Cd concentrations leached from the gel using nitric acid were also plotted in 3.3c, along with the overall partition coefficients (Fig. 3.3b). Overall Cd content in the hydrogel also increased with decreasing ionic strength in solution in agreement with previous studies on other hydrogels.[27, 28] Under the assumption that the overall partitioning of Cd in the gel (Φ) resulted from steric (θ), electrostatic (Π) and chemical (α) interactions, i.e., $\Phi = \theta\, \Pi\, \alpha$ [12], electrostatic interactions were shown to predominate at the low ionic strengths, whereas at $I=10^{-2}$ M, Φ/Π was 1.36±0.06, indicating that the increased Cd in the gel could be attributed primarily to the specific association of Cd with binding sites in the hydrogel.

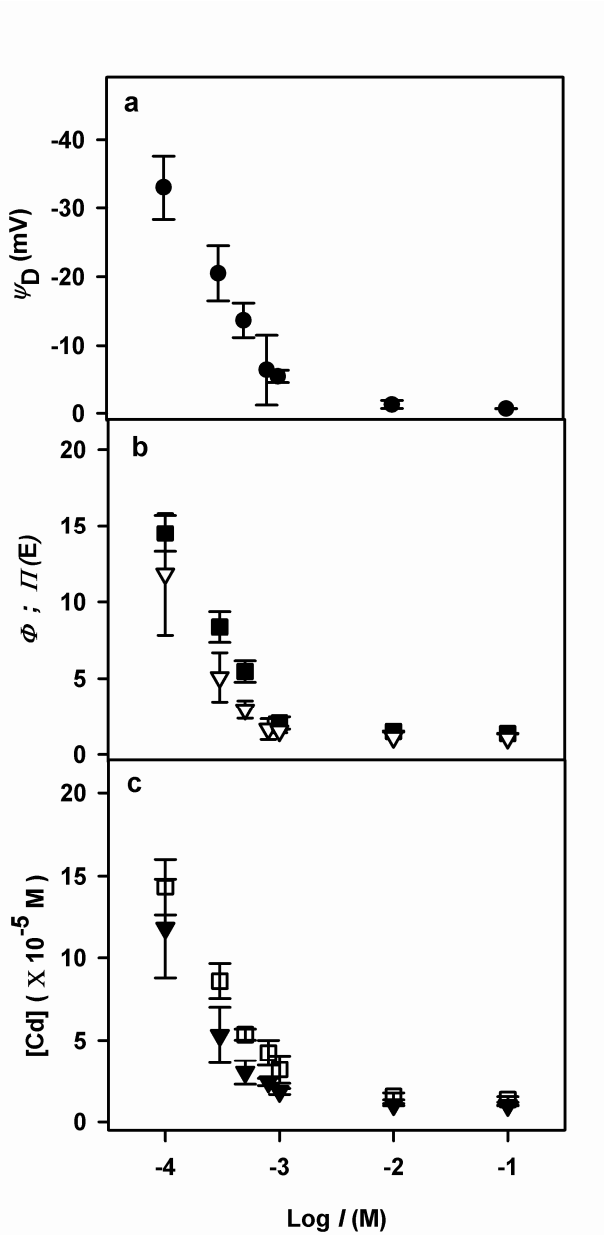

Figure 3.3. (a) Donnan potentials ψ_D (E) (●); (b) partition coefficients $\Pi_D(E)$ calculated from $\psi_D(E)$ (∇); and overall partition coefficients Φ (■); (c) Cd concentrations in the gel measured by leaching Cd from the hydrogel using nitric acid (□) and from $\Pi_D(E)$ values (▼) as a function of ionic strength. Measurements were performed in a low melt (1.5%) agarose gel, $c_{Cd}=10^{-5}$ M, pH=6.0.

3.5.4 Role of pH on Donnan potentials and diffusion

Titration of the agarose gave a pK_A^{int} = 3.9, resulting mainly from agarobiose-substituted pyruvic acid sites in the gel.[12] Indeed, Donnan potentials became less negative as the pH decreased from 6 to 3 (Fig. 3.4a), indicative of the acid p*K*a value.

As above, Donnan potentials were used to calculate the effect of Donnan partitioning on free Cd concentrations in the hydrogel (Fig. 3.4b). Over the examined range of pH, at these ionic strengths (I=5x10^{-4} M except at pH 3 where I=7x10^{-4} M), the effect of protonation was much less pronounced than that of I, with a maximum 3 fold increase of free Cd due to the Donnan effect (observed at pH 6 and 7). Much greater Cd concentrations were associated with the deprotonated gel as compared to values approaching the pK_a (Fig. 3.4c). Once again, Donnan partitioning accounted for nearly all of the observed gel partitioning (Fig. 3.4b). In line with the observation of a decreasing Donnan potential, ΠD_g^m increased as pH was increased from 3 to 7 (Fig. 3.5a).

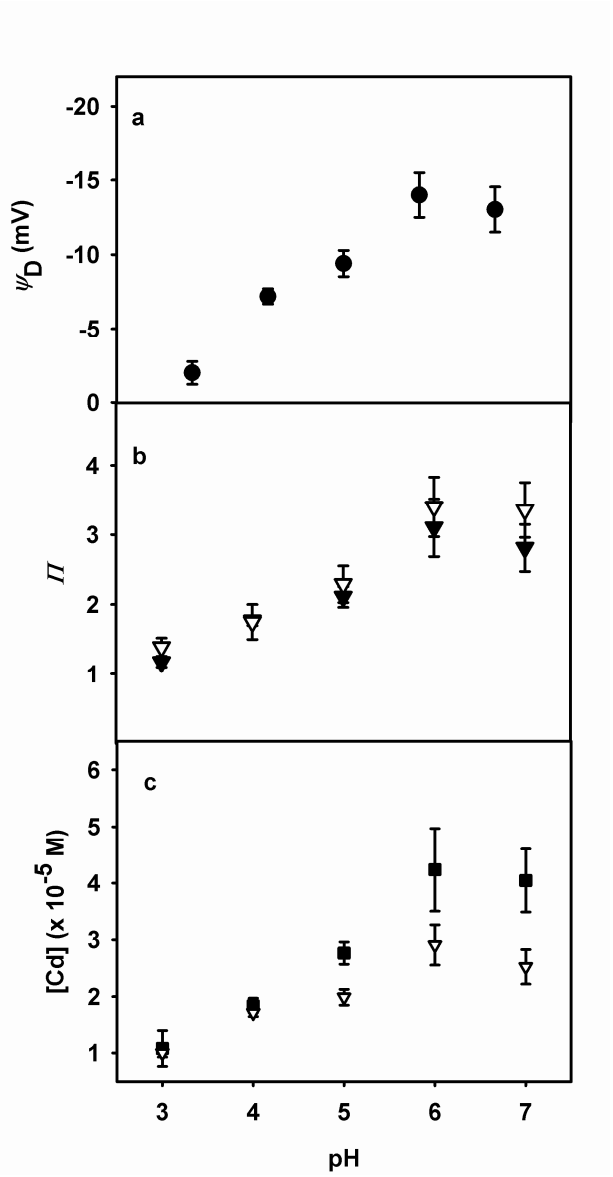

Figure 3.4. (a) Donnan potential as a function of pH in a low melt (1.5%) agarose gel, ψ_D calculated from the half-potential shifts (●); (b) Donnan partition coefficients (Π) as a function of pH in a low melt (1.5%) agarose gel; (c) Total and free Cd concentrations in the gel as a function of pH. Total Cd was measured by leaching the Cd from hydrogel with nitric acid (■) while Cd^{2+} was calculated from Donnan potential measurements (∇). All measurements were performed in a low melt (1.5%) agarose gel; $c_{Cd}=10^{-5}$ M; $I=5\text{x}10^{-4}$ M.

On the other hand, very little or no pH effect was observed for the self-diffusion coefficients (Fig. 3.5b). FCS measurements of self-diffusion were repeated twice: once for

a constant I ($5x10^{-4}$ M, white circles, Fig. 3.5b) and once where additional low and high pH values were acquired (at necessarily higher ionic strengths due to the pH adjustment, black circles, Fig. 3.5b). At these extreme pH values, D_g^s appeared to increase, although it may have been due to the additional ionic strength of the medium. As pH decreased from 9 to 3, protonation of the pyruvic acid sites did not appear to have a significant effect on the self-diffusion of the probe although it is theoretically possible that two effects were taking place simultaneously- increased D due to an increased effective pore size and decreased D due to probe aggregation. Similar to the ionic strength results, effects on the diffusive flux due to an increased chemical gradient (observed in the diffusion cell) greatly overwhelmed the direct effects on the self-diffusion coefficient (observed by FCS).

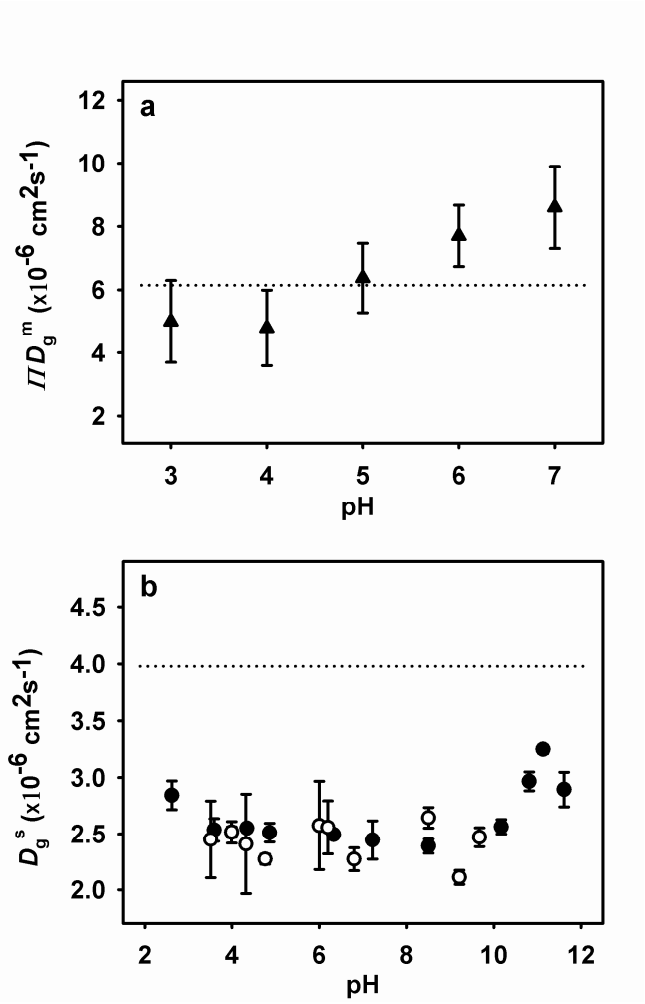

Figure 3.5. (a) Mutual diffusion coefficients (diffusion cell measurements) of Cd as a function of pH for a low melt (1.5%) agarose (▲) c_{Cd} =10^{-5} M; I=10^{-4} M; Dotted line corresponds to the average value for the (self-)diffusion coefficient of Cd in water; (b) Self diffusion coefficients for R6G in the low melt (1.5%) agarose hydrogel as a function of pH, c_{R6G}=2×10^{-8} M, (●) no fix I, (○) I= 5x10^{-4} M; Dotted line corresponds to the average value for the (self-)diffusion coefficient of the $R6G^+$ in water.

3.5.5 Comparison of mutual and self-diffusion

Comparison of all the data was not possible- FCS measurements could only be performed with fluorescent probes while voltammetry required the measurement of

electroactive species (such as Cd(II)). Nonetheless, when ΠD_g^m values (Fig. 3.1) obtained from the diffusion cell measurements for Cd(II) were divided by Π values (Fig. 3.3) determined from the electrochemical measurements, mutual diffusion coefficients could be obtained for Cd^{2+} in the gel (D_g^m, Fig. 3.6). Indeed, mutual diffusion coefficients obtained in this manner for Cd showed a very similar trend to self-diffusion coefficients measured by FCS for R6G (cf. Fig. 3.6 with Figs. 3.2a, 3.5b). The presumed similarity of the D_g^m and D_g^s values suggests that it was possible to average out effects due to gel heterogeneities and interface[29,18,30] effects by making measurements at several different spots in the gel.[1]

---

[1] Self-diffusion and mutual diffusion are two distinct transport events, which are experimentally measured on different time and length scales. In this work, diffusion was probed in hydrogels for which the gel structure (defined by the porosity, tortuosity, fiber radius and volume fraction) played a critical role. In this study, self-diffusion was measured in a probe-equilibrated hydrogel while mutual diffusion was determined from the diffusive flux generated in a gel that was held between two solutions of controlled physicochemistry. Self-diffusion is attributed to the Brownian motion of a probe that is generally measured over ms-s time intervals, across very small length scales (diameter of the FCS confocal volume: 0.2-0.3 μm), whereas, mutual diffusion fluxes were measured over 120 minutes across a gel of thickness≈ 1000 μm. Accordingly, measurements of self-diffusion are much more sensitive to the local gel heterogeneity than are mutual diffusion measurements. For example, in the case of a heterogeneous gel, measurements of self-diffusion in different local zones could result in a large distribution of the diffusion coefficients. For mutual diffusion measurements, the solution/hydrogel interface, especially where a Donnan effect is present, could significantly affect the diffusive flux (and thus the derived D values). In general, it is expected that values of self and mutual diffusion will become more similar for gels as they are more and more homogeneous. Indeed, in this work, the similarity of self and mutual diffusion coefficients in the agarose hydrogel indicated the relative homogeneity of the 1.5% agarose gel. These results are consistent with previous work for agarose where the mutual and self diffusion coefficients for small charged probes were very

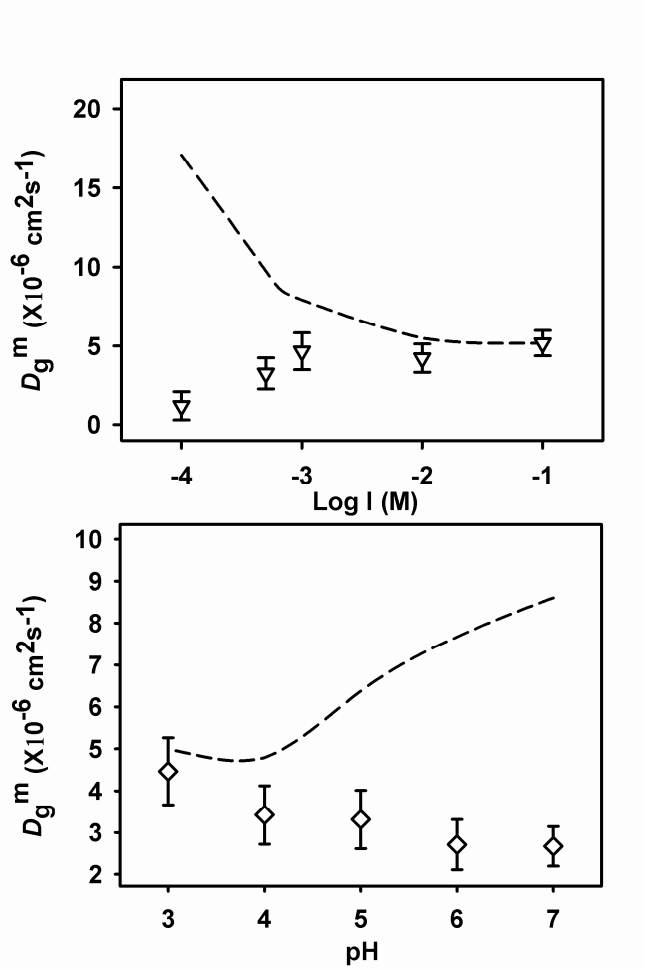

Figure 3.6. Mutual diffusion coefficients as a function of (a) ionic strength (c_{Cd} =10^{-5} M; pH=7) and (b) pH (c_{Cd} =10^{-5} M; I= 5x10^{-4} M) measurements of Cd in a low melt (1.5%) agarose. Dashed lines correspond to a best fit for $\Pi\, D_g^m$ values previously shown in Figs. 3-2a, 3-5b.

---

similar[31]. Therefore, it would appear that for solutes that are much smaller sizes than the gel pore sizes, the self-diffusion coefficients measured in one (small) part of the agarose gel can be extrapolated to the entire hydrogel. This similarity is mainly due to the fact the small probes do not experience anomalous or trapped diffusion in the pores of the gel.

3.6. Conclusion

Electrostatic, specific and steric interactions between solutes and ionic sites in hydrogels can be important effects which affect solute diffusion. The physicochemistry of the bulk solution and the nature of the gel will thus play an important role on solute diffusion, with strong effects observed due to ionic strength and pH variations. Indeed, for an ionic strength variation between 10^{-4} and 10^{-1} M, the mutual diffusion decreased while self-diffusion increased significantly. Similarly, mutual diffusion increased while self-diffusion remained constant for increasing deprotonation of the hydrogel. For the agarose hydrogel, most of the effect resulting from gel charge appeared to be due to increased solute partitioning in the gel rather than direct effects on the diffusion of the charged probes. Increased ionic strength or decreased pH resulted in a reduced Donnan potential such that very few effects were observed above an ionic strength of 10^{-3} M or below a pH of 6. Clearly, changes within the gel resulting from variations in the physicochemistry of the bulk solution, are critical for understanding the diffusion of charged solutes in hydrogels, even for weakly charged gels such as agarose.

3.7. Acknowledgements

The authors gratefully acknowledge the financial support of the *Fonds de recherche du Québec - Nature et technologies* (Team grant program) and the Natural Sciences Research Engineering Council of Canada (NSERC) Discovery Grant program. Helpful discussions with Dr. R.F. Domingos are greatly appreciated.

3.8. Supporting information

An overview of diffusion theory, diffusive fluxes in the DET, concentrations of Cd^{2+} in the diffusion cell versus time (determination of mutual diffusion), molecular structure of the $R6G^{+}$ and details of the Donnan potential calculation for the agarose gel

was published in the original paper. This material can be found in slightly revised form in sections 2.3 and 2.4 of Chapter 2.

3.9. References

1.Hamidi, M.; Azadi, A.; Rafiei, P. Hydrogel Nanoparticles in Drug Delivery. *Advanced Drug Delivery Reviews* **2008,** 60, 1638-1649.

2.Degryse, F.; Smolders, E.; Zhang, H.; Davison, W. Predicting Availability of Mineral Elements to Plants with the DGT Technique: A Review of Experimental Data and Interpretation by Modelling. *Environmental Chemistry* **2009,** 6, 198-218.

3.Town, R. M.; Yezek, L. P.; Van Leeuwen, H. P. Stripping chronopotentiometry at scanned deposition potential (SSCP). Part 8. Metal speciation analysis in gels. *J. Electroanal. Chem.* **2006,** 589, 203-211.

4.Arnott, S.; Fulmer, A.; Scott, W. E.; Dea, I. C.; Moorhouse, R.; Rees, D. A. The Agarose Double Helix and its Function in Agarose Gel Structure. *Journal of Molecular Biology* **1974,** 90, 269-284.

5.Rees, D. A. Structure, Conformation, and Mechanism in the Formation of Polysaccharide Gels and Networks. *Advances in Carbohydrate Chemistry and Biochemistry* **1969,** 24, 267-332.

6.Krueger, S.; Andrews, A. P.; Nossal, R. Small-Angle Neutron-Scattering Studies of Structural Characteristics of Agarose Gels. *Biophysical Chemistry* **1994,** 53, 85-94.

7.Waki, S.; Harvey, J. D.; Bellamy, A. R. Study of Agarose Gels by Electron-Microscopy of Freeze-Fractured Surfaces. *Biopolymers* **1982,** 21, 1909-1926.

8.Pernodet, N.; Maaloum, M.; Tinland, B. Pore size of agarose gels by atomic force microscopy. *Electrophoresis* **1997,** 18, 55-58.

9.Giddings, J. C.; Kucera, E.; Russel, C. P.; Myers, M. N. Statistical theory for the equilibrium distribution of rigid molecules in inert porous network. Exclusion chromatography. . *J. Phys. Chem. B,* **1968,** 72, 4397– 4408.

10.Johansson, L.; Skantze, U.; Lofroth, J. E. Diffusion and Interaction in Gels and Solutions .2. Experimental Results on the Obstruction Effect. *Macromolecules* **1991,** 24, 6019-6023.

11.Amsden, B. Solute Diffusion in Hydrogels. An Examination of the Retardation Effect. *Polymer Gels and Networks* **1998,** 6, 13-43.

12.Fatin-Rouge, N.; Milon, A.; Buffle, J.; Goulet, R. R.; Tessier, A. Diffusion and partitioning of solutes in agarose hydrogels: The relative influence of electrostatic and specific interactions. *Journal of Physical Chemistry B* **2003,** 107, 12126-12137.

13.Nilsson, L. G.; Nordenskiold, L.; Stilbs, P.; Braunlin, W. H. Macroscopic Counterion Diffusion in Solutions of Cylindrical Poly-Electrolytes. *Journal of Physical Chemistry* **1985,** 89, 3385-3391.

14.Petit, J. M.; Zhu, X. X.; Macdonald, P. M. Solute Probe Diffusion in Aqueous Solutions of Poly(vinyl alcohol) as Studied by Pulsed-gradient Spin-echo NMR Spectroscopy. *Macromolecules* **1996,** 29, 70-76.

15.Johansson, L.; Skantze, U.; Lofroth, J. E. Diffusion and Interaction in Gels and Solutions .6. Charged Systems. *Journal of Physical Chemistry* **1993,** 97, 9817-9824.

16.Amsden, B. Solute Diffusion within Hydrogels. Mechanisms and Models. *Macromolecules* **1998,** 31, 8382-8395.

17.Ohshima, H.; Ohki, S. Donnan potential and surface-potential of a charged membrane. *Biophysical Journal* **1985,** 47, 673-678.

18.van Leeuwen, H. P.; Davis, T. A.; Yezek, L. P.; Pinheiro, J. P. Measurement of donnan potentials in gels by in situ microelectrode voltammetry. *Journal of Electroanalytical Chemistry* **2005,** 584, 100-109.

19.Davis, T. A.; Kalis, E. J.; Pinheiro, J. P.; Town, R. M.; van Leeuwen, H. P. Cd(II) Speciation in Alginate Gels. *Environmental Science & Technology* **2008,** 42, 7242-7247.

20.Sangi, M. R.; Halstead, M. J.; Hunter, K. A. Use of the diffusion gradient thin film method to measure trace metals in fresh waters at low ionic strength. *Analytica Chimica Acta* **2002,** 456, 241-251.

21.Zhang, H.; Davison, W. Diffusional characteristics of hydrogels used in DGT and DET techniques. *Analytica Chimica Acta* **1999,** 398, 329-340.

22.Bard, A. J.; Faulkner, L. R., *Electrochemical Methods: Fundamentals and Applications*. Wiley, New York, 2001.

23.Gendron, P. O.; Avaltroni, F.; Wilkinson, K. J. Diffusion coefficients of several rhodamine derivatives as determined by pulsed field gradient-nuclear magnetic resonance and fluorescence correlation spectroscopy. *Journal of Fluorescence* **2008,** 18, 1093-1101.

24.Brendel, P. J.; Luther, G. W. Development of a Gold Amalgam Voltammetric Microelectrode for the Determination of Dissolved Fe, Mn, O-2, and S(-II) in Porewaters of Marine and Fresh-Water Sediments. *Environmental Science & Technology* **1995,** 29, 751-761.

25.Dare-Doyen, S.; Doizi, D.; Guilbaud, P.; Djedaini-Pilard, F.; Perly, B.; Millie, P. Dimerization of Xanthene dyes in Water: Experimental Studies and Molecular Dynamic Simulations. *Journal of Physical Chemistry B* **2003,** 107, 13803-13812.

26.Yezek, L. P.; Van Leeuwen, H. P. Donnan Effects in the Steady-state Diffusion of Metal Ions Through Charged Thin Films. *Langmuir* **2005,** 21, 10342-10347.

27.Zhang, H.; Garmo, O. A.; Davison, W. Interactions of Trace Metals with Hydrogels and Filter Membranes Used in DET and DGT Techniques. *Environmental Science & Technology* **2008,** 42, 5682-5687.

28.Kalis, E. J. J.; Davis, T. A.; Town, R. M.; Van Leeuwen, H. P. Impact of ionic strength on Cd(II) partitioning between alginate gel and aqueous media. *Environmental Science & Technology* **2009,** 43, 1091-1096.

29.Labille, J.; Fatin-Rouge, N.; Buffle, J. Local and Average Diffusion of Nanosolutes in Agarose Gel: the Effect of the Gel/Solution Interface Structure. *Langmuir* **2007,** 23, 2083-2090.

30.Zhang, H.; Davison, W. Performance-Characteristics of Diffusion Gradients in Thin-Films for the in-Situ Measurement of Trace-Metals in Aqueous-Solution. *Analytical Chemistry* **1995,** 67, 3391-3400.

31.Gagnon, M. A.; Lafleur, M. Self-diffusion and mutual diffusion of small molecules in high-set curdlan hydrogels studied by P-31 NMR. *Journal of Physical Chemistry B* **2009,** 113, 9084-9091.

Chapter 4

Diffusion of ions in a calcium alginate hydrogel-Structure is the primary factor controlling diffusion

Mahmood Golmohamadi and Kevin J. Wilkinson, Carbohydrate Polymer, Carbohydrate Polymers 94, 2013, pages 82-87.

4.1. Abstract

Diffusion of solutes has been evaluated in an alginate hydrogel as a function of its structure. The role of solute and gel charge on the diffusion measurements were of particular interest. Diffusion coefficients were measured using fluorescence correlation spectroscopy as a function of solute charge and size, bulk solution ionic strength and pH, and gel density. Diffusion coefficients of fluorescent dextrans with hydrodynamic radii up to 6 nm were reduced by 30% in a 1.8% w/w hydrogel whereas they were reduced by only 2% in a 0.2% w/w hydrogel. The role of ionic strength was examined using various concentrations (10^{-4} to 10^{-1} M) and compositions of ions (Na^{+}, Ca^{2+} or mixtures thereof). The diffusion coefficient of a small charged probe (Rhodamine 6G: $R6G^{+}$) did not change significantly with increasing ionic strength when sodium was used as the counter ion. Similarly, pH variations from 3 to 9 had little impact on the diffusion coefficients of $R6G^{+}$ in the gel. On the other hand, the addition of Ca^{2+} had a significant impact on gel compactness, which led to a significant reduction in solute diffusion. The diffusion coefficient was only moderately influenced by the charge of solutes (from +1 to -2). For the calcium alginate hydrogels, structural modifications resulting from Ca binding were much more important than electrostatic effects due to modifications of the gel Donnan potential.

4.2. Introduction

The diffusive properties of solutes in gels are key to a large number of environmental [1-3], pharmaceutical [4] and biotechnological [5] applications. The diffusion of a solute through a hydrogel will depend upon both physical (e.g. obstruction [6-8]) and chemical (e.g. hydrogen bonding, electrostatic effects [9, 10]) interactions between the two phases, which are dependent upon the physicochemical properties of both the solute and the gel. For example, solute size [11] and charge [12] and the extent of gel crosslinking [13] have been well documented to influence diffusion in hydrogels. For calcium alginate hydrogels, electrostatics have also been thought to play an important role in the diffusion of sodium [14] and bovine serum albumin (BSA)[15] at various ionic strength and pH [16]. Indeed, several recent papers [16-18] have shown that the partitioning and mobility of solute in the gel/solution interface should be significantly increased in alginate gels due to their large Donnan potential. In contrast, a decrease in the diffusion coefficient of charged solutes into hydrogel with increasing electrostatic interaction between the solute and the gel has also been observed[14, 19]. Ionic strength increases and pH decreases can further complicate the above charge effects, first by decreasing the gel Donnan potential, led to decreased partitioning and mobility of solutes in gel/solution interface[20], and secondly, results in increase mobility of solutes into hydrogel caused by an enhanced effective gel pore size through a reduction in the double layer thickness[21], or an increase in the homocoagulation of the diffusing solutes[22]. In order to quantitatively determine the effects of charge on solute diffusion, especially in highly charged gels such as alginate, further investigation is thus required.

In this paper, the diffusion coefficients of a number of charged probes with relatively small sizes were evaluated in order to assess the relative importance of charge interactions on diffusion through a negatively charged calcium alginate hydrogel. The ionic strength (I), pH and nature of the diffusing solutes were systematically varied in order to determine the role of charge effects due to bulk medium on diffusion in an alginate hydrogel.

4.3. Experimental

4.3.1. Materials

Medium viscosity alginate, D-glucono-δ-lactone (GDL), rhodamine 6G (R6G), calcium nitrate and calcium carbonate were purchased from Sigma-Aldrich. Rhodamine 110 (R110) and ultrapure nitric acid were acquired from Fluka. Fluorescently labelled dextrans (Molar masses=3k, 10k, 40k and 70k) and other fluorescent probes-tetramethylrhodamine, methyl ester (TMRM); Oregon green 488 carboxylic acid, succinimidyl ester (Oregon 1C); Oregon green 488 carboxylic acid (Oregon 2C)-were purchased from Invitrogen. For all fluorophores except Oregon 1C and 2C, small quantities of fluorophore were added to Milli-Q water (R > 18 MΩ cm) to obtain stock solutions in the micromolar concentration range. Oregon 1C and 2C were dissolved in 10^{-3} M MOPS (3-(N-morpholino) propanesulfonic acid) at pH 7.2. Samples were prepared by dilution of the stock solutions into an electrolyte solution with a controlled pH and ionic strength in order to obtain a final probe concentration of 20 nM (pH: 3 to 9, I: 10^{-4} to 10^{-1} M). Dilute HNO_3 (Fluka), sodium hydroxide (Sigma) and sodium nitrate (Fluka, analytical grade) were used to adjust the pH and ionic strengths of the solutions. pH was measured using a Metrohm 744 pH meter, calibrated with standard NBS buffers. All products were used without further purification.

4.3.2. Hydrogel preparation

The hydrogel was prepared according to the method of Draget *et al.*[23]. Simply, sodium alginate solutions were stirred overnight. The next day, calcium carbonate ($CaCO_3$) particles were dispersed into the viscous alginate solutions and degassed under vacuum. Finally, a freshly prepared solution of D-glucono-δ-lactone (GDL,3×10^{-2} M) was added to the mixture and stirred for 2 minutes, following which the gel was poured into cylindrical wells (for swelling measurements) or FCS coverslips (for FCS experiments). Gel pieces were left 24 h to solidify and then equilibrated in the desired experimental solutions for another 24 h. In a few selected experiments, hydrogels (cilynders with diameter: 1 cm;

height: 0.5 cm; volume: 1 mL) were first immersed in a 5×10^{-2} M $Ca(NO_3)$- 2×10^{-2} M $Na(NO_3)$ mixture for 48 h prior to transfer into 20 mL of a pH and ionic strength controlled experimental solution for an additional 48 h (solutions were refreshed 3x).

4.3.3. Diffusion measurements

Diffusion coefficients of fluorescent solutes were measured by fluorescence correlation spectroscopy (FCS) using a Leica TCS SP5 laser scanning microscope equipped with an argon ion (Ar^+) laser (excitation at 488 or 514 nm) and a DPSS Nd: YVO_4 laser (excitation at 561 nm). An avalanche photodiode detector was used to quantify fluorescence intensity fluctuations in the small volume (*ca.* 1 μm^3) defined by the confocal optics of the instrument. Fluorescence was measured in the emission ranges of 500-530 nm or 607-683 nm. For any given set of calibrations/experimental measurements, the position of the laser from the bottom of the coverslip was kept constant.

In FCS, variations in fluorescence intensity are attributed to the translational diffusion of fluorophores into and out of the confocal volume. The characteristic time that a fluorescent probe spends in the confocal volume, τ, is determined from an autocorrelation function, *G(t)*:

$$G(\tau) = a + \left(\frac{1}{N}\right)\left(1+\left(\frac{t}{\tau}\right)^{\delta}\right)^{-1}\left(1+\frac{1}{p^2}\left(\frac{t}{\tau}\right)^{\delta}\right)^{-0.5} \qquad (4\text{-}1)$$

where a is the limiting value of *G(t)* for $t \rightarrow \infty$; N is the average number of fluorescent particles diffusing through the confocal volume, t is the measurement time, δ accounts for anomalous diffusion as non-Fickian behaviour of diffusion[24] in the gel and p is the structural parameter (ratio of the transversal, ω_{xy}, to the longitudinal, ω_z, dimension of the confocal volume: $p = \omega_z / \omega_{xy}$). Diffusion coefficients are determined from the measured values of τ:

$$D = \frac{\omega_{xy}^2}{4\tau} \quad (4\text{-}2)$$

Prior to measurements, ω_{xy} is obtained from a calibration of the confocal volume using R110, which has a known diffusion coefficient of 4.42×10^{-10} $m^2 s^{-1}$ [11 22].

Fluorescent probes (typically 2×10^{-8} M) were entrapted to the gel through adding to the gel formation solution before gel formation, and also subsequently it was added to the desired solutions (with the same concentration as it was inside the gel) on the top of a small quantity (0.25 mL) of gel in each of the 8 wells of an FCS cell; solutions were refreshed at least three times over the 24 h period leading up to the FCS measurements. For each experimental condition, diffusion coefficients were measured in the bulk solutions and in the hydrogels under identical conditions. Diffusion was examined as a function of the pH and ionic strength of the bulk solution, the charge and size of the fluorescent probe and the weight fraction of the gel. For each experimental condition, results were obtained at a minimum of 8 different locations in the gel. In addition, experiments were repeated with freshly prepared gels on different days. Means and standard deviations were obtained from all of the repeated measurements (combination of different days and different gel locations). Acquisition times of 100 s were used to optimize the signal-to-noise ratio. Diffusion measured by FCS results from the Brownian motion of the solutes (*self*-diffusion) after equilibration of solute with hydrogel. Indeed, diffusion coefficient is the diffusion coefficient of species when the chemical potential gradient equals zero. Correspondingly, it can be contrasted with *mutual* diffusion, which is directional and driven by a concentration gradient.

4.3.4. Swelling measurements

It was assumed that the swelling of the gel due to changes in the physicochemistry of bulk solution would have an influence on solute diffusion. Swelling was quantified using a swelling factor (S), which was determined from the ratio of the mass of the hydrogel before (m_1) and after (m_2) its equilibration in the experimental solutions:

$$S = m_2 / m_1 \qquad (4\text{-}3)$$

As above, gels were allowed to equilibrate with external solutions for at least 48 h, with at least 3 renewals of the experimental solutions over this period.

4.4. Results and discussion

4.4.1. Effect of probe size and gel concentration on diffusion coefficient

The diffusion coefficients of solutes in hydrogels are generally smaller than those in the bulk solution due to the presence of the polymer network that limits the free volume available for diffusion[8,15,25-28]. This effect was seen for the diffusion of the dextran size standards for several different concentrations of alginate (Fig. 4.1).

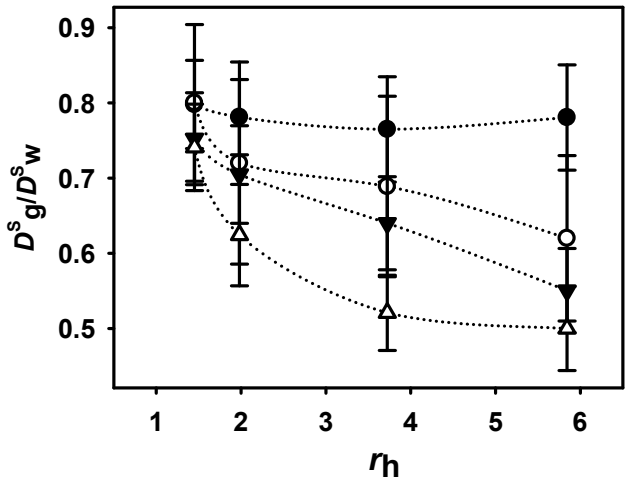

Figure 4.1. Diffusion coefficient of dextrans (3-70 kD) in the calcium alginate hydrogel as a function of their hydrodynamic radii, r_h, and for several densities (%w/w) of alginate: 0.2% (●); 1% (○); 1.4% (▼) and 1.8% (Δ). Error bars correspond to standard deviations of n=15-20 FCS measurements.

The diffusion coefficient of the largest dextran (hydrodynamic radius, r_h, of 6.2 nm) decreased by *ca*. 20% in the 0.2% w/w alginate and by *ca*. 50% in the 1.8% w/w hydrogel when compared to measurements in water (i.e. D^s_g/D^s_w of 0.8 and 0.5,

respectively, where the subscripts refer to the values made in the gel and water). The size of the probe also had an important effect on the diffusion coefficient, especially at the higher gel densities. For example, in the 0.2% alginate, the diffusion coefficient only decreased by an additional 2% for an increase in the hydrodynamic radius of the dextrans from 1.5 nm to 6.2 nm, whereas for the 1.8% alginate, an additional 30% decrease in D^s_g was observed for the same increase in probe size. While there was little difference (7%) among the diffusion coefficients of the smallest probe (3 kD dextran) between the least and most concentrated gel, a much larger effect (36%) was observed for the largest probe (70 kD dextran).

4.4.2. Effect of probe charge on diffusion coefficient

Hydrogels were prepared in $5x10^{-2}$ M $Ca(NO_3)_2$ and $2x10^{-2}$ M $NaNO_3$ (pH 7.0) and then transferred to experimental solutions with variable ionic strengths of 10^{-4}, 10^{-3} or 10^{-2} M with Debye length of 30.4, 9.6 and 3.04 nm, respectively, and a [Ca]/[Na]=3[16]. Three charged fluorophores of similar sizes: $R6G^+$ ($z=^+1$, r_h=0.5 nm), Oregon 1C ($z=^-1$, r_h =0.65 nm) and Oregon 2C ($z=^-2$, r_h=0.58 nm) were used to probe the effect of solute charge on diffusion. At all three ionic strengths, the relative diffusion coefficient (D^s_g/D^s_w) decreased slightly as the charge of solute was varied from +1 to -2 (Fig. 4.2).

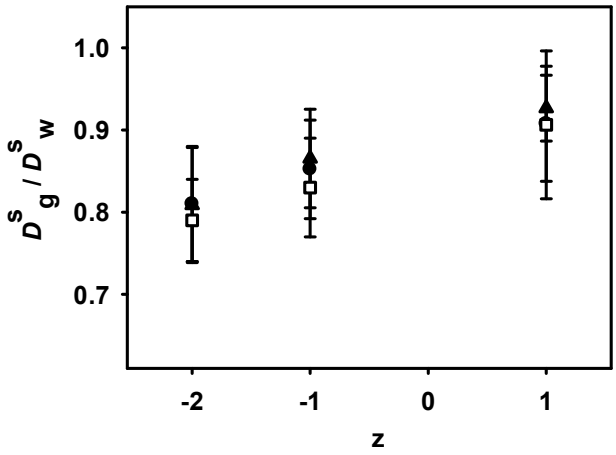

Figure 4.2. Effect of solute charge on diffusion within a calcium alginate hydrogel (1% w/w). Probes corresponded to: $R6G^+$ ($z=^+1$), Oregon 1C ($z=^-1$) and Oregon 2C ($z=^-2$); $I=10^{-4}$ M (□);10^{-3} M (●);10^{-1} M (▲); pH=7.0, [Ca]/[Na] =3/1. Error bars correspond to standard deviations compiled FCS measurements (n=15-20 over several days).

Nonetheless, the high value of the D^s_g/D^s_w ratio under all conditions, indicated that no significant chemical or physical interactions were occurring between the solutes and the hydrogel[19, 29-31]. The results were also consistent with the observation of a constant fluorescence intensity (data not shown), suggesting that little adsorption to the hydrogel was occurring for any of the probes, under any condition. A similar observation of an increasing diffusion coefficient with increasing probe charge (from $^-2$ to $^+1$) has been observed in a bacterial biofilm[31] and has been attributed to a stronger electrostatic repulsion between the anionic probes and the negatively charged hydrogel. Given that the gel pores were at least an order of magnitude larger than the probes, the electrostatic repulsion of negatively charged probes by the gels may be enough to limit their movement in the gel. Note that the accumulation of positively charged probes (and depletion of the negatively charged probes) in the hydrogel[32] is expected to increase the concentration gradient between the gel and the surrounding bulk solution. While such an increase could increase the (mutual) diffusive flux of the probes, it should have little effect on *equilibrium* FCS measurements of the diffusion coefficient (i.e. Brownian motion).

4.4.3. Effect of ionic strength on diffusion and gel structure

Diffusion coefficients for $R6G^+$ were evaluated at several ionic strengths. When $NaNO_3$ was employed as the electrolyte, diffusion coefficients were virtually constant over the entire range of ionic strength (10^{-4}-10^{-1} M; Fig. 4.3a).

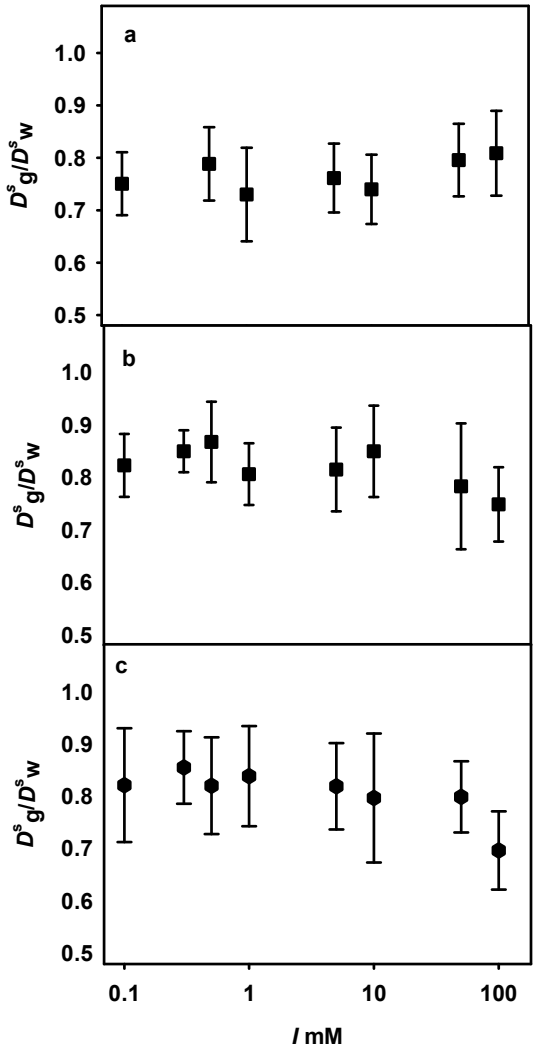

Figure 4.3. Diffusion coefficients of the $R6G^+$ in the 1% w/w hydrogel with respect to that in the water (D^s_g/D^s_w) as a function of ionic strength, I, for a bulk solution containing (a) only $NaNO_3$; (b) only $Ca(NO_3)_2$; (c) a mixture of $NaNO_3$ and $CaCO_3$ ([Ca]/[Na] =3/1). The pH of the solutions was 7. Error bars correspond to standard deviations for compiled measurements (n=30-40 FCS measurements over several days).

In contrast, when $Ca(NO_3)_2$ was employed as the electrolyte or when Ca^{2+} was mixed with Na^+, there was a small but perceptible decrease in D^s_g/D^s_w at the highest ionic strengths (Fig. 4.3b,c). For experiments performed at a constant ionic strength, the diffusion coefficient in the gel clearly decreased for an increasing ratio of Ca/Na (Fig. 4.4).

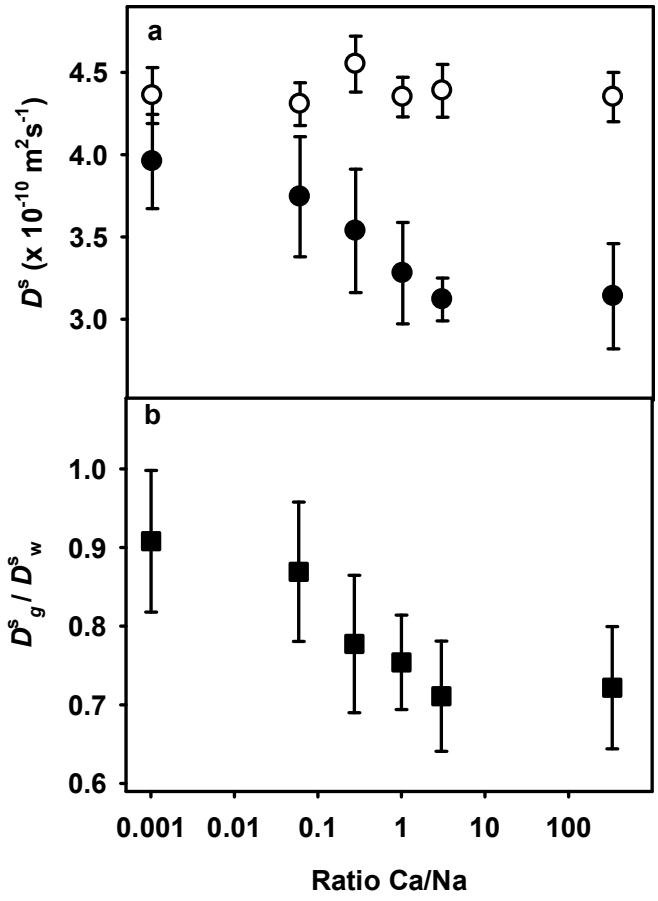

Figure 4.4. (a) Diffusion coefficients of $R6G^+$ in water (○) and in the alginate hydrogel (●); (b) D^s_g/D^s_w (■) at various ratios of Ca/Na for a constant ionic strength of 10^{-1} M. Error bars correspond to standard deviations for compiled measurements (n=30 FCS measurements over several days).

Ionic strength changes can lead to numerous and often contradictory effects on diffusion measurements [21]. For example, an increase in ionic strength leading to an increase in charge screening may: (i) increase diffusion due to effectively larger effective pore sizes (reduction of the Debye layer) (**larger** *D*), (ii) decrease solute-gel interactions ($R6G^+$ is positively charged while the alginate is negatively charged) (**larger** *D*), (iii) increase

homocoagulation of the diffusion probe (**smaller** *D*), or (iv) increase gel compactness (**smaller** *D*). The ionic strengths, in fact, apply all the aforementioned effects by varying the potential profile around the fixed charges into hydrogel through Debye length.

With respect to the above potential explanations, simple calculations based upon the ionic strength suggest that the Debye layer (point i above) would decrease from *ca.* 30 nm at 10^{-4} M to *ca.* 1 nm at 10^{-1} M (supporting information of Chapter 4), potentially leading to a large change in the *effective* pore size for charged substrates. The results evaluating the variation of solute charge (point ii above, Fig. 4.2) suggest that little interaction was occurring between the solute and the gel. Homocoagulation of the probe (point iii above) was not observed under any of the experimental conditions- diffusion coefficients in water were constant across the range of examined ionic strength values.

Gel swelling (point iv above) was measured as the ratio of the gel mass before and after equilibration in solutions of varying ionic strengths (10^{-4} to 10^{-1} M) and composition ($NaNO_3$, Ca $(NO_3)_2$). Swelling is thought to lead to larger pore radii and increased interconnectivity (decreased tortuosity) of the gel. When both Na^+ and Ca^{2+} were added, the swelling ratio decreased with ionic strength, however, gels showed much greater shrinkage for Ca (NO_3) as compared to $NaNO_3$ (Fig. 4.5a).

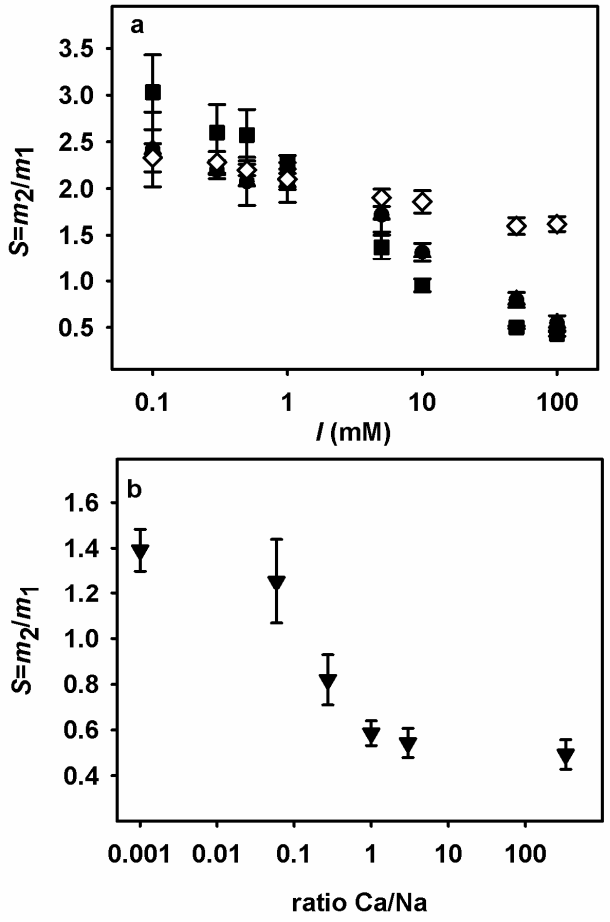

Figure 4.5. (a) Swelling of calcium alginate (1% w/w) in various ionic strengths with only $NaNO_3$ (◊), only $Ca(NO_3)_2$ (▲) and a mixture of $CaCO_3$ and $NaNO_3$ ([Ca]/[Na] =3/1) (■) in the bulk solutions; (b) Swelling of a calcium alginate (1% w/w) for a varying ratios of Ca^{2+} to Na^{+} in the bulk solutions in a constant ionic strength of 10^{-1} M. Error bars correspond to standard deviations for 2 gels.

Indeed, the gel contraction observed with increasing $NaNO_3$ (Fig. 4.5a) is attributed to a decreasing Donnan potential due to charge screening[33-38], whereas compression of gel with increasing $Ca(NO_3)_2$ can be attributed to an increased crosslinking of the carboxylate functional groups[16, 17]. Swelling was also determined for gels that were held at a constant ionic strength (I=10^{-1} M) in the presence of an increasing ratio of Ca to Na (Fig. 4.5b). Consistent with the diffusion measurements (Fig. 4.3), a significant contraction of the gel was observed as the Ca/Na ratio increased. Interestingly, a similar gel contraction in the gel

structure could be obtained by immersing an already formed gel in a 5×10^{-2} M calcium nitrate-2×10^{-2} M sodium nitrate mixture (supporting information, Fig. S4.1); in contrast, no difference in the diffusion coefficients was measured.

Since different electrolyte compositions but similar ionic strength produced perceptibly different diffusion coefficients, the observed change in D^s_g was likely not due to changes to the Donnan potential of the gel[33,35,36] but rather its induced structural modifications [16, 17, 33, 37, 39]. In other words, the significant effect of Ca on diffusion appears to be mainly due to Ca binding to carboxylates and the resulting structural modifications to the gel structure, rather than an effect on the electrostatic interactions between the probe and the gel. However, note that the contraction of gel will result to increased charged density and then enhanced Donnan effect. This simultaneous contrast variation in Donnan effect, indeed, renders hard distinguishing the role of structural than Donnan effect on the mobility of charged probes in the hydrogel.

4.4.4. Effect of pH on diffusion

The pH of the bulk solution can also affect the Donnan potential of the gel via protonation of carboxylate functional groups[18]. Calcium alginate hydrogels were immersed in solutions across the pH range of 3.0 – 9.0 (I=10^{-2} and I=10^{-3} M) for a constant Ca/Na ratio of 3. Although gels were significantly more compressed at 10^{-2} M as compared to 10^{-3} M (Fig. 4.6a), no significant differences in swelling could be attributed solely to the pH changes. pK_a values of M and G monomers that constitute the alginate are in the range of 3.38 and 3.65, respectively[40], and thus only the lowest examined pH would be expected to result in significantly increased protonation of the carboxylate functional groups on the alginate chains. Furthermore, it is possible that the protonation effect leading to decreased charge density of alginate (decreased swelling)[18] was compensated by a decreased concentration of bound calcium (increased swelling).

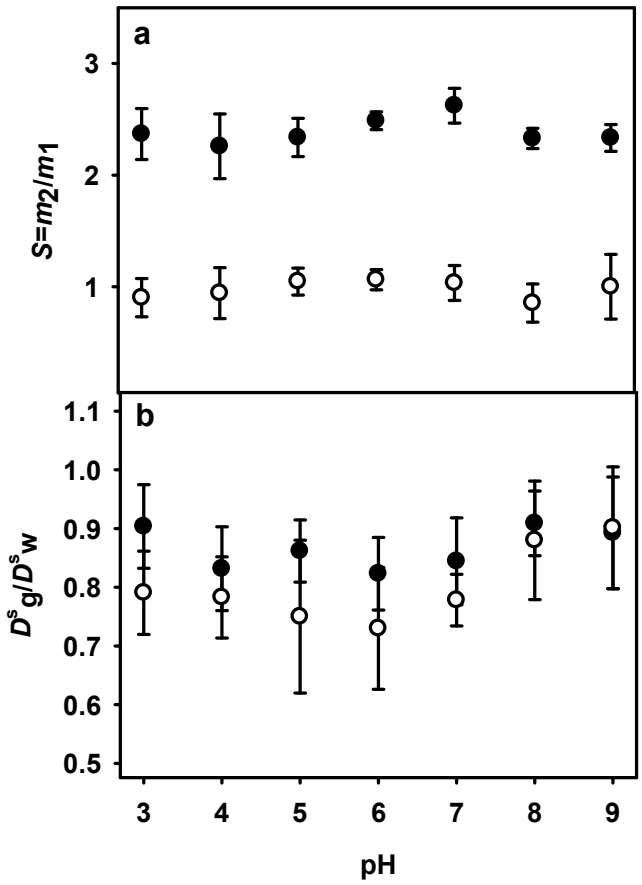

Figure 4.6. (a) Swelling of the calcium alginate (1% w/w) as a function of pH for ionic strengths of 10^{-3} M (●) and 10^{-2} M (○); (b) Ratio of D^s_g/D^s_w for $R6G^+$ in a 1% (w/w) calcium alginate gel across a wide range of pH, at ionic strengths of 10^{-3} M (●) and 10^{-2} M (○). For both experiments, ([Ca]/[Na] =3/1). Error bars correspond to standard deviations for compiled measurements (n=18-20 for FCS measurements; n=2 for swelling measurements).

Similarly, little variation of the diffusion coefficients was observed as a function of pH, although D^s_g/D^s_w values were slightly higher at the extreme pH values (Fig. 4.6b). At low pH, a decrease in the gel Donnan potential could be responsible for increased diffusion of the cationic R6G due to an increase in the effective pore size of the gel (decrease in the charged double layer). At pH 8 and 9, a larger diffusion coefficient could be attributed to gel degradation due to β-elimination[41, 42] or a shift in Ca speciation (formation of $Ca(OH)^+$,

$Ca(HCO_3)^+$), leading to reduced Ca^{2+} complexation. Note that reduced Ca binding would be expected to lead to increased gel swelling, which was not observed. The significant effect of calcium on diffusion coupled to the weak effect observed for both Na^+ and H^+ strongly supports the contention that structural rather than charge effects are mainly controlling diffusion through the alginate gel. Accordingly, it seems that mobility of solutes due to Brownian motions into hydrogel affected mostly by the potential profiles around fixed charges (various Debye lengths) than the total number of fixed charges, determinant mostly to the Donnan potential magnitude.

4.5. Conclusion

Numerous factors influence the diffusion of ions in the alginate hydrogel. For example, the gel Donnan potential was previously shown to have a major influence on *predicted diffusive fluxes* within an alginate gel, due to its large Donnan potential [16]. Mutual diffusive fluxes are mainly due to increased cation concentrations associated with the significant negative charge on the alginate gel (resulting in an increased concentration gradient). Since measurements of *diffusion* (as measured here) result from Brownian motion only, they are likely to depend strongly on the physicochemical structure of the gel. Indeed, diffusion coefficients were shown to vary by up to 30%, however, most of the variability was shown to be due to variations in the gel structure (swelling, compression) rather than charge effects. Correspondingly, Ca had the greatest effect on the gel structure and diffusivity while changes in H^+ and Na^+ resulted in only relatively small effects on the diffusion of charged solutes in the gel. Other effects, such as an increasing negative charge of the probe, were shown to result in significant, but smaller (ca. 10%) decreases in diffusion coefficients. As expected, probe size and gel structure had significant effects on diffusion; however, even these effects were not straightforward when looking at the diffusion of charged solutes. For example, while increasing the density of the calcium alginate gel will decrease its pore sizes and increase obstruction effects, especially for the larger probes [43-45], greater gel charge (and Donnan potential) will also result [21], potentially leading to increased mutual diffusion fluxes. Clearly, diffusive transport in charged gels such as the alginate can only be thoroughly understood by taking into account all of the

effects resulting from charge (solute and gel), size (solute), structure (gel) and concentration gradients.

4.6. Acknowledgements

The authors gratefully acknowledge the financial support of the *Fonds de recherche du Québec - Nature et technologies* (Team grant program) and the Natural Sciences Research Engineering Council of Canada (NSERC) Discovery Grant program.

4.7. References

1.Chen, J. P.; Hong, L.; Wu, S.; Wang, L. Elucidation of interactions between metal ions and Ca alginate-based ion-exchange resin by spectroscopic analysis and modeling simulation. *Langmuir* **2002,** 18, 9413-9421.

2.Davis, T. A.; Llanes, F.; Volesky, B.; Mucci, A. Metal selectivity of Sargassum spp. and their alginates in relation to their alpha-L-guluronic acid content and conformation. *Environmental Science and Technology* **2003,** 37, 261-267.

3.Chang, J. S.; Huang, J. C. Selective adsorption/recovery of Pb, Cu, and Cd with multiple fixed beds containing immobilized bacterial biomass. *Biotechnology Progress* **1998,** 14, 735-741.

4.Pillay, V.; Dngor, C.; Govender, T.; Moopanar, K. R.; Hurbans, N. Drug release modulation from cross-linked calcium algiante microdiscs. 1.Evaluation of the concentration dependency of sodium alginate on drug entrapment capacity, morphology, and dissolution rate. *Drug delivery* **1998,** 5, 25-34.

5.Lim, F.; Sun, A. M. Microencapsulated Islets as Bioartificial Endocrine Pancreas. *Science* **1980,** 210, 908-910.

6.Giddings, J. C.; Kucera, E.; Russel, C. P.; Myers, M. N. Statistical theory for the equilibrium distribution of rigid molecules in inert porous network.Exclusion chromatography. *Journal of Physical Chemistry B* **1968,** 72, 4397– 4408.

7.Johansson, L.; Skantze, U.; Lofroth, J. E. Diffusion and interaction in gels and solutions. 2.Experimental results on the obstruction effect. *Macromolecules* **1991,** 24, 6019-6023.

8.Amsden, B. Solute diffusion in hydrogels. An examination of the retardation effect. *Polymer Gels and Networks* **1998,** 6, 13-43.

9.Fatin-Rouge, N.; Milon, A.; Buffle, J.; Goulet, R. R.; Tessier, A. Diffusion and partitioning of solutes in agarose hydrogels: the relative influence of electrostatic and specific interactions. *Journal of Physical Chemistry B* **2003,** 107, 12126-12137.

10.Nilsson, L. G.; Nordenskiold, L.; Stilbs, P.; Braunlin, W. H. Macroscopic counterion diffusion in solutions of cylindrical poly-electrolytes. *Journal of Physical Chemistry* **1985,** 89, 3385-3391.

11.Petit, J. M.; Zhu, X. X.; Macdonald, P. M. Solute probe diffusion in aqueous solutions of poly(vinyl alcohol) as studied by pulsed-gradient spin-echo NMR spectroscopy. *Macromolecules* **1996,** 29, 70-76.

12.Johansson, L.; Skantze, U.; Lofroth, J. E. Diffusion and interaction in gels and solutions. 6.Charged systems. *Journal of Physical Chemistry* **1993,** 97, 9817-9824.

13.Amsden, B. Solute Diffusion within Hydrogels. Mechanisms and Models. *Macromolecules* **1998,** 31, 8382-8395.

14.Lundberg, P.; Kuchel, P. W. Diffusion of solutes in agarose and alginate gels: H-1 and Na-23 PFGSE and Na-23 TQF NMR studies. *Magnetic Resonance in Medicine* **1997,** 37, 44-52.

15.Amsden, B. Diffusion in polyelectrolyte hydrogel : Application of an obstruction-scaling model to solute diffusion in calcium alginate. *Macromolecules* **2001,** 34, 1430-1435.

16.Kalis, E. J.; Davis, T. A.; Town, R. M.; Van Leeuwen, H. P. Impact of ionic strength on Cd(II) partitioning between alginate gel and aqueous media. *Environmental Science and Technology* **2009,** 43, 1091-1096.

17.Davis, T. A.; Kalis, E. J.; Pinheiro, J. P.; Town, R. M.; Van Leeuwen, H. P. Cd(II) speciation in alginate gels. *Environmental Science and Technology* **2008,** 42, 7242-7247.

18.Kalis, E. J. J.; Davis, T. A.; Town, R. M.; Van Leeuwen, H. P. Impact of pH on Cd(II) partitioning between alginate gel and aqueous media. *Environmental Chemistry* **2009,** 6, 305-310.

19.Holte, O.; Tonnesen, H. H.; Karlsen, J. Effect of charge and size of diffusing probe on the diffusion through calcium alginate gel matrices. *Pharmazie* **2007,** 62, 914-918.

20.Sangi, M. R.; Halstead, M. J.; Hunter, K. A. Use of the diffusion gradient thin film method to measure trace metals in fresh waters at low ionic strength. *Analytica Chimica Acta* **2002,** 456, 241-251.

21.Golmohamadi, M.; Davis, T. A.; Wilkinson, K. J. Diffusion and partitioning of cations in an agarose hydrogel. *Journal of Physical Chemistry A: In press:* **2011**.

22.Wilkinson, K. J.; Gendron, P. O.; Avaltroni, F. Diffusion coefficients of several rhodamine derivatives as determined by pulsed field gradient-nuclear magnetic resonance and fluorescence correlation spectroscopy. *Journal of Fluorescence* **2008,** 18, 1093-1101.

23.Draget, K. I.; Ostgaard, K.; Smidsrod, O. Alginate-based solid media for plant-tissue culture. *Applied Microbiology and Biotechnology* **1989,** 31, 79-83.

24.Banks, D. S.; Fradin, C. Anomalous diffusion of proteins due to molecular crowding. *Biophysical Journal* **2005,** 89, 2960-2971.

25.Martinsen, A.; Storro, I.; Skjakbraek, G. Alginate as Immobilization Material .3. Diffusional Properties. *Biotechnology and Bioengineering* **1992,** 39, 186-194.

26.Aslani, P.; Kennedy, R. A. Studies on diffusion in alginate gels .1. Effect of cross-linking with calcium or zinc ions on diffusion of acetaminophen. *Journal of Controlled Release* **1996,** 42, 75-82.

27.Wang, X. W.; Spencer, H. G. Calcium alginate gels: Formation and stability in the presence of an inert electrolyte. *Polymer* **1998,** 39, 2759-2764.

28.Muhr, A. H.; Blanshard, J. M. V. Diffusion in Gels. *Polymer* **1982,** 23, 1012-1026.

29.Lannuccelli, V.; Coppi, G.; Cameroni, R. Biodegradable intraoperative system for bone infection treatment. I. The drug/polymer interaction. *International Journal of Pharmaceutics* **1996,** 143, 195-201.

30.Garbayo, I.; León, R.; Vílchez, C. Diffusion characteristics of nitrate and glycerol in alginate. *Colloids and Surfaces B: Biointerfaces* **2002,** 25, 1-9.

31.Zhang, Z.; Nadezhina, E.; Wilkinson, K. J. Quantifying diffusion in a biofilm of Streptococcus mutans. *Antimicrobial Agents and Chemotherapy* **2011,** 55, 1075-1081.

32.Davis, T. A.; Yezek, L. P.; Pinheiro, J. P.; van Leeuwen, H. P. Measurement of Donnan potentials in gels by in situ microelectrode voltammetry. *Journal of Electroanalytical Chemistry* **2005,** 584, 100-109.

33.Kuo, C. K.; Ma, P. X. Ionically crosslinked alginate hydrogels as scaffolds for tissue engineering: part 1.Structure, gelation rate and mechanical properties. *Biomaterials* **2001,** 22, 511-521.

34.Morris, E. R.; Rees, D. A. Principles of biopolymer gelation. Possible models for mucus gel structure. *British Medical Bulletin* **1978,** 34, 49-53.

35.Morris, E. R.; Rees, D. A.; Robinson, G.; Young, G. A. Competitive-inhibition of interchain interactions in polysaccharide systems. *Journal of molecular biology* **1980,** 138, 363-374.

36.Rees, D. A. Polysaccharide shapes and their interactions-some recent advances. *Pure and Applied Chemistry* **1981,** 53, 1-14.

37.Saitoh, S.; Araki, Y.; Kon, R.; Katsura, H.; Taira, M. Swelling/deswelling mechanism of calcium alginate gel in aqueous solutions. *Dental Materials Journal* **2000,** 19, 396-404.

38.Stokke, B. T.; Draget, K. I.; Smidsrod, O.; Yuguchi, Y.; Urakawa, H.; Kajiwara, K. Small-angle X-ray scattering and rheological characterization of alginate gels. 1.Ca-alginate gels. *Macromolecules* **2000,** 33, 1853-1863.

39.Liu, X. X.; Qian, L. Y.; Shu, T.; Tong, Z. Rheology characterization of sol-gel transition in aqueous alginate solutions induced by calcium cations through in situ release. *Polymer* **2003,** 44, 407-412.

40.Draget, K. I.; Braek, G. S.; Smidsrod, O. Alginic acid gels: the effect of alginate chemical composition and molecular weight. *Carbohydrate Polymers* **1994,** 25, 31-38.

41.Haug, A.; Larsen, B.; Smidsron, O. The degradation of alginates at different pH values. *Acta Chemica Scandinavica* **1963,** 17 1466–1468.

42.Haug, A. Composition and properties of alginates, Thesis, Norwegian Institute of Technology, Trondheim. 1964.

43.Favre, E.; Leonard, M.; Laurent, A.; Dellacherie, E. Diffusion of polyethyleneglycols in calcium alginate hydrogels. *Colloids and Surfaces a-Physicochemical and Engineering Aspects* **2001,** 194, 197-206.

44.Liu, X. D.; Yu, W. Y.; Zhang, Y.; Xue, W. M.; Yu, W. T.; Xiong, Y.; Ma, X. J.; Chen, Y.; Yuan, Q. Characterization of structure and diffusion behaviour of Ca-alginate beads prepared with external or internal calcium sources. *Journal of Microencapsulation* **2002,** 19, 775-782.

45.Gagnon, M. A.; Lafleur, M. Comparison of the structure and the transport properties of low-set and high-set curdlan hydrogels. *Journal of Colloid and Interface Science* **2011,** 357, 419-427.

4.8. Supporting Information

4.8.1. Debye length calculations in the electrolytes

The Debye length (κ^{-1}) is usually defined as[1]

$$\kappa^{-1} = \sqrt{\frac{\varepsilon_r \varepsilon_0 K T}{2 N_A e^2 I}} \quad \text{(S4-1)}$$

where I is the ionic strength of the bulk solution, ε_0 is the permittivity of free space, ε_r is the dielectric constant, K is the Boltzmann constant, N_A is the Avogadro number, e is the elementary charge and T is the temperature. For a symmetric monovalent electrolyte, Equation S4-1 becomes:

$$\kappa^{-1} = \sqrt{\frac{\varepsilon_r \varepsilon_0 R T}{2 F^2 c_0 I}} \quad \text{(S4-2)}$$

where R is the gas constant, F is the Faraday constant, c_0 is the concentration of the electrolyte. This Equation can be rewritten as follows:

$$\kappa^{-1} = \frac{1}{\sqrt{8\pi \lambda_B N_A I}} \quad \text{(S4-3)}$$

where λ_B is the Bjerrum length of the medium. Equation S4-3 for an aqueous 1-1 electrolyte (such as sodium chloride; Na^+ Cl^-) at room temperature (25 $^\circ$C) can be written as:

$$\kappa^{-1} = \frac{0.304}{\sqrt{I}} \quad \text{(S4-4)}$$

where κ^{-1} is in nm and I has its molar units. This equation indicates that the Debye length can significantly extend from the gel water interface as a function of the ionic strength in bulk medium. For example, for a variation of ionic strength from 10^{-4} -10^{-1} M, κ^{-1} would increase ca. 30 fold.

4.8.2. Internal solution effect on swelling

Although the internal crosslinking of the gels could be achieved by adding calcium carbonate and GDL (as described in the experimental protocol), it is also possible to complex the carboxylate functional groups by adding an intermediate step in which the gels are immersed (48 h) in a solution of 5×10^{-2} M calcium nitrate–2×10^{-2} M sodium nitrate [2] prior to their transfer to the experimental solutions with ionic strengths of 10^{-4}, 10^{-3} or 10^{-2} M mM (constant Ca/Na ratio of 3). Swelling results (Fig. S4.1a) corresponded to the ratio of the mass of a small piece of hydrogel in the final experimental solution with respect to its initial mass, which was measured following the initial gel formation in carbonate/GDL.

Gels were much more compact (approximately 4x) when the additional gelling solution was employed (Fig. S4.1a). Nonetheless, even though the swelling factor was largely influenced by the ionic strength of the solution, gel swelling had only limited effect on the diffusion of $R6G^{+}$. Indeed, despite the large variations in the hydrogel structure (Fig. S4.1a), no significant variations in the diffusion were observed (Fig. S4.1b). Our interpretation is that, in spite of significant gel contraction with increasing Ca, the pore sizes of the hydrogel remained relatively large with respect to the size of the R6G under all experimental conditions.

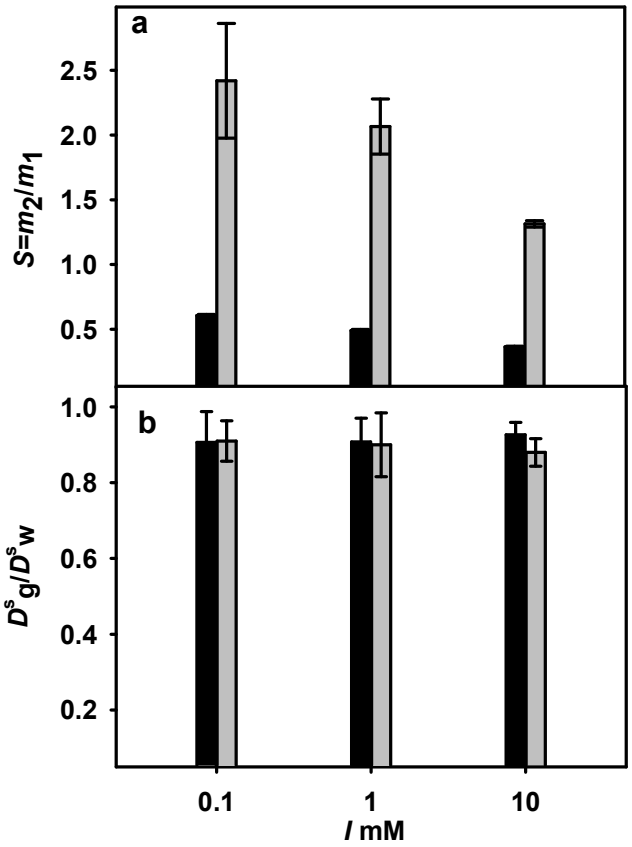

Figure S4.1. (a) Swelling of 1% (w/w) calcium alginate with (■) and without (■) the addition of an intermediate gelation solutions. m_2 is the mass of the gel after preparing the gel in a solution of 5×10^{-2} M $CaNO_3$ and 2×10^{-2} M $NaNO_3$, pH=7; (b) the D^s_g/D^s_w ratio of $R6G^+$ with (■) and without (■) the internal gelation solution, pH=7. Error bars correspond to standard deviations for compiled, duplicated measurements (n=18-20 for FCS; n=2 for swelling measurements).

4.8.3. Modeling size effect

Numerous authors have attempted to describe the diffusion of macromolecular probes in hydrogels as a function of probe size or gel density. In our case, diffusion coefficients were measured for hydrogels with various alginate densities, using dextran probes of variable molar masses (3-70 kD). The D_g/D_w ratio varied with both probe size (i.e. hydrodynamic radius, R_h) and gel density as shown in Fig 4.1. A stretched exponential function can be used to describe the dependency of the diffusion coefficient on solute size [3]:

$$D_g / D_W \propto \exp\left(-A R_h^m\right) \quad \text{(S4-5)}$$

where A is constant for a given hydrogel. The value of m that was fitted from self-diffusion experiments carried out with the various densities of alginate varied from 0.40-0.52, which is similar to the value obtained for numerous analytes in curdlan hydrogels[4] or for polyethylene glycols (PEG) in 2-hydroxyethyl methacrylate and 2-(2′-hydroxyethoxy)ethyl methacrylate hydrogels [5], m=0.50).

Note that no drastic reduction in diffusion was observed over the range of dextran radii tested here, indicating that there was no reptation effect for solute diffusion in this hydrogel [6]. Furthermore, it is possible to conclude that for the range of calcium alginate weight fractions examined here, the dextrans appeared to diffuse as spheres rather than as macromolecules with ellipsoidal or wormlike configurations (in the power law, $D=A\cdot M^{\alpha}$, α was 0.5 rather than -1 or -2, respectively). Reptational effects are observed when solute sizes (R_h) are on the order of correlation length, ξ, i.e., the distance between the polymer fibres composing the network, which generally occurs in very concentrated polymer networks. The value of α was similar to that which has been observed previously for the diffusion of PEG in various densities of calcium alginate.

Three models were tested to see whether the diffusion data could be predicted from the basic physicochemistry of the gels. Philip's model [7] takes into account obstruction effects (Equation S4-6):

$$\frac{D_g}{D_w} = \left[1 + \left(\frac{R_h^2}{k} \right)^{1/2} + \frac{1 R_h^2}{3k} \right]^{-1} \qquad \text{(S4-6)}$$

where k=0.31$r_f^2 \varphi^{-1.17}$, r_f, corresponded to the distance between G-G monomers in the alginate, 3.6 A$^{\circ}$[18], and φ was the volume fraction of the hydrogel. The Amsden model [8] takes into account both hydrodynamic and obstruction factors (Equation S4-7):

$$\frac{D_g}{D_w} = \exp\left[-\pi \left(\frac{R_h + r_f}{r_f} \right)^2 \frac{\varphi}{\left(k_1 + 2\varphi^{1/2} \right)^2} \right] \qquad \text{(S4-7)}$$

where a value of 1.6 was used for the value of k_1 (Amsden, 1998).

Based upon the results of Figure S4.2, neither of the models (Philips and Amsden) was effective in predicting the reduction in diffusion in the alginate as a function of either probe size (cf. Figure S4.2 a,b,c and d) or ionic strength (cf. Figures S4.2 e).

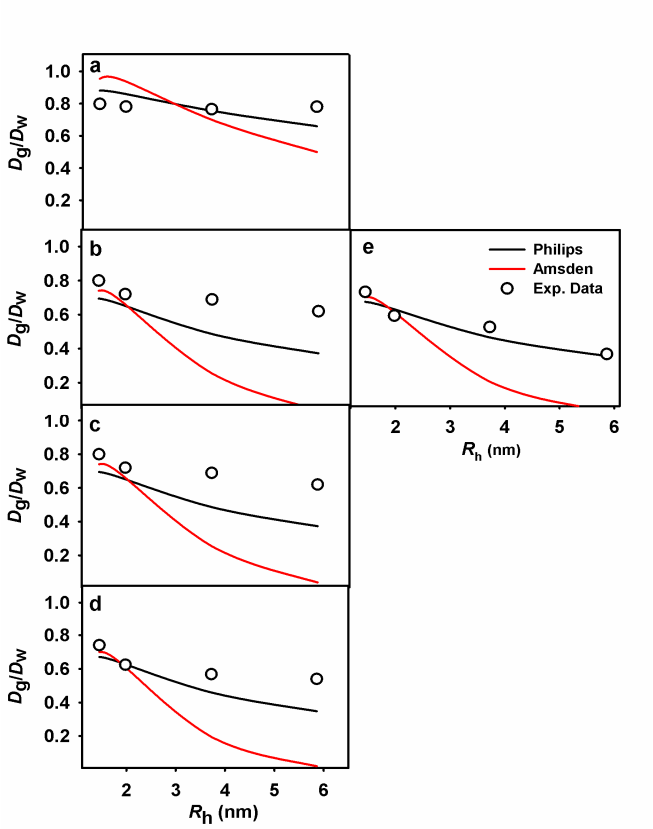

Figure S4.2. D_g/D_w values for dextran probes of various sizes in calcium alginate for an ionic strength I=10^{-2} M [Ca/Na=3/1] [Philips model (solid dark line) and Amsden model (solid red line) for 0.2% (a), 1% (b), 1.4% (c) and 1.8% (d) of calcium alginate] and for ionic strength of 10^{-1} M [Ca/Na=3/1] for Philips model (solid dark line) and Amsden model (solid red line) for only 1% calcium alginate (e).

Some of the deviations from the models may have been due either to the method of gel preparation or to the fact that previous measurements were of mutual diffusion coefficients as opposed to the self-diffusion coefficients determined here. Indeed, the hydrogel was prepared with an internal gelation solution that was different from the external gelation method used in past work. Factors such as the ratio of Ca $(CO_3)_2$ to GDL (D-glucono-δ-lactone) are important as they can determine the extent to which the alginate G-block is involved in the crosslinking of the hydrogel. The doping of greater amounts of calcium into the network can decrease the gel pore size and the use of the internal gelation method for preparing the calcium alginate has been shown to result in larger pore sizes and

a looser network than the technique using external gelation [9]. In any case, based upon the absence of a fit to our data, we concluded that effects other than obstruction and hydrodynamic effects were required to explain the diffusion of the probes in the alginate used in this work.

4.8.4. Effect of alginate Donnan potentials on solute diffusion

Donnan potentials, ψ_D, of the calcium alginate gels have been determined by Kalis et al.[10] by voltammetrically measuring Cd with a Au amalgam microelectrode in the bulk solution and then after the slow insertion into the hydrogel. They determined Donnan potentials in three ways: first, by calculation based upon a known charge density [10, 11], second, directly from the shift in the voltammetric half-wave potential (equivalent to the Donnan potential), and third, from the ratio of limiting currents (Equation 10):

$$\Pi = e^{\frac{-2F\psi_D}{RT}} = \frac{I_g^L}{I_w^L} \times \frac{D_w^m}{D_g^m} \qquad \text{(S4-8)}$$

where the (Donnan) partition coefficient represents the enhancement of metal in the gel due to electrostatic effects [10, 12, 13] and I_g^L / I_w^L is the ratio of limiting currents measured in gel and water, respectively. For each ionic strength, measured limiting current values in the gel and in water were used to generate D_g/D_w values (Equation S4-8) from Donnan potentials that were determined: (i) from the gel charge and the Ohshima equations or (ii) directly from the electrochemical potential shift. Note that in their original paper, Kalis et al. (2009a) assumed D_g/D_w values of 1 (i.e. that Donnan potentials obtained from potential and current measurements were equivalent), which is reflected by the squares (■) and the dotted line calculated from the electrochemical potential shift (Fig. S4.3). Theoretical calculations based upon the gel titration data are given by the circles and the dotted line, whereas the solid line and open triangles represents our measured diffusion coefficients, as determined by FCS for $R6G^+$.

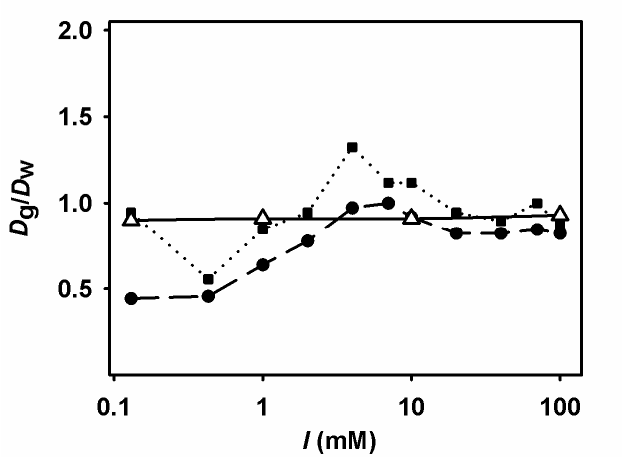

Figure S4.3. Calculated values of D_g/D_w for Cd^{2+} based upon Donnan partition coefficients determined from charge density calculations (filled circles, dashed line) or by using Donnan partition coefficients determined from shifts in voltammetric half wave potentials (filled squares, dotted line). Measured D_g/D_w values for $R6G^+$, as measured by FCS, are shown by the open triangles and solid line; all Cd^{2+} data was taken from Kalis *et al.* (2009a).

From Fig. S4.3, it can be seen that there was a large variability of predicted D_g/D_w values depending on the method that was estimated for their calculation. For example, when D_g/D_w values were based upon charge density measurements, a much larger screening effect, due to ionic strength was predicted (D_g/D_w ranged from 0.44 at very low ionic strength to ca. 1 at highest ionic strength (Table S IV.2). When D_g/D_w values were estimated from the electrochemical measurements of half wave potential and limiting current, values were near 1 (0.6-1.5), as noted in the original paper (Table S IV.2). Given the observed variability of the predicted values, the measured (FCS) values of D_g/D_w are consistent with the prior study.

Table S IV.1. Donnan partition coefficients determined from charge density calculations and from shifts in the voltammetric half wave potential measurements; the measured ratio of limiting currents and D_g/D_w values calculated from the partition coefficients (Equation S4-8). The data used in the calculations have been extracted from Fig. 2b of Kalis *et al*. (2009a).

I ($\times 10^{-3}$ M)	Π(m) determined from charge density	$\Pi(E)$ from $\Delta E_{1/2}$	I_g/I_w	D_g/D_w determined from Π(m)	D_g/D_w determined from $\Pi(E)$	D_g/D_w R6G
0.13	100.0	46.9	44.4	0.44	0.95	0.90
0.43	37.5	30.8	17.1	0.46	0.55	-
1	17.1	12.9	10.9	0.64	0.84	0.91
2	9.5	7.8	7.3	0.78	0.95	-
4	5.4	4.0	5.2	0.82	1.32	-
7	4.0	3.5	4.0	0.82	1.12	-
10	3.0	2.5	2.7	0.82	1.12	0.91
20	2.0	1.7	1.6	0.84	0.95	-
40	1.5	1.4	1.2	0.92	0.89	-
70	1.29	1.18	1.09	0.97	1.00	-
100	1.25	1.09	1.03	1.00	0.87	0.93

4.8.5. References

1.Hückel, E.; Debye, P. On the theory of electrolytes. I. Freezing point depression and related phenomena *Physikalische Zeitschrift* 1923, 24, 185-206.

2.Kalis, E. J. J.; Davis, T. A.; Town, R. M.; Van Leeuwen, H. P. Impact of Ionic Strength on Cd(II) partitioning between Alginate Gel and Aqueous Media. *Environmental Science & Technology* 2009, 43, 1091-1096.

3.Favre, E.; Leonard, M.; Laurent, A.; Dellacherie, E. Diffusion of polyethyleneglycols in calcium alginate hydrogels. *Colloids and Surfaces a-Physicochemical and Engineering Aspects* 2001, 194, 197-206.

4.Gagnon, M. A.; Lafleur, M. Comparison of the structure and the transport properties of low-set and high-set curdlan hydrogels. *J Colloid Interface Sci* 2011, 357, 419-427.

5.Pilar, J.; Kriz, J.; Meissner, B.; Kadlec, P.; Pradny, M. Effect of structure of HEMA-DEGMA hydrogel matrix on diffusion coefficients of PEG tracers. Variation of hydrogel crosslink density by change of polymer concentration. *Polymer* 2009, 50, 4543-4551.

6.Pluen, A.; Netti, P. A.; Jain, R. K.; Berk, D. A. Diffusion of macromolecules in agarose gels: Comparison of linear and globular configurations. *Biophysical Journal* 1999, 77, 542-552.

7.Phillips, R. J.; Deen, W. M.; Brady, J. F. Hindered transport of spherical macromolecules in fibrous membranes and gels. *Aiche Journal* 1989, 35, 1761-1769.

8.Amsden, B. Solute diffusion in hydrogels. An examination of the retardation effect. *Polymer Gels and Networks* 1998, 6, 13-43.

9.Liu, X. D.; Yu, W. Y.; Zhang, Y.; Xue, W. M.; Yu, W. T.; Xiong, Y.; Ma, X. J.; Chen, Y.; Yuan, Q. Characterization of structure and diffusion behaviour of Ca-alginate beads prepared with external or internal calcium sources. *Journal of Microencapsulation* 2002, 19, 775-782.

10.Kalis, E. J.; Davis, T. A.; Town, R. M.; van Leeuwen, H. P. Impact of ionic strength on Cd(II) partitioning between alginate gel and aqueous media. *Environmental Science and Technology* 2009, 43, 1091-1096.

11.Ohshima, H.; Kondo, T. Relationship among the Surface-Potential, Donnan Potential and Charge-Density of Ion-Penetrable Membranes. *Biophysical Chemistry* 1990, 38, 117-122.

12.Davis, T. A.; Kalis, E. J.; Pinheiro, J. P.; Town, R. M.; van Leeuwen, H. P. Cd(II) speciation in alginate gels. *Environmental Science & Technology* 2008, 42, 7242-7247.

13.Kalis, E. J. J.; Davis, T. A.; Town, R. M.; van Leeuwen, H. P. Impact of pH on Cd(II) partitioning between alginate gel and aqueous media. *Environmental Chemistry* 2009, 6, 305-310.

Chapter 5

The role of charge on the diffusion of solutes and nanoparticles (silicon nanocrystals, $nTiO_2$, nAu) in a biofilm

Mahmood Golmohamadi, Rhett J. Clark, Jonathan G.C. Veinot and Kevin J. Wilkinson, Environmental Chemistry, In press.

5.1. Environmental context

The mobility and bioavailability of both contaminants and nutrients in the environment depends, to a large extent, on their diffusion. Because the majority of microorganisms in the environment are embedded in biofilms, it is essential to quantify diffusion in biofilms in order to evaluate the risk of emerging contaminants, including nanomaterials and charged solutes. This study quantifies diffusion, in a model environmental biofilm, for a number of model contaminants of variable size and charge.

5.2. Abstract

The effect of solute and biofilm charge on self-diffusion (Brownian motion) in biofilms is examined. Diffusion coefficients (D) of a number of model (fluorescent) solutes (rhodamine B; tetramethylrhodamine, methyl ester; Oregon Green 488 carboxylic acid, succinimidyl ester and Oregon Green 488 carboxylic acid) and nanoparticles (functionalized silicon, gold and titanium) were determined using fluorescence correlation spectroscopy (FCS). Somewhat surprisingly, little effect due to charge was observed on the diffusion measurements in the biofilms. Furthermore, the ratio of the diffusion coefficient

in the biofilm with respect to that in water (D_b/D_w) remained virtually constant across a wide range of ionic strengths (0.1-100 mM) for both negatively and positively charged probes. In contrast, the self-diffusion coefficients of nanoparticles with sizes >10 nm greatly decreased in the biofilms with respect to those in water. Furthermore, much larger nanoparticles (> 66 nm) appeared to be completely excluded from the biofilms. The results indicated that for many oligotrophic biofilms in the environment, the diffusion of solutes and nanoparticles will be primarily controlled by obstruction rather than electrostatic interactions. The results also imply that most nanomaterials will become significantly less mobile and less bioavailable (to non-planktonic organisms) as they increase in size beyond ca. 10 nm.

5.3. Introduction

Biofilms are architecturally complex communities, which are formed by the adhesion of microorganisms to any surface[1, 2]. In the natural environment, most microorganisms are thought to be encased in a matrix of extracellular polymeric substances (EPS)[3, 4], which is thought to slow the mobility of solutes, including nutrients and contaminants. In parallel to the observation of a greater than predicted resistance to antibiotics[5-7] in medical biofilms, a decreased contaminant bioavailability has been postulated to result from the presence of biofilms in environmental systems[8]. Because diffusion is the predominant transport process in biofilms, the measurement of diffusive fluxes and diffusion coefficients is key to understanding contaminant mobility and bioavailability in the natural environment. Unfortunately, there is currently no consensus on the mechanisms leading to a *reduction* of solute diffusion or bioavailability in a biofilm[9]. In fact, numerous papers have postulated that biofilms could *increase* bioavailability due to the bioconcentration of compounds that are found in the bulk water[10-15].

Although diffusive fluxes are known to be affected by steric[16], chemical[17] and electrostatic[18] interactions with the EPS, most predictive models of solute diffusion only take obstruction (steric interactions) into account[19]. Nonetheless, recent work on model (negatively charged) hydrogels[10, 20] has shown that the predicted diffusive fluxes of

cations could be many fold greater than those in water, due to an accumulation of cations in the gel resulting from its significant Donnan potential. In that case, the accumulation of solutes at the gel-water interface would result in an increased concentration gradient, thereby increasing the mutual diffusion fluxes[11]. In contrast, a significant decrease in the diffusion of cationic antibiotics[21-25] including a quaternary ammonium compound (cetylpyridinium chloride)[17, 26] or amine-modified latex beads[27] has been attributed to electrostatic interactions within the negatively charged biofilm. In recent work with the *Pseudomonas fluorescens* biofilm[28], we showed that the relative diffusion coefficients (D_b/D_w: diffusion coefficient in the biofilm relative to that in water) of a number of model nanoparticles could be well predicted by the obstruction effect, except for a single case of highly stabilized (carboxylated) silver nanoparticles. In that case, the self-diffusion coefficient of the anionic silver nanoparticles was much less than what would be predicted, based on size (obstruction) effects alone. Since Zhang *et al.*[18] showed that self-diffusion coefficients in a *Streptococcus mutans* biofilm decreased with increasing negative charge of the solute probe, we hypothesized that charge might be an important parameter influencing the diffusion of ionic contaminants and charge-stabilized nanoparticles. We further hypothesized that in the negatively charged biofilms, anionic probes would diffuse more slowly than cationic probes, and that electrostatic effects would be eliminated by screening the charges by increasing the ionic strength.

In this paper, we attempt to determine the effect of charge on the diffusion of solutes and nanoparticles in a biofilm at variable ionic strengths. Self-diffusion coefficients were determined by fluorescence correlation spectroscopy (FCS),[29, 30] which is a non-invasive technique whereby the diffusion of fluorescent (or fluorescently labelled) solutes are measured on a size scale of 1 μm^3. Self-diffusion results from the Brownian motion of the solutes and can be contrasted with mutual diffusion, which is directional and driven by a concentration gradient. The results will be useful for evaluating the mobility and bioavailability of charged contaminants and nanoparticles in the natural environment.

5.4. Materials and methods

Rhodamine B (RB, ≥97.0%) and rhodamine 110 (R110, ≥ 99.0%) were obtained from Fluka. The other fluorescent probes: tetramethylrhodamine, methyl ester (TMRM**,** molar mass: 500.9 g mol^{-1}); Oregon Green 488 carboxylic acid, succinimidyl ester (Oregon 1C, molar mass: 509.4 g mol^{-1}); Oregon Green 488 carboxylic acid (Oregon 2C, molar mass: 412.3 g mol^{-1}) and rhodamine 123 (R123, molar mass: 380.8 g mol^{-1}) were purchased from Invitrogen. Small quantities of fluorophore were first added to Milli-Q water (resistance > 18 MΩ cm) or 1 mM 3- (N-morpholin) propanesulfonic acid (MOPS, pH 7.1) to obtain a concentrated stock solution. Fluorophores were then diluted (ca. 10^3-10^4 times to a final concentration of 5-20 nM) in an electrolyte solution with a controlled pH and ionic strength (*I*). For experiments examining *I*, 0.1-100 mM solutions were prepared with $NaNO_3$ (Sigma-Aldrich, 99.0-100.5%). pH was adjusted to 7.1±0.1 using NaOH (Sigma-Aldrich) or HNO_3 (Sigma-Aldrich), where required, and measured using a Metrohm 744 pH meter.

5.4.1. Preparation of biofilms

Biofilms were produced from a strain of *P. fluorescens* (13525) obtained from the American Type Culture Collection (ATCC)[28]. The nutrient broth (NB) medium consisted of 1.5 g L^{-1} glucose, 0.2 g L^{-1} $(NH_4)_2SO_4$, 1.5 g L^{-1} Na_2HPO_4, 750 mg L^{-1} KH_2PO_4, 1.3 g L^{-1} NaCl, 95 mg L^{-1} $MgCl_2$, 44 mg L^{-1} $CaCl_2$, 0.6 mg L^{-1} thiamine and 1.62 mg L^{-1} $FeCl_3$. "Overnight" cultures were prepared in NB medium from frozen (–80°C) cultures. A total of 40 µL of the overnight culture was inoculated into 10 mL of autoclaved NB medium, which was transferred into the 0.5-mL wells of the chambered borosilicate cover glasses (Lab-Tek 155411) used for FCS measurements. The FCS slides were then incubated for 17 h at 26°C. Prior to FCS measurements, solutions on top of the biofilm were replaced with identical experimental solutions, except that they contained the fluorescent probe. Solutions were refreshed and equilibrated (20 min) at least twice before starting FCS experiments.

5.4.2. Fluorescence correlation spectroscopy

In FCS, diffusion times of fluorescently labelled probes are quantified as they pass through a small (~1 μm^3) illuminated volume that is defined by the optics of a confocal microscope (Leica TCS SP5). In this study, fluorophores were excited using an argon ion (excitation at 488 or 514 nm) or a diode-pumped solid state DPSS Nd: YVO_4 laser (excitation at 561 nm) with emission in the ranges of 500-530 nm or 607-683 nm (depending on the probe). An avalanche photodiode detector was used to quantify fluorescence intensity fluctuations. Data acquisition times were minimized by carefully choosing optimized conditions for fluorescence excitation: (1) fluorophore concentrations (5-20 nM), (2) laser power (10-40 μW) and (3) laser wavelengths close to the excitation maxima of the fluorophores. By assuming that no chemical reactions or other dynamic events occurred during the short period in which measurements were made (milisecond to second time scale), temporal intensity fluctuations could be attributed to the translational diffusion of the fluorescent probe[29]. Diffusion times were determined from an autocorrelation function that assumed a three-dimensional Gaussian distribution, $G(t)$, of fluorophores in the confocal volume[30, 31]:

$$G(\tau) = b + \left(\frac{1}{N}\right)\left[\left(f_1\left(1+(\frac{\tau}{\tau_D})^{\delta}\right)^{-1}\left(1+\frac{1}{p^2}(\frac{\tau}{\tau_D})^{\delta}\right)^{-0.5}\right)+ \left((1-f_1)\left(1+(\frac{\tau}{\tau_D})^{\delta}\right)^{-1}\left(1+\frac{1}{p^2}(\frac{\tau}{\tau_D})^{\delta}\right)^{-0.5}\right)\right] \quad (5\text{-}1)$$

where b is the limiting value of $G(t)$ when $\tau\rightarrow\infty$, N is the average number of fluorescent particles in the confocal volume, τ_D is the characteristic diffusion time of the fluorescent species in the sample volume, τ is the delay time, δ accounts for anomalous diffusion in the biofilm and p is the structural parameter, $p=\omega_z/\omega_{xy}$ where ω_{xy} and ω_z are the transversal and longitudinal radii of the confocal volume, respectively. Values of ω_{xy} and ω_z are determined from a calibration of the system with R110, which has a known diffusion coefficient of 4.4×10^{-10} m^2 s^{-1} [32]. Diffusion times, τ_D, of the fluorescent probes were

obtained by fitting the experimental points to Eq. 5-1 and diffusion coefficients were calculated from Equation 5-2:

$$D^s = \frac{\omega_{xy}^2}{4\tau_D} \quad (5\text{-}2)$$

In the biofilms, diffusion times were determined by averaging 20-25 measurements for the solutes and 15-20 measurements for the nanoparticles, obtained in randomly selected zones of the biofilm (variable EPS densities) using acquisition times of 100-120 s. In order to minimize the effect of any macroscopic movement of the microcolonies and to ensure reproducibility, all measurements were performed on an active dampening antivibration table (Table Stable Ltd.) with the laser focused in the most mechanically stable regions of the biofilm, i.e., no more than 10 μm from the coverslip surface (Fig. S6 in supplementary information). Biofilm displacement was tracked by confocal microscopy over the duration of the FCS measurements. Optical errors were reduced by performing reference measurements in the same multiwell cover glass as the sample (constant slide thickness) and by always measuring at defined distances from the slide (constant beam astigmatism). Controls consisted of measurements of the fluorescent probes in an identical experimental medium as that used to replenish the biofilms. Results were presented as a ratio of the diffusion coefficients in the biofilms (D_b) divided by those obtained in the overlying water (D_w). All diffusion measurements were performed at room temperature, 22±1°C. Significant differences among means were identified using an analysis of variance (ANOVA) at $p<0.05$. A Student t-test was used to distinguish between means and for testing whether the slope of a regression line was significantly different from 0.

5.4.3. Nanoparticles (NP)

Diffusion was quantified for several nanoparticles of variable charge. Silicon nanocrystals (Si-NC) with a variably charged methyl undecanoate surface coating were prepared using a published literature procedure[33] (summarized in the supporting information). Gold (nAu) and titanium dioxide ($nTiO_2$) nanoparticles were prepared with either a polyacrylic acid (PAA, negative charge) or a poly diallyl dimethyl ammonium

chloride (PDDA, positive charge) coating. The nanoparticles were labelled with R123 and Oregon 1C by physical adsorption of small concentrations (5-20 nM) of the probe, at concentrations that would not to perturb the overall particle charge (calculated average adsorption of <1 fluorophore per particle). [34] Nanoparticles of nAu and $nTiO_2$ were employed at a concentration of 30 mg L^{-1}, obtained from the dilution of a stock solution. Finally, a fluorescent (Dragon Green) polystyrene nanoparticle (d_H=51 nm) was purchased from Bang laboratories (FS02F). The pH of the nanoparticle suspensions were buffered to pH=7.1 using MOPS (3-(N-morpholino) propanesulfonic acid). Zeta potentials of the nanoparticles were determined using a Malvern Zetasizer Nano-ZS. Hydrodynamic diameters, d_H, of the nanoparticles were determined from measurements of their diffusion coefficients in water using the Stokes-Einstein Equation:[35]

$$D^s = \frac{kT}{3\pi\eta d_H} \tag{5-3}$$

where k is the Boltzmann constant, T is the absolute temperature and η is the solution viscosity.

5.5. Results

The role of solute and biofilm charge on diffusion was examined by employing fluorescent solutes and nanoparticles of variable charge or charge density or by increasing the ionic strength in order to screen the (probe and biofilm) charge. Although this is an intrinsically fluorescent biofilm, it is possible to distinguish its auto-fluorescence from the fluorescence of the probes in two ways: (i) chemically, by selectively bleaching the pyoverdines that are the main contributors to biofilm auto-fluorescence, and (ii) mathematically, because the fluctuation times attributed to the auto-fluorescence are on the order of seconds whereas the small probes diffuse through the confocal volume in the sub-millisecond range[28]. Indeed, auto-fluorescence is taken into account when fitting the correlation decay through the parameter b (Eq. 5-1). The limited tailing of the autocorrelation function for small probes indicates that their adsorption to the biofilm was likely not significant, at least over this time frame (Fig. 5S1).

Diffusion coefficients of the small, variably charged probes (Table V.1) were first evaluated at pH 7.1 at an *I* of 1 mM.

Table V.1. Self-diffusion coefficients measured in water (D^s_w) by FCS, corresponding hydrodynamic radii and molecular charge number (solutes) or zeta potentials (nanoparticles) of the probes used in the diffusion experiments. Values were determined at a pH of 7.1 and an ionic strength of 10^{-3} M (MOPS).

Fluorescent Probes	D^s_w **(x 10^{-10} m^2 s^{-1})**	d_H[a] **(nm)**	**z**	
TMRM	3.87±0.16	1.2	+1	
RB	4.21±0.20	1.1	0	
Oregon 1C	3.87±0.13	1.2	-1	
Oregon 2C	3.67±0.10	1.3	-2	
Silicon Nanoparticles	D^s_w **(x 10^{-10} m^2 s^{-1})**	d_H **(nm)**	ζ[b] **(mV)** Without label	ζ **(mV)** With label
nSi1	1.10±0.21	4.4	-44.2	-42.6
nSi2	0.98±0.16	4.9	-40.5	-39.0
nSi3	1.03±0.16	4.7	-39.6	-38.7
nSi4	1.09±0.13	4.4	-39.3	-37.7
nSi5	0.98±0.16	4.9	-35.4	-33.8
nSi6	1.21±0.12	4.0	-33.8	-32.4
Gold and Titanium Nanoparticles	D_w **(× 10^{-10} m^2 s^{-1})**	d_H **(nm)**	ζ **(mV)** Without label	ζ **(mV)** With label
R123- labelled				
nAu-PAA	0.02±0.01	456.9	-20.0	-19.0
nAu-PDDA	0.42±0.07	11.4	21.3	22.4
nTiO2-PAA	0.05±0.02	105.1	-18.5	-17.7
nTiO2-PDDA	0.06±0.05	83.0	17.8	18.8
Oregon 1C- labelled				
nAu-PAA	0.49±0.15	10.2	-20.0	
nAu-PDDA	0.16±0.08	31.0	20.2	
nTiO2-PAA	0.07±0.04	66.0	-17.8	
nTiO2-PDDA	0.06±0.01	80.0	17.8	

[a] Hydrodynamic diameter calculated from the Stokes-Einstein Equation.
[b] Zeta potential

In the biofilm, diffusion coefficients decreased by 15-25 % with respect to those determined in water (i.e., $D_b/D_w \approx$ 75-85 %, Fig.5.1). Surprisingly, and in contrast to our previous results on thick biofilms of *Streptococcus mutans*[18], (a bacteria generally found on teeth), no significant differences were observed among the diffusion coefficients of four small probes of similar size but variable charge (+1 to -2) (Fig. 5.1).

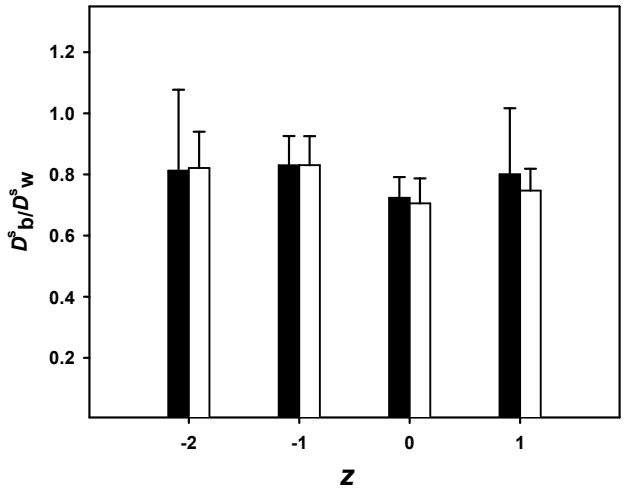

Figure 5.1. D^s_b/D^s_w versus charge of solutes including; TMRM (z=$^+$1), RB (z=0), Org 1C (z= $^-$1) and Org 2C (z= $^-$2); c=20 nM; I=10^{-3} M (▉) and I=10^{-1} M (▉); pH=7.1. Error bars correspond to standard deviations determined for 20-25 FCS measurements in the biofilm.

Similarly, I increases were expected to screen the charge of the biofilm, thereby decreasing its Donnan potential[36] and increasing the effective pore size through a reduction of the double layer thickness[11]. Nonetheless, relative diffusion coefficients showed no significant differences over a range of I (0.1- 100 mM), with diffusion coefficients in the biofilm ranging between 75 % and 85 % of those measured in water at the same I (Fig. 5.2). Note that the small variation in the diffusion coefficient for Oregon 2C, observed at 100 mM, likely resulted from its homocoagulation[32] given that a significantly smaller value was also observed for the measurements made in water.

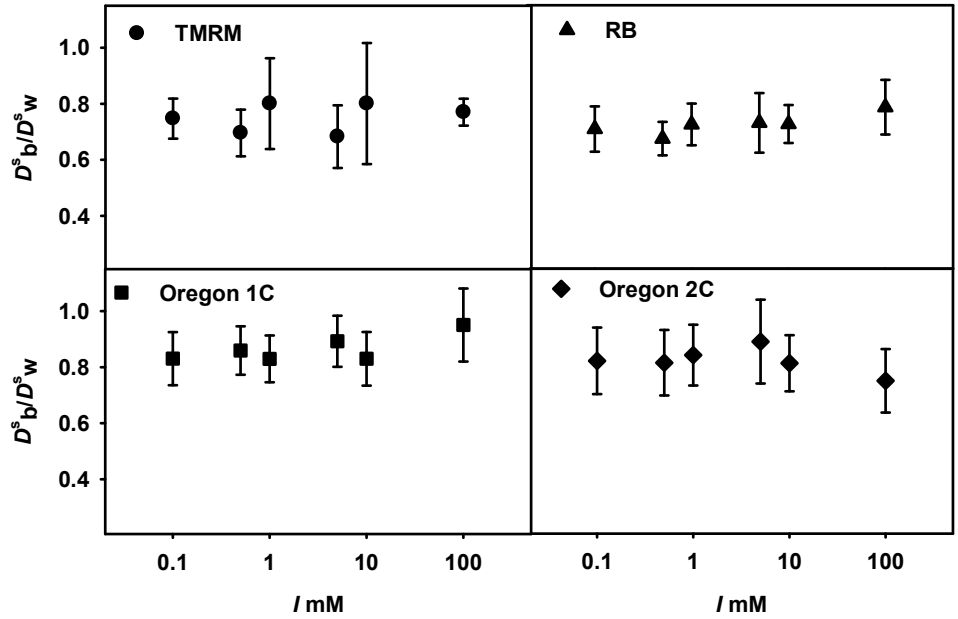

Figure 5.2. Diffusion coefficients in biofilm normalized by those in water (D^s_b/D^s_w) as a function of the ionic strength of the bulk solutions. Four probes of variable charge were evaluated: TMRM (•); RB (▲); Oregon 1C (■); Oregon 2C (♦); pH=7.1. Error bars correspond to standard deviations obtained for n=20-25 FCS measurements.

We hypothesized that the lack of a clear effect of solute or biofilm charge might have been due to the relatively small size of the fluorescent probes as compared to the effective pore size of the biofilm. Therefore, a number of variably charged nanoparticle probes were also examined: (i) a series of Si nanoparticles (nSi) with zeta potentials varying from -33 mV to -44 mV and (ii) positively and negatively charged, surface modified, nAu and $nTiO_2$.

Diffusion coefficients of the nSi labelled with a small quantity of R123 were measured at a constant pH (7.1) and I (1 mM) (Table V.1, Fig. 5.3). Because only a small concentration of label was added, it had only a minimal effect on the surface charge of the nanoparticles (e.g. maximum 2-5% modification of the zeta potential, Table V.1). In water, the sizes of the nanoparticles measured by FCS (average ≈ 5 nm, Table V.1) were consistent with determinations made using high-resolution transmission electron microscopy (data not shown). In the biofilm, diffusion coefficients were ~20-40% of those

in water. Although there were no significant differences in the mean values among the treatment groups (e.g. Fig. 5.3b, ANOVA, p=0.297), the slope of the relative diffusion coefficients (D_b/D_w) as a function of particle charge was significantly different from 0 and positive (slope=0.016 ± 0.006, Student t-test, $p<0.05$). In other words, D_b/D_w decreased by 37 % with increasing negative zeta potential (–33 mV to –44 mV) but repeated measurements from different zones of the same biofilm had an average variability of –38 % (due to the heterogeneity of the biofilm).

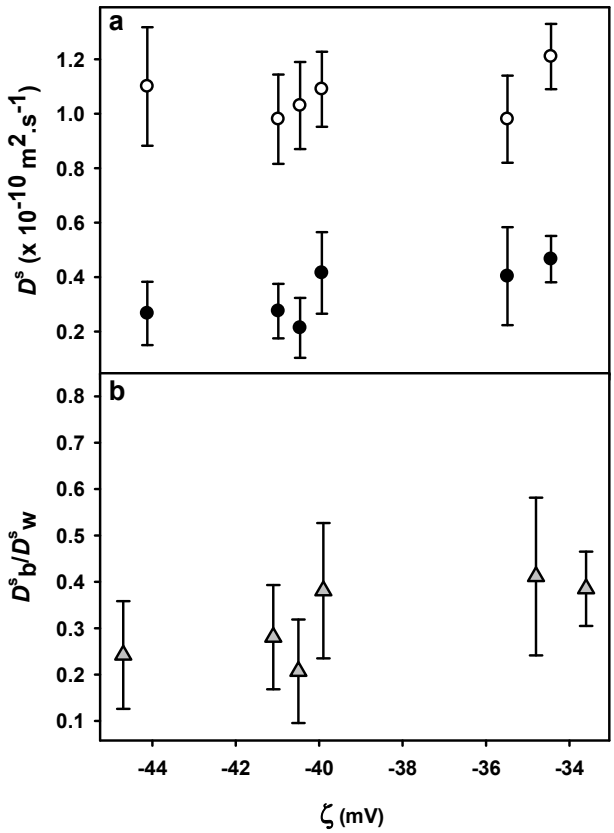

Figure 5.3. (a) Diffusion coefficients of the variably charged nSi in the biofilm (●) and in water (○); (b) the ratio of diffusion coefficients in biofilm to that in water, D^s_b/D^s_w (▲); c=30 mg L^{-1}; I=10^{-3} M; pH=7.1. Error bars correspond to standard deviations obtained for 15-20 FCS measurements.

The role of charge was also probed by comparing oppositely charged nAu and $nTiO_2$ that were obtained by coating the nanoparticles with a positively (PDDA) or

negatively (PAA) charged polymer (Table V.1). In this case, the nanoparticles were post-labelled with a small quantity of similarly charged label ($R123^+$ for the PDDA-coated nanoparticles and Oregon $1C^-$ for the PAA-coated nanoparticles). Note that in water, the size of the NP increased significantly when fluorescent probes of opposite sign were used as the label. For example, when using the similarly charged labels d_H of ~11 nm were obtained for the nAu (10.2 nm for nAu–PAA; 11.4 nm for nAu–PDDA) and ~70-80 nm for the $nTiO_2$ (66 nm for $nTiO_2$–PAA; 83 nm for $nTiO_2$–PDDA). In contrast, with the oppositely charged labels, the nanoparticles appeared to agglomerate, with sizes up to 400 nm for the nAu–PAA and 105 nm for the $nTiO_2$–PAA. Furthermore, for both nAu and $nTiO_2$, fluorescence decreased to a large extent when the oppositely charged probe was used. The statistically insignificant variations in zeta potential that were observed when oppositely charged probes were added (Student t-test, $P \geq 0.20$) suggested that agglomeration was due to bridging rather than the neutralization or screening of particle charge.

In the biofilm, the sign of the particle surface charge had a limited effect on the particle diffusion coefficients. For example, D_b values were nearly constant for negatively (0.07×10^{-10} m^2 s^{-1}) and positively (0.06×10^{-10} m^2 s^{-1}) charged $nTiO_2$ (Fig. 5.4). Interestingly, the relative reduction of the diffusion coefficient in the biofilm (D_b/D_w) was greater for the $nTiO_2$ (0.95 for $nTiO_2$–PAA; 0.93 for $nTiO_2$–PDDA) than it was for nAu (0.23 for nAu–PAA; 0.27 for nAu–PDDA). Furthermore, when the agglomerated nAu and $nTiO_2$ (i.e. the NP with the oppositely charged probes) were examined, a similar conclusion could be made (nAu 0.23-0.27; $nTiO_2$ 0.95-0.93: Fig S3, Supporting information).

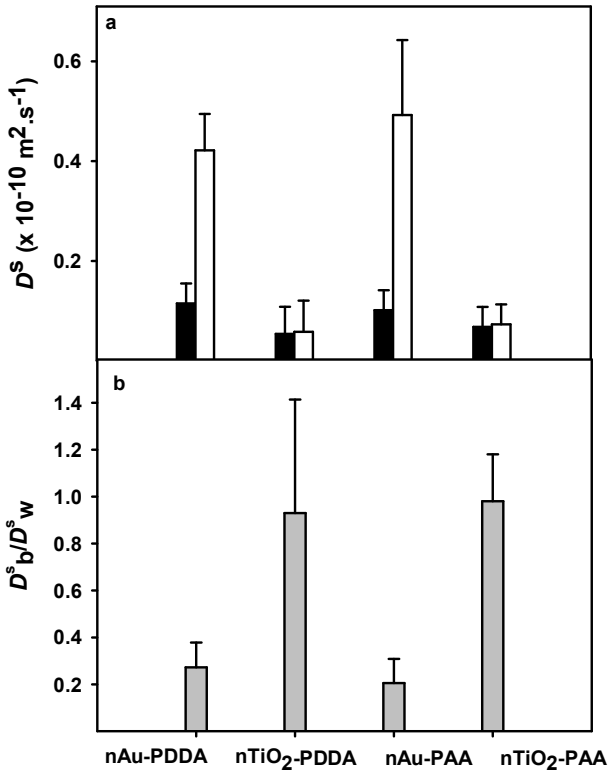

Figure 5.4. Diffusion coefficients of the nanoparticles obtained following their labelling with a similarly charged fluorescent probe (PDDA stabilized particles were labelled with R123 while PAA stabilized particles were stabilized with Org 1C). (a) Diffusion coefficient of nAu and $nTiO_2$ in water, D^s_w (▉) and in the biofilm, D^s_b (▉); (b) ratio of D^s_b/D^s_w (▉) for the stabilized nAu and $nTiO_2$; c=30 mg L^{-1}; I=10^{-3} M (MOPS); pH=7.1. Error bars correspond to standard deviations obtained for 15-20 FCS measurements.

Finally, despite of identical surface coatings, nAu experienced a much greater reduction of its diffusion coefficient in the biofilm as compared to the $nTiO_2$ even though the $nTiO_2$ was composed of larger particles (70-80 nm for $nTiO_2$ as compared to 10-11 nm for nAu). Clearly, the lack of significant differences in the relative diffusion coefficients of positively and negatively charged nanoparticles (e.g. t-test, p=0.35 for negatively charged $nTiO_2$–PAA and positively charged $nTiO_2$–PDDA in Fig. 5.4b) and the observation of significantly different reductions for particles of similar surface coatings strongly suggests that charge was not an important parameter controlling nanoparticle diffusion in the biofilm.

5.6. Discussion

Biofilms can be considered to be highly hydrated, heterogeneous gels in which the EPS produced by adherent bacteria form a polymer network[37]. The nature and organization of the EPS in a biofilm are responsible, in large part, for its porosity and diffusive properties. In polysaccharide hydrogels, it is well established that molecular diffusion is often simply limited by the obstruction of the polymer network, with reduced diffusion observed for larger particles[38] or higher gel densities[39]. Nonetheless, for some hydrogels, electrostatic interactions have been shown to play a key role with respect to the mobility of charged solutes[18, 28]. Under the conditions examined here, the electrostatic effect *did not* appear to be determinant in the transport of the charged solutes or nanoparticles. For example, diffusion of the positively charged probe (R123) was virtually constant within the biofilm (D_b/D_w ≈80 %, Fig. 5.1) over a wide range of I, designed to screen the Donnan potential of the gel. Furthermore, the diffusion coefficients of nSi increased by a small amount (ca. 37 %) as their zeta potentials increased from –44 mV to –33 mV (Table V.1 and Fig. 5.3), possibly within experimental error of the measurements. Finally, the determination of similar diffusion properties for two nanoparticles (nAu, $nTiO_2$) that were embedded in oppositely charged polymer coatings, showed that the nature or charge of the surface coatings did not play a significant role on particle diffusion in the biofilm (Fig. 5.4). Combination of the various results suggested that the charge effect was overwhelmed by other factors including: the size of the analyte (obstruction or size exclusion effect[26, 40, 41]), the affinity of diffusing solutes for specific gel components[39] and the local accumulation of particles due to either the porosity of the matrix or to a Donnan effect[18]. Other factors such as biofilm hydrophilicity[42] and local variations in the biofilm viscosity[27] may have also played a role, but were not specifically tested.

The observation that the self-diffusion coefficients of $nTiO_2$ in water were very similar to those found in the biofilm (i.e. D_b/D_w ≈1) suggested that the *relatively* large $nTiO_2$ may have been excluded from the smaller pores of the EPS[26, 27, 43], i.e. that it was so large that it only diffused into the water-filled voids of the biofilm (a "size exclusion" effect[41]). The observation of a size exclusion effect for the $nTiO_2$ but not for the nSi (d_H ≈ 5 nm; D_b/D_w ≈ 0.32) or the nAu (d_H≈11 nm; D_b/D_w ≈ 0.27) suggested that the effective

pore size of the biofilm was smaller than the size of $nTiO_2$ (i.e. ≤ 66 nm), consistent with a pore size of 50 nm estimated previously for this same biofilm[28]. The large value of D_b/D_w that was obtained for $nTiO_2$ also suggested that specific interactions were not occurring between the $nTiO_2$ and the bacterial biofilm[17, 27], an observation supported by the measurements of a constant background fluorescence for the biofilm during experiments.

The complexity of the biofilm, especially when compared to hydrogels, may also have contributed to the apparent absence of an electrostatic effect on the diffusion. On a microscopic level, diffusion can be influenced by: (1) the chemical heterogeneity of the matrix (composed of polysaccharides, proteins, lipids, bacteria, etc.) and (2) the locally variable architecture of the biofilm matrix[44]. This latter effect can result in localized zones where both the viscosity and Donnan potential can vary greatly and randomly. Indeed, the larger than normal values of standard deviation determined in the biofilms, despite a large number of repeated measurements (n=15-25), attests to biofilm heterogeneities rather than experimental error[27]. Similar observations of biofilm heterogeneity have been observed previously using different biofilms and different analytical techniques (*Streptococcus mutans,* FCS[18]; *Streptococcus oralis,* fluorescence recovery after photobleaching[45]). Nonetheless, even variations of the diffusion coefficients on the order of the standard deviations that were observed were not large when compared to the observed size effects (nanoparticles larger than 66 nm did not appear to penetrate the biofilm and even the diffusion of relatively small nanoparticles (5-11 nm) was reduced by 60-80 % with respect to water).

The biofilms produced here were not well developed, as might be expected in oligotrophic natural systems. Indeed, only a small reduction of the diffusion of R123 was observed, consistent with previous work by de Beer et al.[46], where they followed the diffusion of fluorescein in the *P. fluorescens* biofilm using microinjection coupled to confocal scanning light microscopy. It was possible to increase the development of the biofilm by providing it with additional nutrients over a longer induction period. Indeed, increased biofilm production resulted in a significant reduction in the diffusion of a neutral polystyrene nanoparticle (d_H=51 nm; Fig. 5.5).

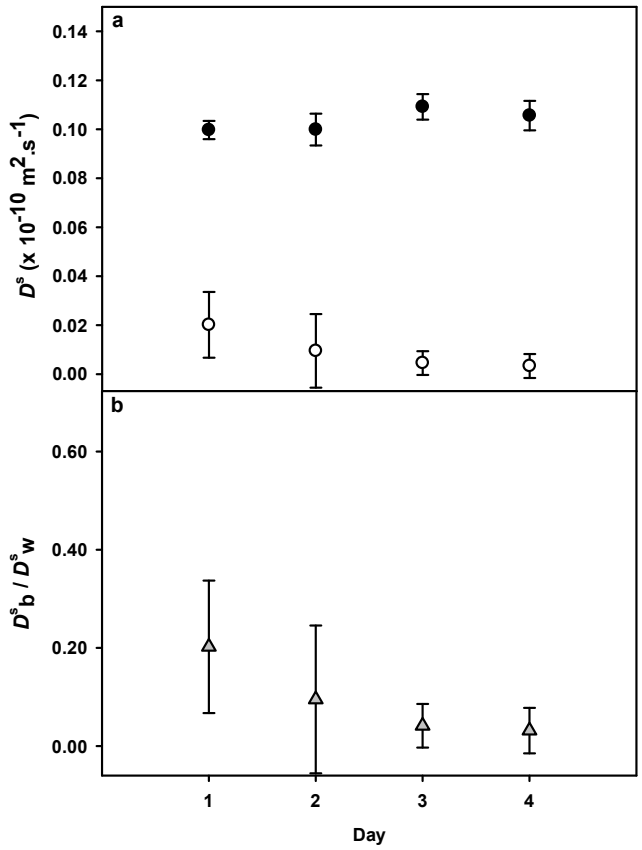

Figure 5.5. (a) The diffusion coefficient of polystyrene nanoparticle (d_H=51 nm) in water (•) and biofilm (○); (b) D^s_b/D^s_w in biofilm and water (▲). Ionic strength=10^{-3} M; pH=7.1. Error bars correspond to the standard deviations from 15-20 measurements.

The increased reduction in the diffusion coefficient with time likely resulted from increased production of EPS. Thicker, more robust biofilms are thus likely to reduce the diffusion of even smaller nanoparticles[28] and may show a greater sensitivity to the charge of the diffusing substrate, with anionic substrates diffusing significantly more slower than cationic ones.[18] Such a result may explain why a more important charge effect was observed previously for a *S. mutans* biofilm produced under conditions of high nutrient availability, whereas it was not observed here.[18]

5.7. Conclusion

Generally, diffusion of solutes in a biofilm results from the characteristics of both the diffusing solute (size, composition, charge, etc.) and the biofilm (bacterial strain, trophic status, etc.). Results from a biofilm of *Pseudomonas fluorescens* indicated that electrostatic interactions were not a major factor affecting diffusion. Neither ionic strength (0.1–100 mM) nor solute or nanoparticle charge appeared to have a major influence on the Brownian motion (i.e. self-diffusion) of solutes or nanoparticles in the biofilm. Rather, obstruction effects appeared to be primarily responsible for the reduction of solute diffusion within the biofilm matrix. These results have important implications when attempting to predict the mobility of nanomaterials in the environment in that they suggest that larger nanoparticles or agglomerated nanoparticles will be much less mobile and bioavailable under natural conditions.

5.8. Acknowledgements

The authors appreciate the donation of the gold and titanium nanoparticles from Dr. Richard Loo and Dr. Cynthia Goh, University of Toronto, Department of Chemistry. The authors also gratefully acknowledge the financial support of the *Fonds de recherche du Québec–Nature et technologies* (Team grant program) and the Natural Sciences Research Engineering Council of Canada (NSERC) through the NRC (The National Research Council)-NSERC (Natural Sciences and Engineering Research Council)- BDC (the Business Development Bank of Canada) Nanotechnology Initiative. Partial financial support was obtained from the Government of Canada through the Department of the Environment.

5.9. References

[1] Branda SS, Vik A, Friedman L, Kolter R. Biofilms: the matrix revisited. Trends in Microbiology. **2005**, 13(1), 20-6.

[2] Costerton JW, Lewandowski Z, DeBeer D, Caldwell D, Korber D, James G. Biofilms, the customized microniche. Journal of bacteriology. **1994**, 176(8), 2137-42.

[3] Flemming HC, Neu TR, Wozniak DJ. The EPS matrix: the "house of biofilm cells". Journal of Bacteriology. **2007**, 189(22), 7945-7.

[4] Sutherland I. Biofilm exopolysaccharides: a strong and sticky framework. Microbiology. **2001**, 147(Pt 1), 3-9.

[5] Stewart PS, Costerton JW. Antibiotic resistance of bacteria in biofilms. Lancet. **2001**, 358(9276), 135-8.

[6] Stewart PS. Mechanisms of antibiotic resistance in bacterial biofilms. International Journal of Medical Microbiology. **2002**, 292(2), 107-13.

[7] Costerton JW, Stewart PS, Greenberg EP. Bacterial biofilms: a common cause of persistent infections. Science. **1999**, 284(5418), 1318-22.

[8] Buffle J, Wilkinson KJ, Van Leeuwen HP. Chemodynamics and bioavailability in natural waters. Environmental Science & Technology. **2009**, 43(19), 7170-4.

[9] Stewart PS. A review of experimental measurements of effective diffusive permeabilities and effective diffusion coefficients in biofilms. Biotechnology and Bioengineering. **1998**, 59(3), 261-72.

[10] Davis TA, Kalis EJ, Pinheiro JP, Town RM, Van Leeuwen HP. Cd(II) speciation in alginate gels. Environmental Science & Technology. **2008**, 42(19), 7242-7.

[11] Golmohamadi M, Davis TA, Wilkinson KJ. Diffusion and partitioning of cations in an agarose hydrogel. The Journal of Physical Chemistry A. **2012**, 116(25), 6505-10.

[12] Battin TJ, Kammer FVD, Weilhartner A, Ottofuelling S, Hofmann T. Nanostructured TiO2: transport behavior and effects on aquatic microbial communities under environmental conditions. Environmental Science & Technology. **2009**, 43(21), 8098-104.

[13] Ferry, J. L., Craig, P., Hexel, C., Sisco, P., Frey, R., Pennington, P. L., Fulton, M. H., Scott, I. G., Decho, A. W., Kashiwada, S., Murphy, C. J., Shaw, T. J., Transfer of gold nanoparticles from the water column to the estuarine food web. Nature Nanotechnology. **2009**, 4(7), 441-4.

[14] Bryers JD, Drummond F. Local macromolecule diffusion coefficients in structurally non-uniform bacterial biofilms using fluorescence recovery after photobleaching (FRAP). Biotechnology and Bioengineering. **1998**, 60(4), 462-73.

[15] Duong TT, Morin S, Coste M, Herlory O, Feurtet-Mazel A, Boudou A. Experimental toxicity and bioaccumulation of cadmium in freshwater periphytic diatoms in relation with biofilm maturity. Science of The Total Environment. **2010**, 408(3), 552-62.

[16] Johansson L, Skantze U, Lofroth JE. Diffusion and Interaction in Gels and Solutions .2. Experimental Results on the Obstruction Effect. Macromolecules. **1991**, 24(22), 6019-23.

[17] Sandt C, Barbeau J, Gagnon M-A, Lafleur M. Role of the ammonium group in the diffusion of quaternary ammonium compounds in *Streptococcus mutans* biofilms. Journal of Antimicrobial Chemotherapy. **2007**, 60(6), 1281-7.

[18] Zhang Z, Nadezhina E, Wilkinson KJ. Quantifying diffusion in a biofilm of *Streptococcus mutans*. Antimicrobial Agents and Chemotherapy. **2011**, 55(3), 1075-81.

[19] Amsden B. Solute diffusion in hydrogels. An examination of the retardation effect. Polymer Gels and Networks. **1998**, 6(1), 13-43.

[20] Kalis EJ, Davis TA, Town RM, Van Leeuwen HP. Impact of ionic strength on Cd(II) partitioning between alginate gel and aqueous media. Environmental Science & Technology. **2009**, 43(4), 1091-6.

[21] Kim H-J, Michael Gias EL, Jones MN. The adsorption of cationic liposomes to Staphylococcus aureus biofilms. Colloids and Surfaces A: Physicochemical and Engineering Aspects. **1999**, 149(1–3), 561-70.

[22] Ahmed K, Gribbon P, Jones MN. The application of confocal microscopy to the study of liposome adsorption onto bacterial biofilms. Journal of Liposome Research. **2002**, 12(4), 285-300.

[23] Gordon CA, Hodges NA, Marriott C. Antibiotic interaction and diffusion through alginate and exopolysaccharide of cystic fibrosis-derived *Pseudomonas aeruginosa*. Journal of Antimicrobial Chemotherapy. **1988**, 22(5), 667-74.

[24] Nichols WW, Dorrington SM, Slack MPE, Walmsley HL. Inhibition of tobramycin diffusion by binding to alginate. Antimicrobial Agents and Chemotherapy. **1988**, 32(4), 518-23.

[25] Campanac C, Pineau L, Payard A, Baziard-Mouysset G, Roques C. Interactions between biocide cationic agents and bacterial biofilms. Antimicrobial Agents and Chemotherapy. **2002**, 46(5), 1469-74.

[26] Marcotte L, Therien-Aubin H, Sandt C, Barbeau J, Lafleur M. Solute size effects on the diffusion in biofilms of Streptococcus mutans. Biofouling. **2004**, 20(4-5), 189-201.

[27] Guiot E, Georges P, Brun A, Fontaine-Aupart MP, Bellon-Fontaine MN, Briandet R. Heterogeneity of diffusion inside microbial biofilms determined by fluorescence correlation spectroscopy under two-photon excitation. Photochemistry and Photobiology. **2002**, 75(6), 570-8.

[28] Peulen TO, Wilkinson KJ. Diffusion of nanoparticles in a biofilm. Environmental Science & Technology. **2011**, 45(8), 3367-73.

[29] Elson EL, Magde D. Fluorescence correlation spectroscopy. I. Conceptual basis and theory. Biopolymers. **1974**, 13(1), 1-27.

[30] Magde D, Elson EL, Webb WW. Fluorescence correlation spectroscopy. II. An experimental realization. Biopolymers. **1974**, 13(1), 29-61.

[31] Fatin-Rouge N, Starchev K, Buffle J. Size effects on diffusion processes within agarose gels. Biophysical Journal. **2004**, 86(5), 2710-9.

[32] Gendron PO, Avaltroni F, Wilkinson KJ. Diffusion Coefficients of Several Rhodamine Derivatives as Determined by Pulsed Field Gradient-Nuclear Magnetic Resonance and Fluorescence Correlation Spectroscopy. Journal of Fluorescence. **2008**, 18(6), 1093-101.

[33] Clark RJ, Dang MKM, Veinot JGC. Exploration of organic acid chain length on water-soluble silicon quantum dot surfaces. Langmuir. **2010**, 26(19), 15657-64.

[34] Leng XJ, Starchev K, Buffle J. Adsorption of fluorescent dyes on oxide nanoparticles studied by fluorescence correlation spectroscopy. Langmuir. **2002**, 18(20), 7602-8.

[35] Monkos K. Determination of the translational diffusion coefficient for proteins from the Stokes-Einstein Equation and viscometric measurements. Some Aspects of Medical Physics - in Vivo and in Vitro Studies. **2010**, 1, 83-9.

[36] Sangi MR, Halstead MJ, Hunter KA. Use of the diffusion gradient thin film method to measure trace metals in fresh waters at low ionic strength. Analytica Chimica Acta. **2002**, 456(2), 241-51.

[37] O'Toole GA. To build a biofilm. Journal of Bacteriology. **2003**, 185(9), 2687-9.

[38] Lawrence JR, Wolfaardt GM, Korber DR. Determination of Diffusion-Coefficients in Biofilms by Confocal Laser Microscopy. Applied and Environmental Microbiology. **1994**, 60(4), 1166-73.

[39] Suci PA, Vrany JD, Mittelman MW. Investigation of interactions between antimicrobial agents and bacterial biofilms using attenuated total reflection Fourier transform infrared spectroscopy. Biomaterials. **1998**, 19(4-5), 327-39.

[40] Lacroix-Gueu P, Briandet R, Leveque-Fort S, Bellon-Fontaine MN, Fontaine-Aupart MP. In situ measurements of viral particles diffusion inside mucoid biofilms. Comptes Rendus Biologies. **2005**, 328(12), 1065-72.

[41] Thurnheer T, Gmur R, Shapiro S, Guggenheim B. Mass transport of macromolecules within an in vitro model of supragingival plaque. Applied and Environmental Microbiology. **2003**, 69(3), 1702-9.

[42] Habimana O, Steenkeste K, Fontaine-Aupart MP, Bellon-Fontaine MN, Kulakauskas S, Briandet R. Diffusion of Nanoparticles in Biofilms Is Altered by Bacterial Cell Wall Hydrophobicity. Applied and Environmental Microbiology. **2011**, 77(1), 367-8.

[43] Takenaka S, Pitts B, Trivedi HM, Stewart PS. Diffusion of macromolecules in model oral biofilms. Applied and Environmental Microbiology. **2009**, 75(6), 1750-3.

[44] Dubertret B, Calame M, Libchaber AJ. Single-mismatch detection using gold-quenched fluorescent oligonucleotides. Nature Biotechnology. **2001**, 19(4), 365-70.

[45] Birmingham JJ, Hughes NP, Treloar R. Diffusion and binding measurements within oral biofilms using fluorescence photobleaching recovery methods. Philosophical Transactions of the Royal Society of London Series B-Biological Sciences. **1995**, 350(1334), 325-43.

[46] de Beer D, Stoodley P, Lewandowski Z. Measurement of local diffusion coefficients in biofilms by microinjection and confocal microscopy. Biotechnology and Bioengineering. **1997**, 53(2), 151-8.

5.10. Supporting information

5.10.1. The Structures and optical information on the fluorescent probes

In order to investigate the impact of charge in the biofilms, several variably charged fluorescent solutes were employed. The structures of probes along with their fluorescence spectra are given in Table SV.1.

Table SV. 1. The structure and fluorescence spectra of small fluorescent probes

Probe	Structure	z[a]	d_H (nm)	Absorption and Emission Spectra
Tetramethylrhodamine, methyl ester (TMRM)[b]	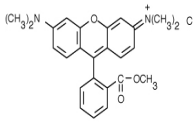	+1	1.24	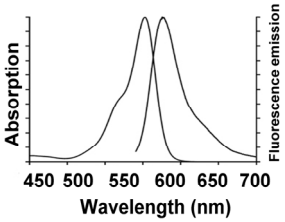
Rhodamine B (RB)[c]	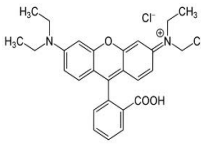	0	1.14	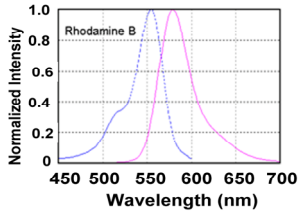
Oregon green 488 carboxylic acid, succinimidyl ester (Oregon Green 1C)[b]	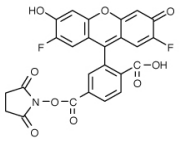	-1	1.22	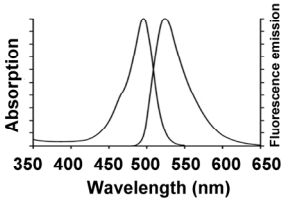
Oregon green 488 carboxylic acid (Oregon Green 2C)[b]	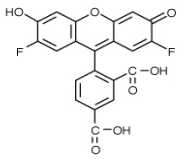	-2	1.32	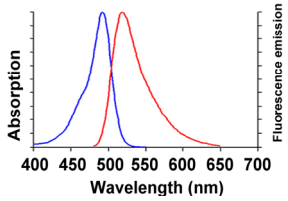

[a]Charge of the fluorescent probes
[b] Spectra were taken from the *www.invitrogen.com.*
[c]Spectra taken from *www.iss.com.*

5.10.2. Preparation of the silicon nanocrystals

The complete synthesis of the silicon nanocrystals can be found in Clark et al.[1]. Briefly, Si-NC was produced in a silica matrix composite by high temperature processing of hydrogen silsesquioxane in methyl isobutyl ketone (HSQ purchased from Dow Corning under the tradename FOx-16) under a slightly reducing atmosphere. One gram of silicon composite was etched with hydrofluoric acid in the presence of ethanol and water in order to liberate the particles from the silica matrix. The particles were then extracted from the water with three portions of toluene and transferred to a flame-dried custom Schlenk flask that was equipped with a quartz sleeve. Methyl undecanoate (0, 10, 25, 50, 100 or 200 μL) was added to the flask. Oxygen was removed from the reaction mixture by applying three freeze-pump-thaw cycles. The reaction was initiated by inserting two UV LEDs (Nichia America Corp., 250 mW at 365 nm, 3.4 eV) into the quartz sleeve and irradiating the mixture for 2 hours. Four mL of undecylenic acid was then added and the reaction was left to react for another 15 hours. Upon completion of the reaction, the clear, colorless supernatant was decanted and the functionalized particles, which were present as a precipitate, were dispersed in ethanol. The suspension was transferred into test-tubes with an excess of toluene, before centrifuging at 1520 g (The Drucker Co., Laboratory Centrifuge, model 614) for 15 minutes. The supernatant was again removed and the solid redispersed in ethanol. This procedure was repeated once more with toluene and once with pentane. Finally, the remaining particles were dispersed in ethanol for storage and characterization. Water suspensions of the surface functionalized Si-NCs were obtained by slowly diluting the Si-NCs with a mixture containing 5 mL of ethanol /5 mL of water. The majority of the ethanol was removed by rotoevaporation and the remaining solution was transferred to dialysis tubes (8-10 kD cellulose ester). Dialysis was carried out in distilled water with the water being changed at least two additional times with a minimum of three hours between changes.

5.10.3. FCS of the probes and nanoparticles in water and biofilm

The correlations of the fluorophore Org 2C and the nSi_1 in water and in the biofilm are shown in Fig. S5.1. For both the diffusion of Org 2C (Fig. S5.1a) and the nSi_1 nanoparticles (Fig. S5.1b), the autocorrelation function was shifted to longer diffusion

times when measurements were made in the biofilm. Furthermore, the greater the density of the biofilm, the greater was the displacement towards longer diffusion times (zones 1, 2, 3 in Fig. S5.1b). Finally, careful comparison of the curves obtained in water for the Org 2C (Fig. S5.1a) with respect to the nSi_1 (Fig. S5.1b) show that the larger particle diffused more slowly.

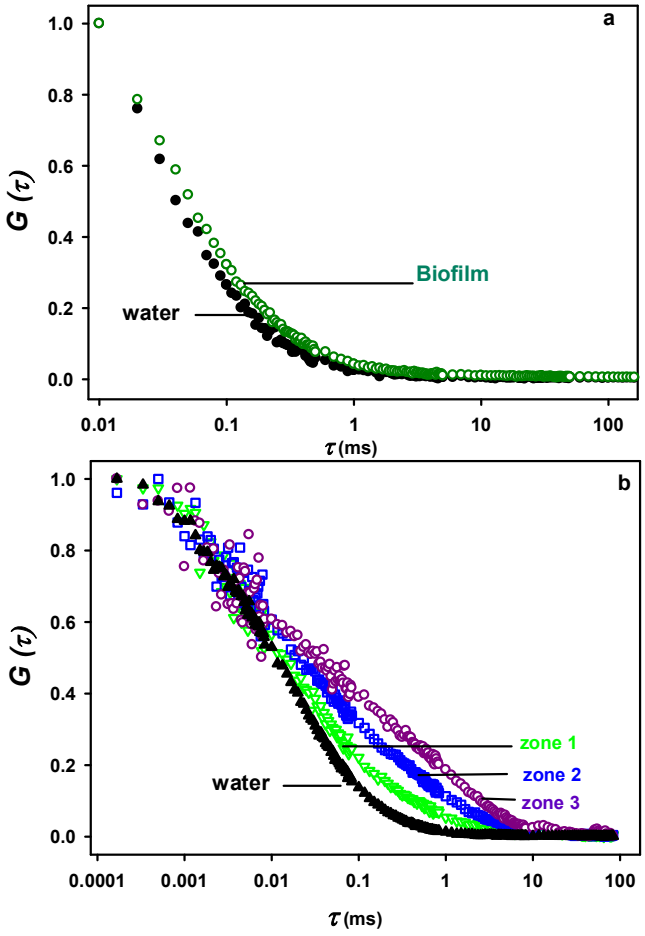

Figure S5.1. (a) The fluorescence correlation of Oregon 2C in water (•) superimposed on that of biofilm (○); c =20 nM; pH=7.1; I=10^{-3} M; laser: 488 nm; laser intensity: 40 μW; acquisition time=60 s; acquisition frequency=10^5 Hz (resolution time: 10 μs); (b) The fluorescence correlation of nSi_1 in water (▲) superimposed on that of variably dense zones of biofilm: less dense part of EPS matrix (zone 1:Δ), intermediate density (zone 2:□), and most dense part of the biofilm (zone 3:○); c_{nSi}=30 mg L^{-1}; pH=7.1; I=10^{-3} M; laser intensity: 40 μW; acquisition time=60 s; acquisition frequency=10^7 Hz (resolution time: 0.1 μs).

5.10.4. Background fluorescence of the biofilm

For several samples, a background signal appearing in the FCS correlations of the biofilms was observed. It was attributed to either the sorption of fluorescent nanoparticles to the biofilm matrix or to the autofluorescence of the biofilm. Indeed, the auto-fluorescence of the biofilm is known to result in large part from the water soluble pyoverdines that are produced by the bacteria and associated with the PS matrix[2, 3]. Nonetheless, since FCS is based on the analysis of fluorescence intensity fluctuations, constant background fluorescence does not generally influence the measured diffusion times. On the other hand, the overall movement of (a fluorescent) biofilm can lead to fluctuations of the fluorescence signal; however, they are generally at much longer correlation times. For example, translational diffusion times of τ_D >0.5 s were attributed to the background movement of the biofilm, much greater than the corresponding diffusion times that were obtained for the fluorescent probes (τ_D <30 μs) and nanoparticles (τ_D <2 ms). While the background fluorescence makes quantification of the fluorescence fluctuation signal more difficult (e.g. blue line, Fig. 5.S2), the background signal can be corrected through the introduction of a constant parameter *b* in the Gaussian model (e.g. dashed red line, Fig. 5.S2). The small modelled value for *b* can lead to very significant differences in the diffusion coefficient for the nanoparticles (Table SV.2).

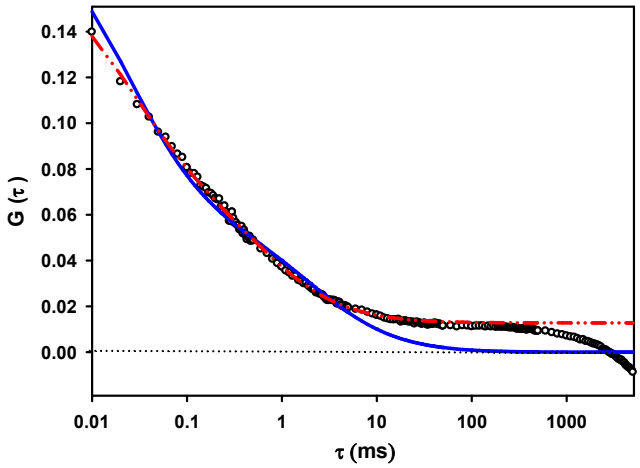

Figure S5.2. FCS correlation curves for the diffusion of the nSi_6 nanoparticle. Black points (○) are experimental data obtained with a significant background signal. The solid blue line is the fitted line obtained without taking into account the constant displacement, while the dashed red line takes into account the background fluorescence through the use of the parameter *b* (Equation 5-1); *c*=30 mg L^{-1}; pH=7.1; *I*=10^{-3} M; laser: 488 nm; laser intensity: 40 μW; acquisition time=60 s; acquisition frequency=10^5 Hz, resolution time= 10 μs.

Table SV. 2. Diffusion coefficients of nanoparticle of nSi_6 in biofilm with and without correction of background signal.

	D_{R123} ($\times 10^{-10}$ $m^2.s^{-1}$)	D_{nSi6} ($\times 10^{-10}$ $m^2.s^{-1}$)	ω_{xy} (μm)	ω_z (μm)	*b*	χ^2 *
Solid blue line	440	4.6	0.21	1.35	-	5.1
Dashed red Line	440	15.5	0.21	1.35	1.28×10^{-2}	0.34

* *chi-squared distribution*

5.10.5. Labelling nanoparticles with oppositely charged probes

When the labelling of the nAu and $nTiO_2$ nanoparticles was performed with fluorescent probes of opposite charge (R123 and Org 1C), diffusion coefficients were reduced significantly with respect to the results obtained with similarly charged probes (Fig. 5.4). Nonetheless, in spite of the agglomeration of the probes in water, similar conclusions could be drawn as for the non-aggregated probes (Fig. S5.3), i.e. diffusion was slowed for the nAu more than for the $nTiO_2$, since the D^s_b/D^s_w values were very similar to those found with non-aggregated probes.

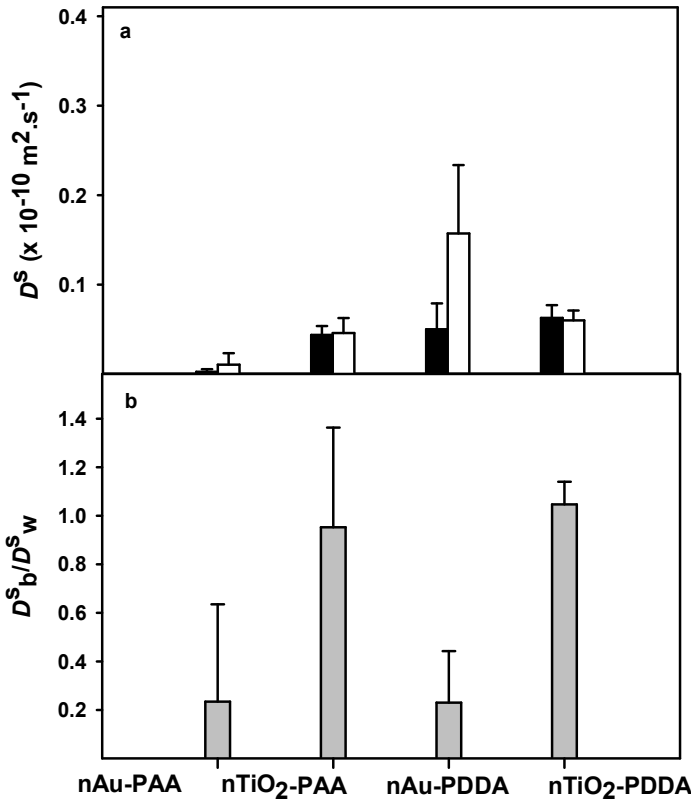

Figure S5.3. Diffusion coefficients obtained when the nanoparticles were labelled with oppositely charged fluorescent probes: (a) diffusion coefficient of nAu and $nTiO_2$ in the biofilm, D^s_b (■) and in water, D^s_w (■). NPs were labelled with rhodamine 123 and Oregon 1C; (b) the ratio of D^s_b/D^s_w (■) for nAu and $nTiO_2$. NPs were labelled with R123 and Org 1C; c=30 mg L^{-1}; I=10^{-3} M (MOPS); pH=7.1. Error bars correspond to the standard deviations of n=15-20 for FCS measurements.

5.10.6. Agglomeration of nanoparticles

Agglomeration of the nanoparticles was sometimes observed in solutions that were left to age or under specific physicochemical conditions. Agglomeration could be detected by following the NP with time or by cross correlating the two FCS channels (two colours) (Fig. S5.4).

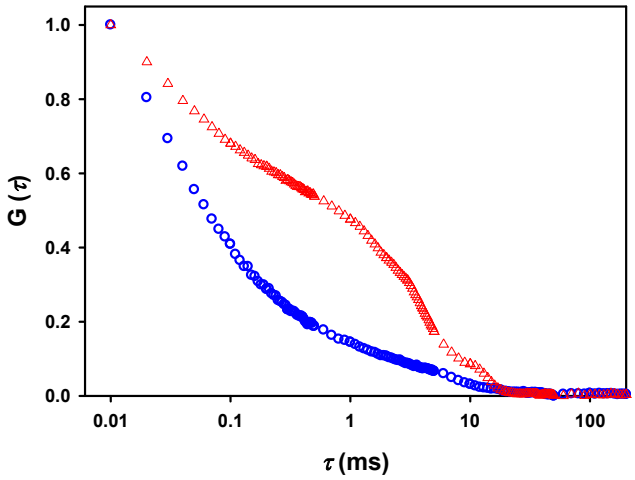

Figure S5.4. FCS cross-correlation curves for the nSi_2 nanoparticles in water (pH=7.1, I=10^{-3} M) as shown by the blue circles (○); distortions in cross-correlation curves due to the agglomeration of nanoparticle of nSi_2 in water were detected for nanoparticles that were aged (Δ) 3 weeks.

5.10.7. Nature of the biofilm and biofilm measurements

The *Pseudomonas* biofilm has been characterized previously in in our lab using confocal laser microscopy (Fig. S5.5) [3]:

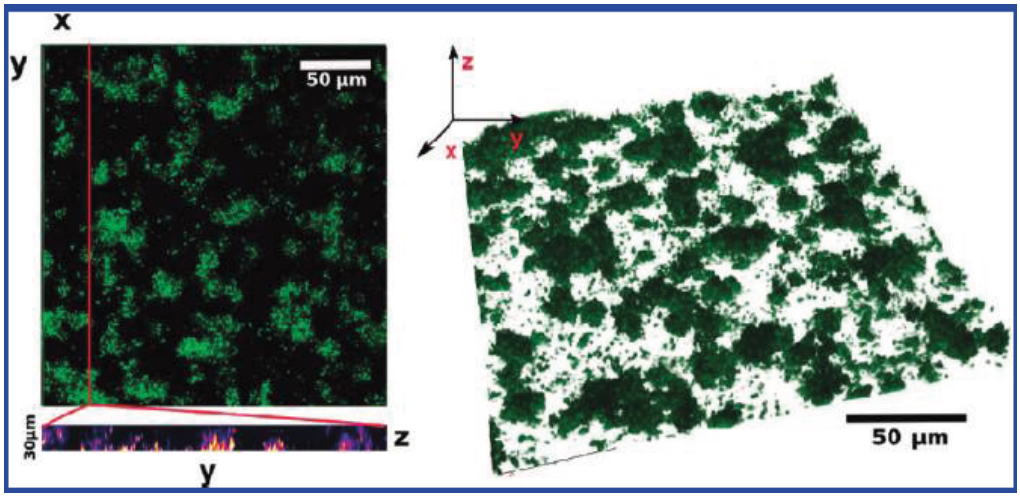

Figure S5.5. CSLM images of the *Pseudomonas fluorescens* biofilm [3].

The average thickness of biofilm was around 10-30 μm (Fig. S5.6). Diffusion measurements in the biofilm were performed at a distance of 10 μm from the coverslip while "bulk solution" measurements were performed 100 μm above the coverslip (Fig. S5.6).

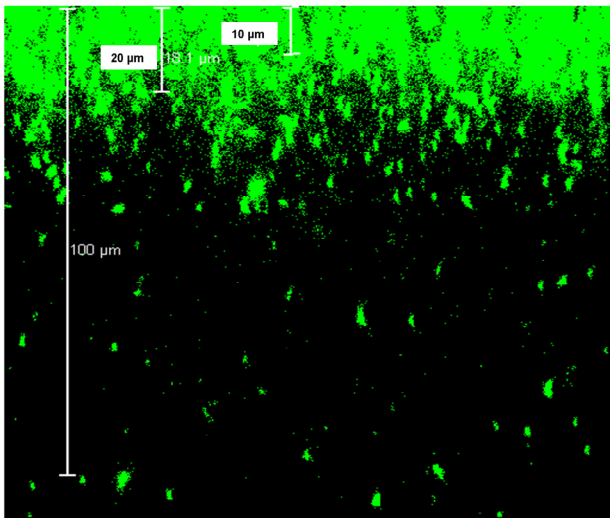

Figure S5.6. CSLM imaging of the *Pseudomonas fluorescens* biofilm in the XZ direction.

The main reason that numerous spots in biofilm were scanned (15-25 replicates) was in order to average out effects due to biofilm heterogeneity. Much of the complexity is due to the nature of the EPS and the accompanying water channels in the cell clusters.

5.10.8. Reference

[1] Clark RJ, Dang MKM, Veinot JGC. Exploration of organic acid chain length on water-soluble silicon quantum dot surfaces. Langmuir. 2010, 26(19), 15657-64.

[2] Elliott RP. Some Properties of Pyoverdine, the Water-Soluble Fluorescent Pigment of the Pseudomonads. Applied Microbiology. 1958, 6(4), 241-6.

[3] Peulen TO, Wilkinson KJ. Diffusion of nanoparticles in a biofilm. Environmental Science & Technology. 2011, 45(8), 3367-73.

Chapter 6

Conclusion and future perspectives

6.1. Overview

This dissertation has investigated the diffusion of variably charged solutes of different sizes through a biofilm. The study was designed to determine, on one hand, the impact of solute characteristics (size and charge) on their diffusion through biofilms, and on the other hand, to evaluate the effect of the biofilm structure on the mobility of solutes. In order to understand the impact of biofilm complexity on diffusion, two model hydrogels (agarose and alginate) were first considered as simple models in order to identify the important parameters affecting the mobility of solutes and macromolecules. Results obtained by the diffusion cell, fluorescence correlation spectroscopy and microelectrode voltammetry allowed us to better understand transport in both the hydrogels and biofilms. The study revealed the significant impact of electrostatic interactions on diffusion, under certain conditions. Accordingly, it was recognized that not only was mutual diffusion affected by the Donnan effect but in fact, it appeared to react in an opposite manner to what was observed for the self-diffusion. On the other hand, contrary to expectations, little Donnan effect was observed for diffusion measurements made in the highly charged alginate hydrogel. On the other hand, data in the alginate demonstrated the critical role of the size and charge of the solutes in controlling diffusion. When cations were added to the gel, structural effects on the gel seemed to predominate over charge effects. Finally, self-diffusion measurements in a *P. fluorescens* biofilm allowed us to show that the size of solutes and the physical structure of the biofilm played major roles in controlling diffusion when compared to other important factors such as solute charge.

6.2. Applications for hydrogels

For ***agarose***, this study found that electrostatic, specific and steric interactions between solutes and ionic sites in hydrogels were effective in reducing the rate of diffusion. It also showed that the variations in physico-chemistry of the bulk solution (ionic strength and pH) had a significant impact on the diffusion via variations in the physico-chemical environment of the hydrogel. Partitioning of cations between the gel and bulk solution appeared to arise mainly from electrostatic interactions rather than chemical interactions. Accordingly, at very low ionic strength, agarose showed a significant Donnan potential. This Donnan potential was reduced with increased ionic strength or decreased pH of bulk solution. This study indicated that the physico-chemistry of the bulk solution and its subsequent impact on the gel were clearly critical for understanding the diffusion of charged solutes in the agarose hydrogel.

For ***alginate***, the structure of the hydrogel was greatly influenced by the ionic strength and pH of bulk solutions, however, diffusion showed only moderate variations as a function of the ionic strength and pH. In fact, most of the variability in the self-diffusion coefficients appeared to be due to variations in the structure of the gel (swelling, compression) rather than any modification of the charge of alginate hydrogel. Among the major factors affecting the alginate matrix, the presence of calcium played a major role in the gel structure while the presence of Na^+ or pH changes resulted in relatively small effects on diffusion. In addition, the density of the alginate greatly affected diffusion in the hydrogel. This effect was stronger for larger solutes. Furthermore, for an increasing size of probe (dextrans: 10-70 kD), a reduction in the ratio D^s_g/D^s_w was observed in the alginate.

Environmental applications- The diffusion measurements of solutes within the hydrogels may be used to interpret physical, chemical or even biological events in a wide variety of biotechnological fields ranging from environmental applications, analytical (e.g. separation[1]), environmental or biomedical (e.g. drug delivery[2]) applications. In most of these applications, it is known that the hydrogel hinders the diffusion of the solutes. At the same time, Donnan potentials are known to be important for numerous colloidal systems and metal speciation techniques in low ionic strength media. For example, modeling of metal speciation using the non-ideal competitive adsorption (NICA-Donnan)[3]

or the Windermere humic acid (WHAM)[4] models relies upon the accurate interpretation of Donnan potential data. In addition, for several metal speciation techniques such as the DET (diffusive equilibration in thin films) and DGT (diffusive gradients in thin-films), in which a gel layer is used, the Donnan effect becomes extremely important when interpreting metal speciation when the nature of bulk solutions vary. These results are also applicable to other techniques such as voltammetric gel integrated microelectrodes[5] in which the solute has to diffuse through a thin film of gel to reach the surface of a microelectrode. This study suggested that variations in the physico-chemistry of the bulk solution would lead to variations in the diffusive transport in the hydrogels leading to differences in the measured metal speciation. For example, the 12-15 fold enhanced accumulation of free cations that was seen in the agarose gel (as compared to the bulk solution) when the ionic strength decreased from 10^{-4} to 10^{-1} M could lead to a significant overestimation of the analytical signal of a gel-based sensor. This situation is schematically shown in Fig. 6.1 (modified from[6-8]), which compares the steady-state fluxes for the free metal ion in a hydrogel with or without Donnan enhancement.

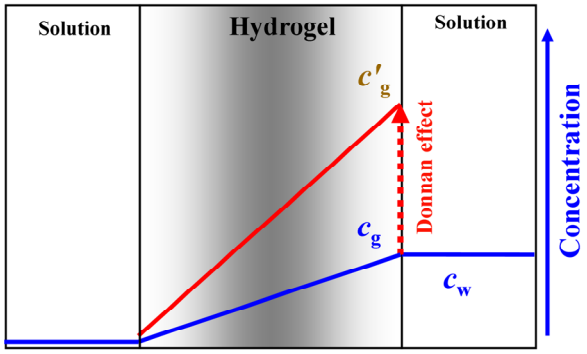

Figure 6.1. Schematic of the role of the Donnan potential on mutual diffusive fluxes through a hydrogel. Solute concentrations (c_w) and concentration gradients are presented in the gel without Donnan effect (c_g, blue line) and with Donnan (c'_g, red line).

The enhanced metal ion concentrations and diffusion values that would be observed in low ionic strength solutions are in fact observed in metal speciation analysis when using DET[9] and DGT[10]. Indeed, in the work of Sangi et al[6], the apparent mutual diffusion coefficient of Cd^{2+} increased in the low ionic strength of river water when measured with

DET[11]. Furthermore, metal speciation measured with DGT[12] gave larger concentrations when measurements were made in fresh waters. The results obtained in this thesis, including the partition coefficients and Donnan values, can be applied to these applications in order to better interpret metal speciation measurements. The results of this thesis indicate that it would be necessary to do the calibration with standard solutions with the same ionic strength and pH as the test solutions. Using calcium alginate as a thin layer film for the various applications would not be advisable as it has higher charge density and substantial swelling was observed at low ionic strengths as compared to agarose.

Moreover, the cell walls of microorganisms mainly consist of polysaccharide hydrogels, and thus the Donnan effect could potentially result in the accumulation of charged solutes at the cell membrane surface[13]. The presence of a Donnan effect would result in the different speciation in the cell wall as compared to the bulk solution. For example, as is mentioned above, the free ion concentration in the agarose gel can be 12-15 fold higher than in the bulk solution (Fig. 6.1). In such a case, metal bioaccumulation (or bioavailability) could be substantially higher than predicted on the basis of the free ion concentration. The Donnan phenomenon can be shown in Fig. 6.2 (modified from Kalis et al[14]). For no Donnan potential, the concentration profile appears continuous (solid line in Fig. 6.2.). However, in the presence of a Donnan potential, the concentration profile varied according to the partition coefficients and the thickness of the diffusion layer (dotted line in Fig. 6.2). As the Free Ion Activity model and the Biotic Ligand Model[15] are directly related to the activity of the free metal ions, then the presence of a charged gel layer can be problematic in the interpretation of these models.

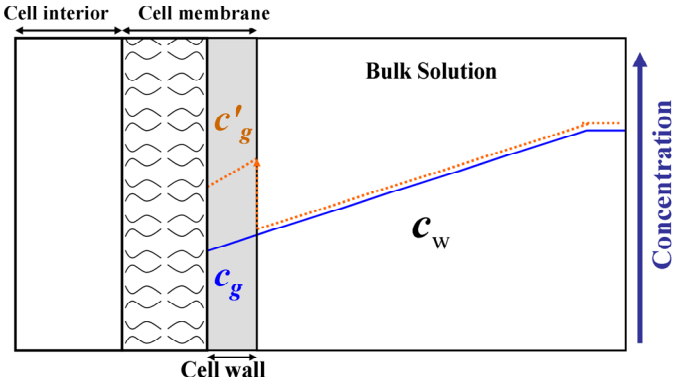

Figure 6.2. Schematic representation of the Donnan effect on speciation in bulk solution and cell membrane. Concentration profiles without Donnan effect (c_g , $\Pi_D = c_g/c_w=1$, solid blue line) and with Donnan effect (c'_g, $\Pi_D=c'_g/c_w>1$, dotted red line) in cell membrane; c_w is the concentration on the solution side of the water–membrane interface.

Biotechnological applications- Agarose (or alginate) gels can be used as biomaterials for the delivery of bioactive agents to the body[16-18], biosensors[19], as well as for encapsulation of cells for both biomedical and fermentation purposes[20]. Our results obtained for diffusion in hydrogels might be used to help explain solute transport in the above applications for large drug molecules such as proteins. In these applications, gels play the role of a barrier layer in order to provide a controlled release system. This barrier can be used as (1) a polymer membrane system in which the drug is encapsulated within a reservoir inside the supported polymer membrane or (2) the drug is homogeneously dispersed within the alginate polymer matrix. In both cases, it is vital to determine the drug diffusion rates. The results in this thesis indicated that these rates can be obtained by careful selection of the gel composition with respect to the size of the drug molecule and the composition of bulk solution. For example, in the case of agarose, different diffusion effluxes would be expected in low ionic strengths as opposed to high ionic strengths. For alginate, the situation is expected to be more complicated given that the hydrogel can swell differently under different conditions. Nonetheless, as observed in all cases, diffusion was strongly dependant upon molecular sizes.

Self and mutual diffusion coefficients- the mutual and self diffusion of a solute can have different values depending upon the physico-chemistry of bulk solutions and type of the hydrogels. Thus, differences in diffusion coefficients will be seen according to the nature of measurement methods. While self-diffusion is measured in local zones, mutual diffusion is averaged over larger distances. Hence, any heterogeneity in the hydrogel can result in much larger variations of values of the self-diffusion coefficients as compared to mutual diffusion coefficients. Indeed, small variations could be seen for small charged probes such as R6G in the agarose hydrogel. Future measurements of self-diffusion coefficients would be useful to elucidate more information about the structure and configuration of the hydrogel matrices. We suggest that the two types of diffusion should be carefully distinguished when interpreting the flux measurements in solid matrices. For example, when using the devices such as the DGT or DET, measurements of mutual diffusion may increase until equilibration whereas self-diffusion will be constant with time, but more spatially variable.

6.3. Applications for Biofilms

For ***biofilms***, in general, the results of this thesis can likely be used to help explain phenomena including (i) the immune response of bacteria due to antibody excess in a biofilm (ii) the bioavailability of antimicrobial peptides to bacterial communities (iii) the bioavailability of antimicrobial enzymes (iv) nutrient gradient profiles within biofilms and (v) gene transfer. It appears that in all the aforementioned events, diffusion plays a key role. In such a case, the architecture of the biofilm will be a key parameter, limiting the diffusion of solutes and nanoparticles. In fact, this work suggested that among the various energetic contributions to the diffusion flux (steric exclusion, hydrophobic and electrostatic interactions), the obstruction effects due to EPS architecture appeared to be mainly responsible for the slower diffusion of solutes within the biofilm matrix (in opposition to our earlier results on agarose). Investigations with variably charged nanoparticles suggested that the diffusion was primarily influenced by steric effects and for large nanoparticles (>50 nm, $D^s_b/D^s_w \approx 1$), a size exclusion effect[21, 22]. These results might explain the behaviour of larger colloids or bacteriophages in the environment. Indeed, the results suggested that the

biofilms are the active barriers to the diffusing solutes especially in the case of larger macromolecules. Accordingly, it has been shown that bacteria in the biofilms demonstrated a higher resistance to environmental stresses (disinfection, antibiotic treatment, phage attack) than their planktonic homologues. These results, therefore, may explain the protection of bacteria, for example, from antibodies[23] or macrophages and antibiotics[24]. At the same time, results from this work showed that there is little to prevent diffusion of particles in biofilm clusters, especially in zones with lower levels of EPS. This penetration into local zones with lower densities of EPS can be problematic, for example, in the milk industry where infection appears to be due to the bacteriophages of lactic acid producing bacteria in the fermentation process[25]. In view of the results of this thesis, the phage may have the capacity to diffuse into biofilms of *L. lactic* formed in dairy plants. Due to the EPS, the bacteriophage can be protected from the outside environments. The exclusion of larger particles from the biofilms may also explain the bacterial community resistance to the biocides. It was observed previously[26] that the strong resistance to a chemical biocide exhibited by *Pseudomonas aeruginosa* POA1 was associated with the formation of EPS in a three-dimensional mushroom-like structure. Our results also showed that in some zones of EPS, which are denser than the rest, diffusion is more hindered. This observation, may be of particular importance to the current development of bacteriophage therapy[27]. Also, the reduced diffusion of nanoparticles and some of the charged solutes can perhaps explain the reduction in the susceptibility of the biofilm to antibiotics and antimicrobial agents.

It was shown in this thesis that the diffusive flux depends on the characteristics of both the diffusing solutes and biofilms. For biofilms, the charge of the disinfectant will thus be critical with respect to targets requiring disinfection. In addition, the charge effect will be determinant in the bioremediation process, for example, for arsenic[28] bioremediation by *Thiomonas genus* in wastewater treatment. In the absence of the convective flow, diffusion becomes the primary process controlling contaminant transport. A Donnan effect in the biofilm could influence the amount of contaminant which could leak into a groundwater[29]. Nonetheless, the charge effect in the biofilm, for *P. fluorescens*, was moderate for most conditions of a loosely forming biofilm. This moderate effect might be overwhelmed by several other factors contributing to the diffusion process, including the size of the analyte (obstruction effect)[30-32], the hydrophilicity of biofilm[33], the affinity of the diffusing solutes

for specific gel components[34], local alterations of viscosity[35] and the local accumulation of particles due to either porosity of the matrix.[36] Certainly, more studies are needed to distinguish the factors affecting diffusion into biofilms.

6.4. Techniques

Several advanced analytical techniques were optimized and new research directions developed in this study. For example, diffusion equilibration cells and fluorescence correlation spectroscopy (FCS) were successfully applied to measure the self and mutual diffusion measurements in biofilms and hydrogels. FCS as a non-invasive technique that was able to measure diffusion coefficients focuses in small zones of the hydrogel or biofilm. The local heterogeneity information can be revealed with FCS by measuring diffusion or imaging local zones of EPS. Also, FCS can be used to get detailed information on the gel-water interface by scanning a distance extending through the interface. Future work in this area could result in a better understanding of the transport phenomena at the interface of the EPS and the bulk solution. Microelectrode voltammetry was used to reveal enhancements in the solute concentrations in the gels. For heterogeneous hydrogels, the Donnan profile could be measured by slicing the hydrogel and measuring the Donnan potential on each surface. Moreover, the slicing of the hydrogels used in the diffusion cell technique would provide diffusion coefficients across a gel of limited thickness. The information mentioned above could help us gain information about the gel or even biofilm heterogeneity. The protocols developed in this thesis may be a valuable tool to examine hydrogels and biofilms.

6.5. Future perspectives

Future studies will be required to quantify the role of both biofilm heterogeneity and the chemistry of the nanoparticles on their fate and diffusive fluxes in the environment. On one hand, the heterogeneity of the biofilm matrix will need to be evaluated in more detail using various imaging techniques equipped with FCS. Also, other biofilms should be

obtained and examined with variable growth media and biofilm development times. The interaction of nanoparticles with biofilms could be elucidated mechanistically by examining genetically modified biofilms with variable EPS compositions. Moreover, hydrogels with similar complexity to the biofilms, either synthesized or found naturally, could potentially be used as better models to explain diffusion in the biofilms. Future experiments measuring overall diffusive fluxes would be highly useful in this context. Moreover, the synthesis of nanoparticles with various surface chemistries and compositions could help us elucidate more about the mechanisms leading to the bioavailability of nanoparticles. Future measurements of diffusion coefficients, Donnan potential and gel (biofilm) will surely provide us with a better physico-chemical understanding of these highly complex systems.

6.6. References

1.Takagi, R.; Hori, M.; Gotoh, K.; Tagawa, M.; Nakagaki, M. Donnan potential and zeta-potential of cellulose acetate membrane in aqueous sodium chloride solutions. *Journal of Membrane Science* **2000,** 170, 19-25.

2.Tonnesen, H. H.; Karlsen, J. Alginate in drug delivery systems. *Drug Development and Industrial Pharmacy* **2002,** 28, 621-630.

3.Milne, C. J.; Kinniburgh, D. G.; Tipping, E. Generic NICA-Donnan model parameters for proton binding by humic substances. *Environmental Science & Technology* **2001,** 35, 2049-2059.

4.Tipping, E.; Hurley, M. A. A unifying model of cation binding by humic substances. *Geochimica et Cosmochimica Acta* **1992,** 56, 3627-3641.

5.Tercier, M. L.; Buffle, J. Antifouling membrane-covered voltammetric microsensor for in situ measurements in natural waters. *Analytical Chemistry* **1996,** 68, 3670-3678.

6.Sangi, M. R.; Halstead, M. J.; Hunter, K. A. Use of the diffusion gradient thin film method to measure trace metals in fresh waters at low ionic strength. *Analytica Chimica Acta* **2002,** 456, 241-251.

7.Yezek, L. P.; van Leeuwen, H. P. An electrokinetic characterization of low charge density cross-linked polyacrylamide gels. *Journal of Colloid and Interface Science* **2004,** 278, 243-250.

8.Davis, T. A.; Kalis, E. J. J.; Pinheiro, J. P.; Town, R. M.; van Leeuwen, H. P. Cd(II) speciation in alginate gels. *Environmental Science & Technology* **2008,** 42, 7242-7247.

9.Zhang, H.; Davison, W. Diffusional characteristics of hydrogels used in DGT and DET techniques. *Analytica Chimica Acta* **1999,** 398, 329-340.

10.Alfaro-De la Torre, M. C.; Beaulieu, P. Y.; Tessier, A. In situ measurement of trace metals in lakewater using the dialysis and DGT techniques. *Analytica Chimica Acta* **2000,** 418, 53-68.

11.Scally, S.; Davison, W.; Zhang, H. Diffusion coefficients of metals and metal complexes in hydrogels used in diffusive gradients in thin films. *Analytica Chimica Acta* **2006,** 558, 222-229.

12.Peters, A. J.; Zhang, H.; Davison, W. Performance of the diffusive gradients in thin films technique for measurement of trace metals in low ionic strength freshwaters. *Analytica Chimica Acta* **2003,** 478, 237-244.

13.Davis, T. A.; Kalis, E. J.; Pinheiro, J. P.; Town, R. M.; van Leeuwen, H. P. Cd(II) speciation in alginate gels. *Environmental Science & Technology* **2008,** 42, 7242-7247.

14.Kalis, E. J. J.; Davis, T. A.; Town, R. M.; van Leeuwen, H. P. Impact of pH on Cd-II partitioning between alginate gel and aqueous media. *Environmental Chemistry* **2009,** 6, 305-310.

15.Niyogi, S.; Wood, C. M. Biotic ligand model, a flexible tool for developing site-specific water quality guidelines for metals. *Environmental Science & Technology* **2004,** 38, 6177-6192.

16.Peppas, N. A., Ed, *Hydrogels in medicine and pharmacy; CRC Press: Boca Raton, FL,*. 1987.

17.Kim, S. W.; Bae, Y. H.; Okano, T. Hydrogels: swelling, drug loading, and release *Pharmaceutical Research* **1992,** 9, 283.

18.Lee, P. I., Synthetic hydrogels for drug delivery. In Controlled Release Systems: Fabrication Technology; Hsieh, D., Ed.; CRC Press: Boca Raton, FL. In 1988.

19.Ratner, B. D., Biomedical applications of synthetic Polymers.In comprehensive polymer science; Aggarwal, S. L., Ed.;Pergamon Press: Toronto,. In 1989; Vol. 7, p 201.

20.Jen, A. C.; Wake, M. C.; Mikos, A. G. Hydrogels for cell immobilization. *Biotechnology and Bioengineering* **1996,** 50, 357.

21.Dulkeith, E.; Ringler, M.; Klar, T. A.; Feldmann, J.; Munoz Javier, A.; Parak, W. J. Gold nanoparticles quench fluorescence by phase induced radiative rate suppression. *Nano Letters* **2005,** 5, 585-589.

22.Dulkeith, E.; Morteani, A. C.; Niedereichholz, T.; Klar, T. A.; Feldmann, J.; Levi, S. A.; van Veggel, F. C.; Reinhoudt, D. N.; Moller, M.; Gittins, D. I. Fluorescence quenching of dye molecules near gold nanoparticles: radiative and nonradiative effects. *Physical Review Letters* **2002,** 89, 203002.

23.Ramphal, R.; Lhermitte, M.; Filliat, M.; Roussel, P. The binding of anti-pseudomonal antibiotics to macromolecules from cystic-fibrosis sputum. *Journal of Antimicrobial Chemotherapy* **1988,** 22, 483-490.

24.Vrany, J. D.; Stewart, P. S.; Suci, P. A. Comparison of recalcitrance to ciprofloxacin and levofloxacin exhibited by Pseudomonas aeruginosa bofilms displaying rapid-transport characteristics. *Antimicrobial Agents and Chemotherapy* **1997,** 41, 1352-1358.

25.Brussow, H. Phages of dairy bacteria. *Annual Review of Microbiology* **2001,** 55, 283-303.

26.Davies, D. G.; Parsek, M. R.; Pearson, J. P.; Iglewski, B. H.; Costerton, J. W.; Greenberg, E. P. The involvement of cell-to-cell signals in the development of a bacterial biofilm. *Science* **1998,** 280, 295-298.

27.Summers, W. C. Bacteriophage therapy. *Annual Review of Microbiology* **2001,** 55, 437-451.

28.Dictor, M. C.; Battaglia-Brunet, F.; Garrido, F.; Baranger, P. Arsenic oxidation capabilities of a chemoautotrophic bacterial population: Use for the treatment of an arsenic contaminated wastewater. *Journal De Physique IV* **2003,** 107, 377-380.

29.Park, C. K.; Baik, M. H. Diffusion of some chemical species through a granite considering their geochemical properties. *Korean Journal of Chemical Engineering* **2009,** 26, 1279-1285.

30.Peulen, T. O.; Wilkinson, K. J. Diffusion of nanoparticles in a biofilm. *Environmental Science & Technology* **2011,** 45, 3367-3373.

31.Suci, P. A.; Geesey, G. G.; Tyler, B. J. Integration of Raman microscopy, differential interference contrast microscopy, and attenuated total reflection Fourier transform infrared spectroscopy to investigate chlorhexidine spatial and temporal distribution in Candida albicans biofilms. *Journal of Microbiological Methods* **2001,** 46, 193-208.

32.Lacroix-Gueu, P.; Briandet, R.; Leveque-Fort, S.; Bellon-Fontaine, M. N.; Fontaine-Aupart, M. P. In situ measurements of viral particles diffusion inside mucoid biofilms. *Comptes Rendus Biologies* **2005,** 328, 1065-1072.

33.Habimana, O.; Steenkeste, K.; Fontaine-Aupart, M. P.; Bellon-Fontaine, M. N.; Kulakauskas, S.; Briandet, R. Diffusion of nanoparticles in biofilms Is altered by bacterial cell wall hydrophobicity. *Applied and Environmental Microbiology* **2011,** 77, 367-368.

34.Suci, P. A.; Vrany, J. D.; Mittelman, M. W. Investigation of interactions between antimicrobial agents and bacterial biofilms using attenuated total reflection Fourier transform infrared spectroscopy. *Biomaterials* **1998,** 19, 327-339.

35.Guiot, E.; Georges, P.; Brun, A.; Fontaine-Aupart, M. P.; Bellon-Fontaine, M. N.; Briandet, R. Heterogeneity of diffusion inside microbial biofilms determined by fluorescence correlation spectroscopy under two-photon excitation. *Photochemistry and Photobiology* **2002,** 75, 570-578.

36.Zhang, Z.; Nadezhina, E.; Wilkinson, K. J. Quantifying diffusion in a biofilm of streptococcus mutans. *Antimicrobial Agents and Chemotherapy* **2011,** 55, 1075-1081.